

# A Field Theoretic Study of Matter Under Extreme Conditions

A THESIS

submitted for the Award of Ph.D. degree of

MOHANLAL SUKHADIA UNIVERSITY

BY

Bhaswar Chatterjee



FACULTY OF SCIENCE

MOHANLAL SUKHADIA UNIVERSITY

UDAIPUR

Year of submission: 2011



*To*  
*my parents*



# DECLARATION

I, **Mr. Bhaswar Chatterjee**, S/o Mr. Nandalal Chatterjee, resident of F-206, PRL residences, Navrangpura, Ahmedabad 380009, hereby declare that the research work incorporated in the present thesis entitled, “**A Field Theoretic Study of Matter under Extreme Conditions**” is my own work and is original. This work (in part or in full) has not been submitted to any University for the award of a Degree or a Diploma. I have properly acknowledged the material collected from secondary sources wherever required. I solely own the responsibility for the originality of the entire content.

**Date:**

**Bhaswar Chatterjee**  
(Author)



# CERTIFICATE

I feel great pleasure in certifying that the thesis entitled, “**A Field Theoretic Study of Matter Under Extreme Conditions**” by Mr. Bhaswar Chatterjee under my guidance. He has completed the following requirements as per Ph.D regulations of the University.

- (a) Course work as per the university rules.
- (b) Residential requirements of the university.
- (c) Regularly submitted six monthly progress reports.
- (d) Presented his work in the departmental committee.
- (e) Published minimum of one research papers in a referred research journal.

I recommend the submission of thesis.

**Date:**

**Dr. Hiranmaya Mishra**

**(Thesis Supervisor)**

Associate Professor, THEPH,  
Physical Research Laboratory,  
Ahmedabad - 380 009.

Countersigned by

**Head of the Department**



---

## Acknowledgements

*I express my sincere and deepest gratitude to Dr. Hiranmaya Mishra, under the guidance of whom, the work reported in this thesis has been carried out. His deep insight in the subject and vast experience helped me immensely in learning the subject. Discussion with him was a great pleasure as he always gave importance to my views and was always patient with me. It was a great experience to work with him and I consider myself fortunate to have him as my supervisor.*

*I greatly acknowledge the assistance I got from my other collaborator, Dr. Amruta Mishra. It was a pleasing experience to work with her and the discussions we had during WHEPP-11 helped me clearing many doubts. Despite her demanding schedule, she always managed time to help us with new ideas and useful comments.*

*I thank Prof. Saurabh Rindani, Prof. Ravindra Amritkar, Prof. Subhendra Mohanty, Prof. Jagannath Banerjee, Dr. Jitesh Bhatt, Dr. Raghavan Rangarajan, Dr. Namit Mahajan, Dr. Partha Konar, Dr. Srubabati Goswami, Dr. Dilip Angom and Dr. R.P. Singh for the courses they taught and many fruitful discussions. They were always very much encouraging and supportive and made me feel comfortable.*

*I thank Prof. J. N. Goswami, the Director, Prof. Utpal Sarkar and Prof. A. K. Singhvi, former Deans, and Prof. Anjan Joshipura, Dean of PRL for providing necessary facilities and encouragements to carry out research work.*

*I thank all the staffs of PRL computer center for providing excellent computational and internet facilities.*

*I specially thank Amjad, Soumya, Rabiul, Tapas, Ketan, Sandeep, Suman, Anand, Vimal, Ashwini, Arvind, Pankaj, Ashok, Sreekanth, Vineet, Santosh, Bhavik, Vishal, Akhilesh, Zeen, Purnendu, Tarun Gulab, Monojit, Avdhesh, Subrata, Naveen (all), Sudhanwa for there unconditional support and many memorable experiences with them.*

*The support I got from my parents, my sister and Sirshendu is something beyond acknowledgement. They were always with me for whatever reason it*

*may be and the encouragement I received from them is will never fade away.*

***Bhaswar***

---

## ABSTRACT

Our understanding of matter under the influence of extremely high temperature or extremely high baryon densities is limited due to lack of conclusive theoretical tools or experimental evidence. However, the heavy ion collision experiments and the data obtained from compact stars might shed some light on what happens to matter under the influence of temperature of the order of few billions of kelvin or baryon density few times higher than the normal nuclear matter density. Nucleons are expected to be crushed and quarks are supposed to be the relevant degrees of freedom at such extreme conditions. The difficulties in analyzing the behavior of the quark matter arise because of the non perturbative nature of strong interaction under such extreme conditions. However, at asymptotically high density, when the strong coupling is small, a first principle calculation shows the QCD ground state to be a 3-flavor color superconductor (CSC) where all three lightest quarks participate in Bardeen-Cooper-Schrieffer (BCS) type Cooper pairing. At intermediate densities, 2-flavor CSC has been suggested. At lower densities, when the coupling is large, the Cooper pairs might shrink in size to become locally bound diquarks and thus may give rise to Bose-Einstein condensation (BEC). There may be other superfluid phases depending on the mismatch in the densities of different flavors. These superfluid phases are valid at small temperature and at higher temperature, system is expected to pass on to a state with deconfined quarks and gluons known as quark gluon plasma (QGP). Confinement-deconfinement transition and chiral transition are two aspects that play a crucial role in the phase structure of quark matter. Strong  $CP$  violation has also been suggested at high temperature and density. Along with high temperature and baryon density, the presence of magnetic fields may also affect the phase structure. This is important as strong magnetic field can be present in the compact stars and ultra strong magnetic fields can be created in heavy ion collision experiments. The study of the phase structure is not possible in the normal framework of QCD. The only first principle calculational tool available is the lattice QCD, but it fails at finite densities because of the fermion sign problem. The other

way is to use effective theories which replicate QCD in certain limits. In this thesis, we shall use such effective theories to study the transition from BCS phase to BEC phase, the effects of strong magnetic field on chiral symmetry breaking (CSB) and the interplay of strong  $CP$  violation and CSB.

In the first part of this thesis, the transition from BCS phase to BEC phase in a relativistic system with two species of fermions is investigated in a field theoretic model using a variational construct for the ground state. The superfluid gap equation is obtained by minimizing the thermodynamic potential. The phase structure is studied as a function of the coupling as well as the difference in chemical potential of the two species. With coupling, the transition from BCS to BEC turns out to be a crossover. It is observed that the antiparticles play an important role for strong coupling even if the corresponding Fermi momentum is small. For unequal number densities of the pairing species, stable gap less modes with one Fermi surface are seen in deep BEC regime. The effect of fluctuations of the condensate field have also been investigated in a nonperturbative manner with a quartic coupling for the condensates. For stronger fluctuations, the transition from superfluid phase to normal matter phase changes from a second order to a first order transition.

In the second part, we have investigated CSB in hot and dense matter in presence of strong magnetic field again with a variational construct for the ground state in a 3-flavor Nambu-Jona-Lasinio (NJL) model. The Kobayashi-Maskawa-'t Hooft (KMT) six quark determinant interaction term is included in the Lagrangian to induce flavor mixing. At zero baryon density and high temperature, the chiral transition remains a crossover even for magnetic field strength  $eB = 10m_\pi^2$ . The magnetic catalysis of CSB is also observed. However, at finite densities, the chiral transition is a first order transition and the transition chemical potential decreases with increase in magnetic field. For zero temperature, after chiral symmetry is restored, the order parameter shows oscillation similar to the de Hass van Alphen effect for magnetization in metals. Inclusion of magnetic field makes the equation of state steeper. Further, the pressure can be anisotropic if the magnetization of the matter is significant.

Within our model, this anisotropy starts to become relevant for field strengths around  $10^{18}$  Gauss. Such anisotropy of pressure parallel and perpendicular to the magnetic field can affect the structure of neutron stars.

In the final part, we have investigated the strong  $CP$  violation and the interplay of CSB and strong  $CP$  violation at finite temperature and density with variational approach for 3-flavor NJL model with the KMT term. The effect of  $CP$  violation is included through a phase  $\theta$  in the KMT term. No  $CP$  violation is seen for  $\theta = 0$  however, spontaneous  $CP$  violation happens for  $\theta = \pi$ . In the range from  $\theta = 0$  to  $\theta = \pi$ , the scalar and the pseudo scalar condensates behave in a complimentary manner and the constituent quark mass remains almost the same. The  $CP$  restoring transition with temperature at zero density is a crossover for  $\theta \neq \pi$  whereas it becomes a second order one for  $\theta = \pi$ . For finite density, the transition is a first order one but it becomes a second order one for high temperature. The first order transitions are associated with metastable  $CP$  restored states.



---

## LIST OF PUBLICATIONS

### A. Publications related to the thesis work

1. “BCS-BEC crossover and phase structure of relativistic systems: A variational approach”  
Bhaswar Chatterjee, Amruta Mishra, Hiranmaya Mishra  
Phys. Rev. D **79**, 014003 (2009) [arXiv:0804.1051 [hep-ph]]
2. “Vacuum structure and chiral symmetry breaking in strong magnetic fields for hot and dense quark matter”  
Bhaswar Chatterjee, Amruta Mishra, Hiranmaya Mishra  
Phys. Rev. D **84**, 014016 (2011) [arXiv:1101.0498 [hep-ph]]
3. “Strong CP violation and chiral symmetry breaking in hot and dense quark matter”  
Bhaswar Chatterjee, Amruta Mishra, Hiranmaya Mishra  
[arXiv:1111.4061 [hep-ph]] (Communicated for publication)

### B. Conference Proceedings

1. “Chiral symmetry breaking in 3-flavor Nambu-Jona Lasinio model in magnetic background”  
Bhaswar Chatterjee, Amruta Mishra, Hiranmaya Mishra  
Nucl. Phys. A **862-863**, 312-315 (2011) [arXiv:1102.0875 [hep-ph]]  
*Presented at 6th International Conference on Physics and Astrophysics of Quark Gluon Plasma (ICPAQGP), Goa, India, 6-10 Dec 2010*



# Contents

<b>Abstract</b>	<b>iii</b>
<b>List of Publications</b>	<b>vii</b>
<b>1 Introduction</b>	<b>1</b>
1.1 Strong interaction . . . . .	2
1.1.1 Asymptotic freedom . . . . .	3
1.1.2 Confinement . . . . .	4
1.2 Extreme conditions and QCD . . . . .	6
1.2.1 Existence of extreme conditions . . . . .	6
1.2.2 Techniques for calculation . . . . .	7
1.3 The QCD phase diagram . . . . .	8
1.3.1 Chiral symmetry breaking (CSB) . . . . .	11
1.3.2 Strong CP violation . . . . .	15
1.3.3 Color superconductivity (CSC) . . . . .	19
1.4 Outline of the thesis . . . . .	29
<b>2 Relativistic BCS-BEC crossover</b>	<b>31</b>
2.1 BCS-BEC crossover in mean field approximation . . . . .	32
2.1.1 The ansatz for the ground state . . . . .	33
2.1.2 Evaluation of thermodynamic potential and gap equation	36
2.1.3 Numerical analysis and the phase structure . . . . .	42
2.2 BCS-BEC crossover with condensate fluctuations . . . . .	49
2.2.1 The new improved ground state . . . . .	51
2.2.2 Thermodynamic potential and gap equation . . . . .	52

---

2.2.3	Numerical analysis of the crossover . . . . .	56
2.3	Summary . . . . .	59
<b>3</b>	<b>Chiral symmetry breaking in a magnetic background</b>	<b>61</b>
3.1	Dirac spinors in a magnetic field . . . . .	62
3.2	Ground state and chiral order parameter . . . . .	65
3.3	Thermodynamic potential and gap equation . . . . .	70
3.4	Results and discussions . . . . .	77
3.5	Summary . . . . .	89
<b>4</b>	<b>Strong CP violation at finite temperature and density</b>	<b>91</b>
4.1	NJL model with CP violating term . . . . .	93
4.2	Ground state and order parameters . . . . .	94
4.3	Effective potential and gap equations . . . . .	96
4.4	Analysis of the phase structure . . . . .	99
4.5	Summary . . . . .	105
<b>5</b>	<b>Summary and outlook</b>	<b>107</b>

# List of Figures

1.1	<i>The theoretically proposed phase diagram of QCD. . . . .</i>	9
1.2	<i>Ratio of the coherence length <math>\xi_c</math> and the average inter quark distance <math>d_q</math> as a function of the chemical potential. This figure is taken from Ref.[19] . . . . .</i>	27
2.1	<i>Gap parameter (left panel) and the scaled chemical potential <math>(\mu - m)/(\epsilon_f - m)</math> (right panel) in units of Fermi energy as a function of the coupling. The dotted line corresponds to the case where antiparticle contributions are not included and the solid line corresponds to inclusion of the antiparticle contributions. . .</i>	43
2.2	<i>(Left panel) Superfluid gap (solid line) and chemical potential (dotted line) in units of Fermi energy as functions of the coupling. (Right panel) Number densities of particles, <math>\rho_-</math> (solid line) and antiparticles, <math>\rho_+</math> (dotted line) in units of <math>k_f^3/3\pi^2</math> as functions of the coupling. . . . .</i>	44
2.3	<i>Ratio of critical chemical potential difference to the gap as a function of the coupling strength <math>\eta</math>. Gapless phase appear for <math>\eta &gt; 1.9</math>. Solid line denotes absence of gapless modes. The dotted line corresponds to gapless modes for quasi particles of species ‘1’ and the dashed line indicates the regime where quasi antiparticles of species ‘2’ also become gapless. . . . .</i>	46

- 2.4 (Left panel) Quasi particle dispersion relation for species ‘1’ for  $\eta = 2.1$  and  $\delta_\mu/\Delta_0 = 1.125$ ,  $\Delta_0$  being the gap at  $\delta_\mu = 0$ . (Right panel) Dispersion relations for quasi particle of species ‘1’ (solid line) and for quasi antiparticle of species ‘2’ (dotted line) for  $\eta = 3$  and  $\delta_\mu/\Delta_0 = 1.195$ . . . . . 47
- 2.5 (Left panel) Superfluid gap as a function of difference in number densities of the condensing species. This is plotted for  $\eta = 2.1$ . (Right panel) Number density distribution for the two species. Solid line corresponds to species ‘1’ and the dashed line corresponds to species ‘2’. This plot corresponds to  $\eta = 3$  and  $\delta_\mu/\Delta_0 = 1.195$ . . . . . 48
- 2.6 (Left panel) Fermion chemical potential and gap in units of Fermi energy as functions of the crossover parameter. (Right panel) Number densities of fermions and bosons in units of total number density as functions of the crossover parameter. In both the plots, The solid (black), dotted (blue) and dashed (red) curves correspond to  $\lambda_R=0, 0.5$  and  $2$  respectively. . . . . 57
- 2.7 (Left panel) Critical temperature  $T_c$  and the chemical potential at  $T = T_c$  in units of Fermi energy as a function of the crossover parameter. The solid (black), dotted (blue) and dashed (red) curves correspond to  $\lambda_R=0, 0.5$  and  $2$  respectively. (Right panel) Superfluid gap as a function of temperature for quartic coupling  $\lambda_R = 5$ . The dotted line corresponds unstable solutions with higher thermodynamic potential as compared to  $\Delta = 0$ . . . . . 58
- 3.1 Constituent quark masses as functions of magnetic field at  $T = \mu = 0$ . (Left panel) Effect of the KMT determinant interaction term is included. (Right Panel) The KMT term is ignored, i.e.  $K = 0$ . The solid curves, the dotted curves and the dash-dotted curves represent the constituent masses of  $u, d$  and  $s$  quarks respectively in both the plots. . . . . 78

3.2	<i>Constituent masses of the <math>u</math> quark, <math>M_u</math> (left panel) and the <math>s</math> quark, <math>M_s</math> (right panel) as functions of temperature for different strengths of magnetic field at <math>\mu = 0</math>.</i>	80
3.3	<i>Constituent masses of <math>u</math> quark (left panel) and <math>d</math> quark (right panel) as functions of <math>\mu_q</math> for different strengths of magnetic field at <math>T = 0</math>.</i>	81
3.4	<i>Constituent mass of <math>s</math> quark (left panel) and baryon density (right panel) as functions of <math>\mu_q</math> for different strengths of magnetic field at <math>T = 0</math>.</i>	81
3.5	<i>Oscillation of <math>u</math> quark mass with magnetic field. We have taken <math>\mu_q = 380</math> MeV and <math>T = 0</math>.</i>	82
3.6	<i>Constituent masses of <math>u</math> quarks (left panel) and <math>s</math> quarks (right panel) as functions of <math>\mu_q</math> at <math>T = 0</math> for different strengths of magnetic field for charge neutral matter.</i>	83
3.7	<i>Constituent masses of <math>u</math> and <math>s</math> quarks as functions of baryon density in units of nuclear matter density <math>\rho_0</math> for different strengths of magnetic field at <math>T = 0</math>.</i>	84
3.8	<i>Constituent masses of <math>u</math> and <math>s</math> quarks as functions of <math>\mu_q</math> for charge neutral matter for different strengths of magnetic field at <math>T = 40</math> MeV.</i>	85
3.9	<i>Equations of state for charge neutral matter at <math>T = 0</math> (left panel) and <math>T = 40</math> MeV (right panel) for different strengths of magnetic field.</i>	85
3.10	<i>(Left panel) Magnetization in units of <math>\Lambda^2</math> as a function of magnetic field. (Right panel) <math>P_{\parallel}</math> and <math>P_{\perp}</math> of strange quark matter as functions of the magnetic field in units of pressure <math>P_0</math> for <math>eB = 0</math>. In both the plots, the magnetic field in units of <math>m_{\pi}^2</math> is plotted in a logarithmic scale and we have taken here <math>T = 0</math> and <math>\mu_u = \mu_d = 0.4</math> GeV.</i>	88

- 
- 4.1  $\theta$  dependence of scalar and pseudo scalar condensates for  $u$  quark (left panel) and the effective potential (right panel) at  $T = \mu_q = 0$ . . . . . 100
- 4.2 (Left panel) Temperature dependence of the constituent mass of  $u$  quark for  $\theta = \mu_q = 0$ . (Right panel) Constituent mass of  $u$  and  $s$  quark as functions of chemical potential at  $\theta = T = 0$ . . . 100
- 4.3 Constituent mass of  $u$  quark and the contributions from scalar and pseudo scalar condensates as a function of temperature at  $\mu_q = 0$  for  $\theta = \pi/2$  (left panel) and  $\theta = \pi$  (right panel). . . . . 101
- 4.4 The nature of transition of the scalar (left panel) and pseudo scalar (right panel) condensates with temperature at  $\mu_q = 0$  for different values of  $\theta$ . . . . . 102
- 4.5 Constituent masses of  $u$  and  $s$  quarks along with the contributions from scalar and pseudo scalar channels as functions of quark chemical potential  $T = 0$  for  $\theta = \pi/2$  (left panel) and  $\theta = \pi$  (right panel). The pseudo scalar contribution for strange quarks is negligible in this range of chemical potential. . . . . 103
- 4.6 (Left Panel) Contribution from the pseudo scalar condensates to the  $u$  quark mass as a function of  $\mu_q$  for different temperatures for  $\theta = \pi$ . (Right panel) The phase diagram for  $CP$  restoring transition in the  $T - \mu$  plane for  $\theta = \pi$ . The region between the solid line and the dotted line represents the unstable  $CP$  restored phase with  $\Omega$  higher than the  $CP$  violated phase. . . . . 104

# Chapter 1

## Introduction

The basic motivation of high energy physics is to understand the nature of different elementary and composite particles and the different types of interaction among them. The matter in this universe is fully comprised of two types of elementary fermions: leptons and quarks. There are six different types of leptons (electron, muon, tau and their corresponding neutrinos) and six different types of quarks (up, down, charm, strange, top and bottom) along with the corresponding antiparticles.

These different quarks and leptons interact with each other through four different types of interactions : gravitational, weak, electromagnetic and strong interaction. Among them, gravity is the least known as we do not yet have a quantum theory of gravity. Electromagnetic and weak interactions are much better understood and they have been successfully unified in  $SU(2)_L \times U(1)_Y$  gauge theory, called the electro-weak theory which is also known as standard model (SM) of particle physics [1]. The perturbative aspects of strong interaction has also been successfully incorporated in the SM by the gauge group  $SU(3)_C \times SU(2)_L \times U(1)_Y$  [2]. However, there is no conclusive theory which can predict the low energy behavior of strong force. Difficulties arise because of the non perturbative nature of strong interaction at low energy. The motivation of this thesis is to study some aspects of strong interaction in the non perturbative regime. In the next section, we shall briefly discuss strong interaction along with its basic aspects.

## 1.1 Strong interaction

Strong interaction is the strongest of the fundamental forces in nature and the particles which participate in strong interactions are the hadrons or more fundamentally, the quarks and gluons. The charge of strong interaction is called color charge and gluons act as the force carrier. The gluonic interaction among quarks and antiquarks leads to formation of color singlet composite particles called hadrons. There are two types of hadrons present in nature: mesons and baryons. Mesons are quark-antiquark bosonic states and baryons are three quark fermionic states.

The theory of strong interaction is described by quantum chromodynamics (QCD). Similar to quantum electrodynamics, QCD is based on a gauge principle. But unlike QED, this is a Yang-Mills gauge theory with the gauge group being the local  $SU(3)_C$ . The gauge invariant QCD Lagrangian is given as

$$\mathcal{L}_{QCD} = \bar{\psi}_a^i (i\gamma^\mu \partial_\mu - m_i) \psi_a^i + g A_\mu^A \bar{\psi}_a^i \gamma^\mu T_{ab}^A \psi_b^i - \frac{1}{4} G_{\mu\nu}^A G^{A\mu\nu}, \quad (1.1)$$

where  $\psi_a^i$  is the quark field in the fundamental representation of  $SU(3)_C$  with flavor index  $i$  and color index  $a$ .  $A_\mu^A$  is the vector gauge field of  $SU(3)_C$  and represents gluons here.  $G_{\mu\nu}^A = \partial_\mu A_\nu^A - \partial_\nu A_\mu^A + gf^{ABC} A_\mu^B A_\nu^C$  is the gluonic field strength tensor. The generators of  $SU(3)_C$  are defined as  $T_{ab}^A = \frac{1}{2} (\lambda^A)_{ab}$ , where  $\lambda^A$  are the Gell-Mann matrices.  $m_i$  is the current quark mass and  $g$  is the coupling constant of QCD.

If we take the quark mass to be zero, the Lagrangian in Eq.(1.1) has flavor symmetry since strong interaction does not discriminate between different quark flavors. With  $N_f$  massless quark flavors, the QCD Lagrangian is symmetric under the global chiral symmetry group  $SU(N_f)_L \times SU(N_f)_R$ . Then the total symmetry group of QCD is  $SU(N_f)_L \times SU(N_f)_R \times U(1)_B \times U(1)_A$ . Where  $U(1)_B$  and  $U(1)_A$  correspond to baryon number symmetry and axial symmetry respectively. The chiral symmetry of QCD is only an approximate symmetry since quarks are not really massless and it is spontaneously broken to  $SU(N_f)_V$  in QCD vacuum with the formation of chiral condensates which

give masses to the hadrons. The vector symmetry  $U(1)_B$  corresponding to baryon number symmetry is an exact symmetry. The axial  $U(1)_A$  symmetry also breaks through chiral anomaly and this also breaks the charge parity ( $CP$ ) symmetry. Though the gauge invariance allows a  $CP$  violating  $\theta$  term in the Lagrangian, the value of  $\theta$  is extremely small in nature. This smallness of  $\theta$  is not explained and this is known as the strong  $CP$  problem. We shall discuss about the chiral symmetry breaking (CSB) and strong  $CP$  problem later in more details.

QCD has two very important properties arising from self interaction of gluons : the asymptotic freedom and confinement. QCD processes at high energies become calculable because of asymptotic freedom whereas confinement describes formation of hadrons at lower energies. There is no fixed energy boundary to separate these two phases. Asymptotic freedom is theoretically well understood and tested but the mechanism of confinement is still a mystery. The study of confinement, CSB and strong  $CP$  requires understanding of low energy QCD. To understand QCD in the low energy regime, it is necessary to study QCD under the influences of extreme conditions like high temperature or baryon density. There might be many interesting phases of matter under the influence of these extreme conditions where the dominant interaction is the strong interaction.

Now, we shall briefly discuss about asymptotic freedom and confinement. Then in the next section, we shall discuss about the extreme conditions, their existence and their influence on the phases of strongly interacting matter and various interesting phenomena including CSB and strong  $CP$  violation.

### 1.1.1 Asymptotic freedom

QCD has a surprising property that causes the coupling strengths to become arbitrarily small when the energy scales become arbitrarily high or equivalently the length scales become arbitrarily small. This is known as asymptotic freedom [2]. At very high energy scales, quarks behave like free particles allowing perturbative calculation described by DGLAP equation [3] in deep

inelastic processes in QCD, on the other hand at low energies, the strong coupling becomes large making analytic calculation of QCD processes difficult and sometimes impossible.

Asymptotic freedom arises because of screening and anti screening by virtual quark-antiquark pairs and virtual gluons respectively in a polarized QCD vacuum. The number of flavors decides whether a gauge theory is asymptotically free or not. This is obtained by calculating the beta function. Beta function denotes the dependence of gauge coupling,  $g$  on the energy scale,  $\mu$ . To lowest non trivial order, the beta function for a  $SU(N)$  gauge theory with fermions in the fundamental representation has been derived as

$$\beta(g) = \frac{\partial g}{\partial \log \mu} = -\frac{g^3}{(4\pi)^2} \left[ \frac{11N}{3} - \frac{2N_f}{3} \right]. \quad (1.2)$$

It is evident from Eq.(1.2) that, for QCD with three colors, the number of flavors,  $N_f$ , should be more than 16 for beta function to be positive. Since we have only 6 quarks, the QCD beta function is negative and it is an asymptotically free gauge theory. The running coupling of QCD is given by

$$\alpha_S(Q) = \frac{2\pi}{b_0 \log \frac{Q}{\Lambda}}, \quad (1.3)$$

where  $\alpha = g^2/4\pi$  and  $b_0 = -(4\pi)^2\beta(g)/g^3$ . Here  $Q$  denotes the momentum transfer and  $\Lambda$  is called the QCD scale. Experiments suggest a value of  $\Lambda \approx 200$  MeV. Strong coupling becomes large for distances larger than  $\sim 1/\Lambda$ , which is roughly the size of light hadrons.

### 1.1.2 Confinement

Confinement is another very important property of QCD which prevents free quarks to exist in nature. Except the top quark, all other quarks form hadrons almost as soon as they are created. Top quark has a lifetime of about  $5 \times 10^{25}$  seconds which is approximately 20 times less than the time scale of strong interaction and so it decays before forming hadrons. The other quarks can

never be observed at a more fundamental level than at hadronic level.

To understand the mechanism of confinement, Wilson loops were introduced [4]. which is defined as a path ordered exponential of a gauge field  $A_\mu$  along a closed curve  $C$ . The gauge invariant Wilson loop is given by

$$W_C = \mathcal{P} e^{i \oint_C A_\mu dx^\mu}, \quad (1.4)$$

Where  $\mathcal{P}$  is the path ordering operator. At  $T = 0$ , if  $W_C$  increases with area then it implies confinement and if  $W_C$  increases with the perimeter of the loop then it implies deconfinement. Though Wilson loops does not describe the mechanism of confinement, it sheds some light on the confinement-deconfinement phase transition. However the most widely used method to address this phase transition is the use of Polyakov loop which is essentially the thermal Wilson loop. It has been shown theoretically that, in the absence of quarks, the thermal Wilson loop with periodic boundary conditions is the order parameter for confinement [5]. At finite temperature, after defining  $\tau = it$ , in the absence of the spatial components of the gauge field  $A_\mu$ , the Polyakov loop can be written as

$$L(\mathbf{X}) = \mathcal{P} e^{i \int_0^\beta A_0(\mathbf{X}, \tau) d\tau}. \quad (1.5)$$

If  $A_0$  is taken to be constant,  $L = \exp(i\beta A_0)$  when  $A_0$  is Hermitian and  $L = \exp(\beta A_0)$  when  $A_0$  is anti Hermitian [6, 7]. The free energy of a quark-quark pair separated by a distance  $X$  in the infinitely heavy quark limit is given by  $\langle \bar{\Phi}(\mathbf{X}) \Phi(\mathbf{0}) \rangle$  [5, 7], where

$$\Phi(\mathbf{x}) = \frac{1}{N_C} \langle \text{Tr}_C L(\mathbf{x}) \rangle \quad \text{and} \quad \bar{\Phi}(\mathbf{x}) = \frac{1}{N_C} \langle \text{Tr}_C L^\dagger(\mathbf{x}) \rangle. \quad (1.6)$$

In the confined phase, the energy required to separate two quarks increases with the separation distance. So  $\Phi$  serves as the order parameter.  $\Phi = 0$  implies confinement,  $\Phi \neq 0$  implies deconfinement and  $\Phi = 1$  implies total deconfinement [8].

## 1.2 Extreme conditions and QCD

By the term ‘extreme conditions’, we refer to mainly extremely high temperature and extremely high density. By extreme temperature, we mean temperature ranging up to few hundreds of MeV ( $1 \text{ MeV} = 1.16 \times 10^{10} \text{ Kelvin}$ ). By extreme densities, we refer to densities up to few times the nuclear matter density,  $\rho_0 = 10^{14} \text{ gm/cc}$ . To study the properties of matter under these conditions is very important because the dominant interaction there is the strong interaction and these conditions significantly affect the strong dynamics. In addition to the above mentioned extreme conditions, extremely high magnetic fields also play a significant role in modifying the QCD dynamics. Now, we shall discuss about the existence of these extreme conditions and the tools available for studying their influence on matter. Then in the next section, we shall discuss about the various phases of matter subject to these extremities.

### 1.2.1 Existence of extreme conditions

In the early universe, when the universe was only a few microseconds old, the temperature was of the order of the QCD scale which corresponds to few hundreds of MeV. In the present universe, such high temperatures might be seen in new born neutron stars. Neutron stars are the best places in our universe where these extreme conditions can be observed. The temperature inside a new born neutron star is  $\sim 10^{12}$  kelvin though because of cooling, it falls to  $\sim 10^6$  kelvin in few years. The density of a neutron star is  $\sim 10^{15} \text{ gm/cc}$  in its core which is approximately 10 times the normal nuclear matter density. Neutron stars are usually associated with very strong magnetic fields ranging from  $10^{13}$  Gauss on the poles of radio pulsars [9] to  $10^{16}$  Gauss on the surface of magnetars [10].

In laboratories also, some of these extreme conditions have been realized for a very short span of time. In the high energy heavy ion collision experiments, temperature that is comparable to that of  $10^{-5}$  second old universe has been created in small regions. This has been achieved at SPS accelerator in CERN,

at RHIC in BNL and latest at the LHC in CERN. Heavy ion collision processes are associated with ultra strong magnetic fields. The strengths of magnetic fields are estimated to be of hadronic scale of the order of  $eB \sim 2m_\pi^2$  ( $m_\pi^2 \simeq 10^{18}$  Gauss) at RHIC [11, 12] to  $eB \sim 15m_\pi^2$  at LHC [12]. The most difficult part is the creation of ultra high densities in laboratories. All the above mentioned colliders mostly operate at zero or very low densities. The future planned FAIR experiment is supposed to be carried out at a higher chemical potential ( $\mu_q \sim 200$  MeV).

### 1.2.2 Techniques for calculation

The dominant interaction in matter under extreme conditions is the strong interaction. It is very difficult to do analytic calculation there because we don't have a conclusive theory. The main difficulty arises from the largeness of QCD coupling. Asymptotically high temperature or density make the situation simpler as the weak coupling approximation holds quite good then. The situation is very different in densities relevant to the neutron stars or the nuclear matter or temperature relevant for the early universe as the coupling becomes really large. There are some methods which have been successful to some extent. One of them is the lattice QCD, the only first principle calculational tool. This is a brute force computational method and results of lattice QCD matches to a good extent with the colliders operating at high temperature but low density. Lattice QCD fails at higher densities because of fermion sign problem. Another method is to use effective models. Effective models are models with some properties of QCD but they are easier to manipulate in the low energy regime. Some popular models are sigma model, bag model and Nambu-Jona-Lasinio (NJL) model. Bag model includes the effect of confinement through an additive energy density. The NJL model is perhaps the most widely used effective model, studied extensively for high densities as well as high temperatures. NJL model has no gluon and the strong interaction is replaced by a four-fermion interaction term [13]. The model is constructed from interacting Dirac fermions with chiral symmetry very much similar to

the construction of Cooper pairs with electrons in Bardeen-Cooper-Schrieffer (BCS) theory of superconductivity [14, 15]. NJL model is very much useful in exploring the finite density behavior. Even at ultra high densities, the weak coupling calculation and the NJL model calculation yield quite similar magnitudes for quantities like superfluid gap. The confinement problem has also been addressed in Polyakov loop extended NJL (PNJL) model [16].

### 1.3 The QCD phase diagram

At ordinary temperature or density, the strong force confines the quarks inside hadrons whose size is around  $1 \text{ fm}$  (which corresponds to  $\Lambda_{QCD} = 200 \text{ MeV}$ ). When the temperature reaches the QCD scale or the density is so high that the average inter-quark separation becomes less than  $1 \text{ fm}$  (quark chemical potential,  $\mu_q \sim 400 \text{ MeV}$ ), then hadrons are melted and it is logical then to consider not the hadrons but the quarks as the basic degrees of freedom. Such phases of matter is called the quark matter. At high temperature, according to the theoretical prediction, the quarks and gluons become deconfined and this phase is the quark gluon plasma (QGP) and the suggested phase of quark matter at high density is a superconducting phase called color superconductor (CSC). The suggested phases of quark matter at different temperature and chemical potential is shown in the conjectured QCD phase diagram in Fig.[1.1].

We call it a conjectured phase diagram because theoretically or experimentally, it is not well known. The relevant thermodynamic quantities are temperature  $T$  and baryon chemical potential  $\mu_B$ . The vacuum corresponds to  $T = \mu_B = 0$ . The ordinary matter is consisted of nucleon droplets surrounded by vacuum and this is the case up to the phase boundary between hadron gas and nuclear matter. This boundary lies at around  $\mu_B = 900 \text{ MeV}$  where a liquid-gas phase transition takes place. As we increase the chemical potential keeping the temperature low, at some critical value of  $\mu_B$ , different effective theories suggest a transition from nuclear matter to quark matter. The nature of quark matter emerging from squeezing of nucleons at intermediate densities

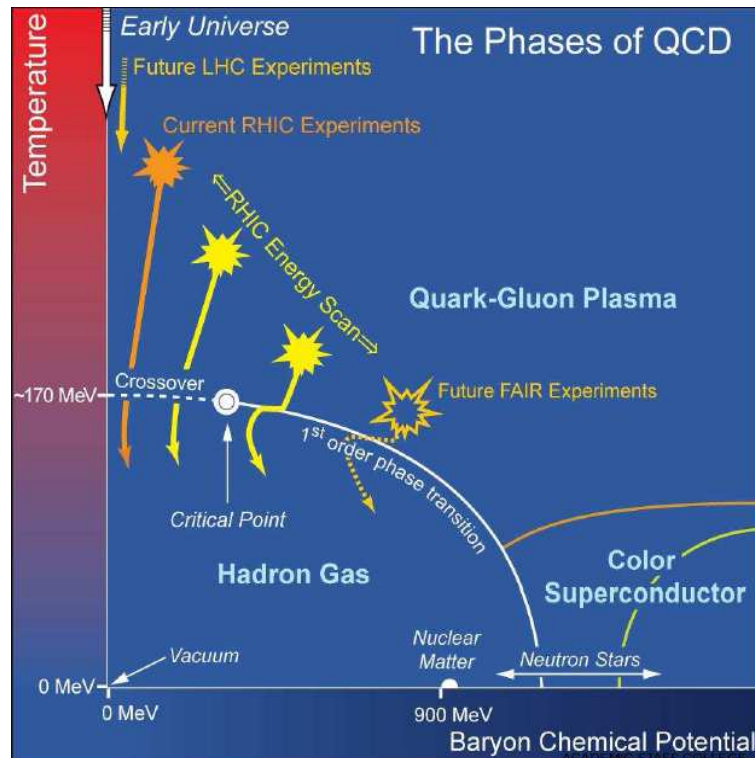


Figure 1.1: *The theoretically proposed phase diagram of QCD.*

(few times  $\rho_0$ ) is an open problem. However, different effective theories suggest the possibility of one of various types of CSC phases. The essence of these CSC phases is the BCS type of superconductivity. However, unlike electrons in BCS theory, quarks come in different flavors and colors. This difference along with different constraints like charge neutrality (relevant for neutron stars) may lead to the possibility of many different types of superconducting phases over a range of chemical potential as well as the difference in chemical potential of different flavors of quarks.

At asymptotically high densities ( $\mu_q \gg m_u, m_d, m_s$ ), QCD calculation predicts quark matter to be in color-flavor locked (CFL) phase which is CSC phase with pairing among all the three quark flavors [17]. At intermediate densities, a varieties of phases have been suggested. In this regime, it is expected that strange quarks are either absent or do not form condensates. So the pairing is restricted to the two lightest flavors. The most widely studied phase in this regime is the 2-flavor CSC (2SC) phase where  $u$  and  $d$  quarks of different color form Cooper pairs [18]. The mechanism of 2SC pairing is similar

to the BCS pairing. As the density decreases, the quark matter might pass on from 2SC phase to Bose-Einstein condensed (BEC) state with bound diquarks [19, 20]. Few other interesting states of matter have been proposed when constraints like charge neutrality are imposed which implies a mismatch in the chemical potential of different flavors. Near the paired-unpaired transition boundary, such a mismatch may induce the Fulde-Ferrel-Larkin-Ovchinnikov (FFLO) phase which involves Cooper pairs with finite momentum [21]. This phase is known as the crystalline superconducting phase. Phases with effective Fermi surfaces have also been suggested for stronger coupling and mismatch in the densities of different flavors of quarks. Superfluidity involving one such Fermi surface is called the interior gap superfluidity and phases with two such effective Fermi surfaces are known as breached pairing phases [22].

Now as the temperature is increased keeping the chemical potential low, at first we get a gas of hadrons (mainly pions). Then at a critical temperature,  $T_C \sim 170$  MeV which corresponds to  $\sim 10^{12}$  kelvin, deconfined quarks, antiquarks and gluons are formed as the thermal fluctuations break up the hadrons. Such deconfined phase is called the QGP phase. The transition from hadronic phase to QGP phase is expected to be a crossover. The  $T_C$  has been predicted by lattice QCD calculations [23]. The QGP is the theoretically predicted state of matter when the universe was only a few microseconds old. At higher densities also, QGP is the expected state of matter when the temperature is as high as  $10^{12}$  kelvin. The confinement-deconfinement phase boundary was also thought to be the boundary for chiral transition. The low density and low temperature region is supposed to be the region chiral symmetry is broken and it is supposed to be restored at high density or temperature. However, some phases, relevant at high density might also break chiral symmetry. So it is now not clear whether deconfinement phase transition and chiral transition follows the same path or not.

In the following, we shall discuss in some detail, three different aspects of strong interaction in the context of the QCD phase diagram : CSB, strong CP violation and CSC.

### 1.3.1 Chiral symmetry breaking (CSB)

Chiral symmetry is a symmetry of the Lagrangian which allows independent transformation of the left-handed and right-handed components of the Dirac fields. Let us consider the fermionic part of the QCD Lagrangian with the two lightest quarks,

$$\mathcal{L} = \bar{u}i\not{D}u + \bar{d}i\not{D}d - m_u\bar{u}u - m_d\bar{d}d. \quad (1.7)$$

If we ignore the current quark masses, then the Lagrangian in Eq.(1.7) has  $SU_V(2)$  isospin symmetry. In terms of the left-handed and right-handed components of the quark doublet  $Q$ , the Lagrangian can be written as

$$\mathcal{L} = \bar{Q}_L i\not{D}Q_L + \bar{Q}_R i\not{D}Q_R, \quad (1.8)$$

where the left-handed and right-handed components of the quark doublet are given by

$$Q_L = \left(\frac{1 - \gamma^5}{2}\right) Q \quad \text{and} \quad Q_R = \left(\frac{1 + \gamma^5}{2}\right) Q \quad (1.9)$$

The Lagrangian in Eq.(1.8) is symmetric under separate unitary transformations of  $SU_A(2)$  given by

$$\begin{aligned} Q_L &\rightarrow e^{i\theta_L} Q_L & \text{and} & & Q_R &\rightarrow Q_R, \\ Q_L &\rightarrow Q_L & \text{and} & & Q_R &\rightarrow e^{i\theta_R} Q_R. \end{aligned}$$

This symmetry is called the chiral symmetry. A mass term like  $m\bar{Q}Q$  in the Lagrangian explicitly breaks the chiral symmetry as it mixes the left-handed and the right-handed quarks,

$$m\bar{Q}Q = m\bar{Q}_L Q_R + m\bar{Q}_R Q_L.$$

The QCD Lagrangian respects the chiral symmetry only approximately as the  $u$  and  $d$  quarks are not really massless. Chiral symmetry is spontaneously broken in the QCD vacuum with a non zero vacuum expectation value of  $\bar{Q}Q$ . The explicit mechanism of CSB is not known. Since it is a non perturbative

phenomenon, lattice QCD or some effective models are used to study CSB. The NJL model is especially useful as it features the generation of Fermion masses through dynamical CSB. The mechanism of CSB in NJL model closely follows the BCS theory of superconductivity as it features quark-antiquark pair condensation in vacuum through some attractive channel. Now we shall discuss CSB in 2-flavor NJL model through Green's function approach [24].

For two flavors of quarks with equal masses, the NJL Lagrangian with the scalar and pseudo scalar terms is given by

$$\mathcal{L}_{NJL} = \bar{\psi} (i\cancel{\partial} - m) \psi + G \left[ (\bar{\psi}\psi)^2 + (\bar{\psi}i\gamma^5\boldsymbol{\tau}\psi)^2 \right], \quad (1.10)$$

where  $\boldsymbol{\tau} = (\tau^1, \tau^2, \tau^3)$  are the Pauli matrices in the flavor space. We have suppressed the flavor and color indices here. The Lagrangian has isospin symmetry as  $m_u = m_d = m$ . In the mean field approximation, using the Feynman rules for a four-fermion interaction, the self energy associated with the scalar vertex  $(\bar{\psi}\psi)^2$  and that with the pseudo scalar vertex  $(\bar{\psi}i\gamma^5\boldsymbol{\tau}\psi)^2$  can respectively be written as

$$\Sigma^S = 2G [Tr\{iS(x, x)\} - iS(x, x)], \quad (1.11)$$

$$\Sigma^{PS} = 2G (i\gamma^5\boldsymbol{\tau}) [Tr\{iS(x, x)\} - iS(x, x)] (i\gamma^5\boldsymbol{\tau}), \quad (1.12)$$

where  $Tr$  denotes a trace over the color, flavor and spinor indices.  $S(x, x)$  is the time ordered single particle Green's function defined as  $iS(x, x') = \langle T\psi(x)\bar{\psi}(x') \rangle$ . This propagator satisfies

$$(i\cancel{\partial}_x - \Sigma) S(x, x') = \delta^{(4)}(x - x'), \quad (1.13)$$

where  $\Sigma$  is the total self energy given by  $\Sigma = m + \Sigma^S + \Sigma^{PS}$ . It is easy to identify  $\Sigma$  as the mass of the particle in the system,  $\Sigma = M$ . The solution of Eq.(1.13) in the momentum space is given by

$$S(p) = \frac{\not{p} + M}{p^2 + M^2}. \quad (1.14)$$

Now, inserting the Fourier transform of the propagator, given in Eq.(1.14) in Eq.(1.11) and Eq.(1.12) and adding them, the mass gap equation can be written as

$$\Sigma = M = m + iG [2N_C N_f + 1] \int \frac{d^4 p}{(2\pi)^4} \text{tr} S(p), \quad (1.15)$$

where the trace is over the spinor indices only. Eq.(1.15) gives the constituent mass  $M$  of the quarks. Now, Eq.(1.15) contains divergence whose origin can be traced back to the four-fermion contact interaction. Since NJL model is non renormalizable, some regularization schemes need to be imposed. One such scheme is the three momentum cutoff scheme. In this method, a three momentum cutoff,  $\Lambda$  satisfying  $|\mathbf{p}| < \Lambda$ , is imposed after carrying out the  $p_0$  integration in Eq.(1.15). If we neglect the exchange term in Eq.(1.15), then it has the form

$$M = m + 4GN_C N_f M \int^\Lambda \frac{d^3 p}{(2\pi)^3} \frac{1}{E_p}, \quad (1.16)$$

with  $E_p = \sqrt{p^2 + M^2}$ . Eq.(1.16) is a self consistent equation for the constituent quark mass  $M$  and it can be analytically calculated as

$$\int^\Lambda \frac{d^3 p}{(2\pi)^3} \frac{1}{E_p} = \frac{1}{4\pi^2} \left[ \Lambda \sqrt{\Lambda^2 + M^2} - M^2 \sinh^{-1} \frac{\Lambda}{M} \right].$$

In the limit of vanishing current quark mass, Eq.(1.16) will always have a trivial solution for  $M = 0$  and the corresponding phase is called Wigner phase for which, the chiral condensate,  $\langle \bar{\psi} \psi \rangle = 0$ . On the other hand if a non zero  $M$  exists, then the chiral condensate is given as

$$\langle \bar{\psi} \psi \rangle = -2N_C N_f M \int \frac{d^3 p}{(2\pi)^3} \frac{1}{E_p}. \quad (1.17)$$

Such a phase is known as the Nambu-Goldstone phase. The difference in energy density between the Nambu-Goldstone phase and the Wigner phase is given as

$$\langle \delta T^{00} \rangle = \langle T^{00} \rangle_{NG} - \langle T^{00} \rangle_W \simeq \frac{\Lambda^2 M^2}{8\pi^2} \left[ 1 - \frac{\pi^2}{GN_C N_f \Lambda^2} \right]. \quad (1.18)$$

A negative  $\langle \delta T^{00} \rangle$  implies that the Nambu-Goldstone phase is energetically favored over the Wigner phase. From Eq.(1.18), it is evident that  $\langle \delta T^{00} \rangle$  is negative beyond a critical value of  $G$ ,  $G_C \Lambda^2 = \pi^2 / N_C N_f$ . Below  $G_C$ , the Nambu-Goldstone phase will not be favored over the Wigner phase.

The momentum cutoff,  $\Lambda$ , and the four-fermion coupling,  $G$ , are fixed by choosing a value for the current quark mass and fitting to the pion decay constant and the mass of pion. If the current quark mass,  $m$  is taken to be zero then, for  $\Lambda = 653$  MeV and  $G \Lambda^2 = 2.14$ , the constituent quark mass,  $M$ , turns out to be 313 MeV in the two flavor case [24].

At finite temperature and density, Eq.(1.16) gets modified due to the thermal contribution of quarks and antiquarks and is given as

$$M = m + 4GN_C N_f M \int^{\Lambda} \frac{d^3 p}{(2\pi)^3} \frac{1}{E_p} [1 - n_-(p) - n_+(p)], \quad (1.19)$$

with  $n_{\mp}(p) = [\exp\{\beta(E_p \mp \mu)\} + 1]^{-1}$  being the quark and antiquark distribution functions respectively. The chiral order parameter in Eq.(1.17) also gets modified and is given as

$$\langle \bar{\psi} \psi \rangle = -2N_C N_f M \int \frac{d^3 p}{(2\pi)^3} \frac{1}{E_p} [1 - n_-(p) - n_+(p)]. \quad (1.20)$$

It has been shown that strong magnetic field acts as a catalyzer of CSB [25, 26, 27] as it enhances the constituent quark mass. But recently it has been shown using ADS-CFT correspondence that magnetic field may also induce a lower critical  $\mu_B$  for chiral symmetry restoration [28]. This phenomena has been termed as inverse magnetic catalysis (IMC). The effect of magnetic field on CSB can play a significant role in the structure of the neutron stars as they are usually associated with very high magnetic field. The study of the effect of magnetic field on CSB is essential in the context of heavy ion collision experiments also as ultra high magnetic fields  $\sim 10^{18}$  Gauss are produced there and an interesting phenomenon induced by strong magnetic field called chiral magnetic effect (CME) [29] has been predicted which may explain the charge separation observed in STAR experiment [44].

In the above, we have discussed CSB in 2-flavor NJL model using the Green's function method. CSB can also be studied in NJL model using Bogoliubov-Valatin approach which involves an explicit construction of a BCS like variational ground state. In chapter-3, we shall study the effect of magnetic field on CSB in 3-flavor NJL model with a Kobayashi-Maskawa-'t Hooft (KMT) determinant interaction term in the Bogoliubov-Valatin approach.

### 1.3.2 Strong CP violation

Strong interaction is known to respect the parity ( $P$ ) and charge parity ( $CP$ ) symmetry to a large extent. The QCD Lagrangian that we have considered in Eq.(1.1) is symmetric under  $P$  and  $CP$  transformations in the vanishing quark mass limit. The axial current density  $J_{\mu 5}^f = \bar{\psi}_f \gamma_\mu \gamma_5 \psi_f$  corresponding to the Lagrangian in Eq.(1.1) is conserved in the vanishing quark mass limit as

$$\partial^\mu J_{\mu 5}^f = 2m_f i \bar{\psi}_f \gamma_5 \psi_f. \quad (1.21)$$

For  $m_f = 0$ , the right hand side becomes zero implying exact conservation of the axial current density. However, these classical symmetries of QCD comes under question because of the Adler-Bell-Jackiw anomaly [30] which is also known as the  $U(1)_A$  axial anomaly [31]. Because of this anomaly, the axial current density is not conserved even in the vanishing quark mass limit and the divergence of the axial current is given as

$$\partial^\mu J_{\mu 5}^f = 2m_f i \bar{\psi}_f \gamma_5 \psi_f + \frac{N_f g^2}{32\pi^2} F_{\mu\nu}^a \tilde{F}^{a\mu\nu}, \quad (1.22)$$

where  $F_{\mu\nu}^a$  is the gluon field strength tensor and  $\tilde{F}^{a\mu\nu} = \epsilon^{\mu\nu\rho\sigma} F_{\rho\sigma}^a$  is the dual field strength tensor. This anomalous divergence of the axial current density should correspond to a pseudo scalar meson with roughly the same mass as pion which has never been observed. This is the  $U(1)_A$  problem. This problem was theoretically solved by showing that because of instanton effects,  $U(1)_A$  should not result in a physical meson [32, 33]. This anomalous axial current

can be obtained by adding a  $\theta$ -term, which is allowed in principle by the gauge invariance of QCD, to the Lagrangian in Eq.(1.1) as

$$\mathcal{L}_{QCD}^{\theta} = \mathcal{L}_{QCD}^{\theta=0} + \mathcal{L}^{\theta} = \mathcal{L}_{QCD}^{\theta=0} + \frac{\theta}{64\pi^2} g^2 F_{\mu\nu}^a \tilde{F}^{a\mu\nu}, \quad (1.23)$$

where  $\mathcal{L}_{QCD}^{\theta=0}$  is the Lagrangian we have considered in Eq.(1.1) and  $\theta$  is a number. For non zero values of  $\theta$ , the  $P$  and  $CP$  invariance of QCD is lost when such a term is included. From the Lagrangian in Eq.(1.23), the divergence of axial current can be written as

$$\partial^{\mu} J_{\mu 5}^f = 2m_f i \bar{\psi}_f \gamma_5 \psi_f + \frac{N_f g^2 \theta}{32\pi^2} F_{\mu\nu}^a \tilde{F}^{a\mu\nu}. \quad (1.24)$$

The  $CP$  violating  $\theta$ -term manifests its effect in the electric dipole moments (EDM) of the hadrons. The current experimental upper bound on the neutrons EDM is  $|d_n| < 2.9 \times 10^{-26} e \text{ cm}$  [34]. A careful analysis from this value of EDM of neutron yields an upper bound,  $|\theta| < 0.7 \times 10^{-11}$  [35]. The reason behind such unnatural smallness of  $\theta$  is not yet known and this is the strong  $CP$  problem. Possible explanation of this problem has been suggested by promoting  $\theta$  into a dynamic axion field [36]. These axion fields emerge as Nambu-Goldstone boson corresponding to the spontaneous breaking of an additional chiral symmetry : the Peccei-Quinn symmetry [37].

The Vafa-Witten theorem forbids spontaneous violation of  $P$  or  $CP$  in the QCD vacuum for  $\theta = 0$  [38]. However, this theorem need not hold for QCD at finite isospin density [39] or finite temperature [40] where  $P$  odd operators, which are not Lorentz invariant, are allowed to have non zero expectation values. Moreover, the Dashen phenomenon allows degenerate vacuum states which spontaneously break  $P$  and  $CP$  for  $\theta = \pi$  [41].

The heavy ion collision experiments might produce excited vacuum states which breaks  $P$  and  $CP$  [42]. It has been proposed that near the deconfinement phase transition, the QCD vacuum might possess  $P$  and  $CP$  odd states with locally non vanishing  $\theta$  [43]. However, the prediction that opened new ways of observing  $P$  and  $CP$  violating effects in the heavy ion collision experiments

in presence of strong magnetic field is the chiral magnetic effect (CME). This predicts separation of electric charges along the axis of the magnetic field because of the spatial variation of the topological charge distribution [29]. The experimental results obtained by STAR Collaboration at RHIC also suggests such charge separation resulting from  $P$  and  $CP$  odd effects [44].

Because of the non perturbative nature of strong interaction at finite temperature and density, the study of these  $P$  and  $CP$  violating effects require lattice QCD or effective models. Though NJL model does not have any  $CP$  violation term, it can still be used with the inclusion of a six fermion determinant interaction term in the Lagrangian. Such a term was first introduced to account for the large mass of the pseudo scalar meson  $\eta'$  ( $m_{\eta'} = 958$  MeV) [45] and later, this vertex was derived as an instanton induced quark interaction [33]. This vertex is called the Kobayashi-Maskawa-'t Hooft (KMT) vertex and is expressed as

$$\mathcal{L}_{KMT}^0 = \det \bar{\psi}_i (1 - \gamma_5) \psi_j + h.c.,$$

where  $i, j = 1, 2, 3$  are the flavor indices. To incorporate the effect of the  $\theta$ -term in the Lagrangian in Eq.(1.23), a phase factor is introduced in the KMT term and then the NJL Lagrangian can be written as

$$\begin{aligned} \mathcal{L}_{NJL}^{KMT} &= \bar{\psi} i \not{\partial} \psi - \bar{\psi} m \psi + \sum_{a=0}^8 G [(\bar{\psi} \lambda_a \psi)^2 + (\bar{\psi} i \lambda_a \gamma_5 \psi)^2] \\ &+ K [e^{-i\theta} \det \bar{\psi}_i (1 - \gamma_5) \psi_j + h.c] \\ &= \mathcal{L}_0 + \mathcal{L}_{SB} + \mathcal{L}_S + \mathcal{L}_{KMT}, \end{aligned} \quad (1.25)$$

where the quark field  $\psi_i$  has three colors ( $N_c = 3$ ) and three flavors ( $N_f = 3$ ). This Lagrangian incorporates dynamical CSB, the  $U(1)_A$  axial anomaly and the explicit symmetry breaking through the current quark mass. To check the symmetries of the Lagrangian in Eq.(1.25), it is useful to define

$$\Phi_{ij} = \bar{\psi}_i (1 - \gamma_5) \psi_j = 2\bar{\psi}_{iR} \psi_{jL} \quad (1.26)$$

with  $\Phi_{ij}^\dagger = \bar{\psi}_i (1 + \gamma_5) \psi_j = 2\bar{\psi}_{iL} \psi_{jR}$  where  $\psi_{iL}$  and  $\psi_{iR}$  are the left handed

and right handed fields respectively. Under the  $SU(3)_L \times SU(3)_R$  global chiral transformations defined as

$$\psi_{iL} \rightarrow [U(\theta_L)]_{ij} \psi_{jL} \equiv L_{ij} \psi_{jL} \quad \text{and} \quad \psi_{iR} \rightarrow [U(\theta_R)]_{ij} \psi_{jR} \equiv R_{ij} \psi_{jR}, \quad (1.27)$$

with  $U(\theta) = \exp(i \sum_{a=1}^8 \lambda_a \theta_a / 2)$ , the bosonic operators are transformed as

$$\Phi_{ij} \rightarrow L_{ik} \Phi_{kl} R_{lj}^\dagger \quad \text{and} \quad \Phi_{ij}^\dagger \rightarrow R_{ik} \Phi_{kl}^\dagger L_{lj}. \quad (1.28)$$

So the bosonic operators and their hermitian conjugates are respectively the  $(3, \bar{3})$  and  $(\bar{3}, 3)$  representations of  $SU(3)_L \times SU(3)_R$ . It is easy to see that the Lagrangian in Eq.(1.25) has  $SU(3)_L \times SU(3)_R$  invariance.  $\mathcal{L}_S$  is also invariant under  $U(1)_V \times U(1)_A$  transformations defined as

$$\psi_L \rightarrow e^{i\alpha} \psi_L \quad \text{and} \quad \psi_R \rightarrow e^{i\beta} \psi_R. \quad (1.29)$$

Under this transformation, the bosonic operators transform as

$$\Phi \rightarrow e^{i(\alpha-\beta)/2} \Phi \quad \text{and} \quad \Phi^\dagger \rightarrow e^{-i(\alpha-\beta)/2} \Phi^\dagger. \quad (1.30)$$

The KMT term is invariant under  $U(1)_A$  only when  $\alpha = \beta$  which is the  $U(1)_V$  transformation. So  $\mathcal{L}_{KMT}$  is invariant under  $SU(3)_L \times SU(3)_R \times U(1)_V$  but not invariant under  $U(1)_A$ . In addition to the KMT term, the mass term is also not invariant under  $U(1)_A$ . From the Lagrangian in Eq.(1.25), the axial anomaly equation is given as

$$\partial^\mu J_{\mu 5} = 2mi\bar{\psi}\gamma_5\psi + 2iN_f K (e^{-i\theta} \det\Phi - h.c.). \quad (1.31)$$

Comparing Eq.(1.31) with Eq.(1.24), it can be said that the effect of the gluon operator  $\frac{g^2}{32\pi^2} F_{\mu\nu}^a \tilde{F}^{a\mu\nu}$  is simulated by the determinant operator  $(e^{-i\theta} \det\Phi - h.c)$  in the quark sector. We shall discuss the strong CP violation through the KMT determinant interaction term in detail in chapter-4.

### 1.3.3 Color superconductivity (CSC)

Color superconductivity (CSC) is relevant for the high density and low temperature regime of the QCD phase diagram. Let us consider the case of ultra high density where quarks are the relevant degrees of freedom and they are weakly interacting. The distribution function at zero temperature is then given by

$$f_F(k) = \theta(\mu - E_k), \quad (1.32)$$

where  $E_k = \sqrt{k^2 + m^2}$  is the dispersion relation for a free quark of mass  $m$  and momentum  $\mathbf{k}$  ( $k = |\mathbf{k}|$ ).  $\mu$  is the chemical potential given by  $\mu = \sqrt{k_f^2 + m^2}$ , with  $\mathbf{k}_f$  being the Fermi momentum. The distribution function in Eq.(1.32) implies that up to Fermi level, all the states are filled and beyond that all the states are empty. This kind of distribution of quarks makes the ground state unstable in presence of some attractive interaction (even arbitrarily small) among the quarks because of Cooper instability [14] arising from formation of Cooper pairs around the degenerate Fermi surface. Since the Cooper pairs are bosonic in nature, they can form Bose-Einstein condensate at  $T = 0$  leading to a superconducting state very much similar to the BCS theory of superconductivity at low temperature [15]. Here, unlike the electrons in BCS type of low temperature superconductivity, quarks are of different flavors and they are associated with the non abelian color charge. This kind of superconductivity with quark matter is called color superconductivity (CSC). This has been reviewed in Ref.[46].

The ground state of quark matter at asymptotically high density has been predicted to be a CSC phase from perturbative QCD calculation [18]. At large enough densities, when the interaction strength is weak, the dominant interaction is the one gluon exchange interaction and this can be studied from the first principles of QCD. In presence of a finite chemical potential, the QCD Lagrangian, given in Eq.(1.1) is modified and it is given by

$$\mathcal{L}_{QCD} = \bar{\psi}_a^i (i\gamma^\mu \partial_\mu + \gamma^0 \mu - m_i) \psi_a^i + g A_\mu^A \bar{\psi}_a^i \gamma^\mu T_{ab}^A \psi_b^i - \frac{1}{4} G_{\mu\nu}^A G^{A\mu\nu}, \quad (1.33)$$

Since it is reasonable to neglect the current quark masses at high densities, the Lagrangian in Eq.(1.33) has approximate  $SU(2)_L \times SU(2)_R$  global chiral symmetry. We can neglect constituent quark masses generated by dynamical symmetry breaking also as the chiral condensate,  $\langle \bar{\psi}\psi \rangle$  which is responsible for the constituent quark masses, melts down at higher densities.

In the one gluon exchange approximation, the scattering amplitude for quark-quark scattering is proportional to the color structure of the interaction vertex in Eq.(1.33) which is given by

$$\sum_{A=1}^{N_C^2-1} T_{aa'}^A T_{b'b}^A = -\frac{N_C+1}{4N_C} (\delta_{aa'}\delta_{b'b} - \delta_{ab'}\delta_{a'b}) + \frac{N_C-1}{4N_C} (\delta_{aa'}\delta_{b'b} + \delta_{ab'}\delta_{a'b}). \quad (1.34)$$

The first term In Eq.(1.34) corresponds to the attractive antitriplet channel while the second term corresponds to the repulsive sextet channel. The attractive channel plays the key role in Cooper pairing. This antisymmetry of the attractive channel is reflected in the color structure of the Cooper pairs, given by

$$\langle (\bar{\psi}^C)_a^i \gamma^5 \psi_b^j \rangle \sim \varepsilon^{ij} \epsilon_{abc}, \quad (1.35)$$

where  $\psi^C = C\bar{\psi}^T$  is the charge conjugated spinor and  $C = i\gamma^2\gamma^0$  is the charge conjugation matrix. The condensate is antisymmetric in flavor of because of antisymmetry in color and Dirac indices. The arbitrary orientation of this condensate in the color space can be modified conveniently through global color transformations. The convention is to choose the condensate to point towards blue quark,  $\langle (\bar{\psi}^C)_a^i \gamma^5 \psi_b^j \rangle \sim \varepsilon^{ij} \epsilon_{ab3}$ . This means that the blue quarks do not participate in the Cooper pairing and they give rise to gapless quasi particles. To study 2-flavor CSC (2SC) in dense matter, instead of Dirac spinor, it is convenient to use 8-component Nambu-Gorkov spinor given by

$$\Psi = \begin{bmatrix} \psi \\ \psi^C \end{bmatrix}. \quad (1.36)$$

In Nambu-Gorkov basis, the inverse quark propagator in the ground state of

2SC has off-diagonal elements,

$$S^{-1} = \begin{bmatrix} [G_0^+]^{-1} & \Delta^- \\ \Delta^+ & [G_0^-]^{-1} \end{bmatrix}, \quad (1.37)$$

where

$$[G_0^\pm]^{-1} = \gamma^\mu k_\mu \pm \mu \gamma_0 \quad (1.38)$$

are the inverse Dirac propagators for massless quarks ( $G_0^+$ ) and charge-conjugated quarks ( $G_0^-$ ). The off-diagonal components are given by,  $\Delta^- = -i\epsilon^3 \epsilon \gamma^5 \Delta$  and  $\Delta^+ \equiv \gamma^0 (\Delta^-)^\dagger \gamma^0 = -i\epsilon^3 \epsilon \gamma^5 \Delta^*$ , where  $\Delta$  is the diquark gap. From the inverse propagator in Eq.(1.37), the quark propagator can be written as

$$S = \begin{bmatrix} G^+ & \Xi^- \\ \Xi^+ & G^- \end{bmatrix}, \quad (1.39)$$

where the diagonal and the off-diagonal elements of the quark propagator are given by

$$G^\pm = \left[ (G_0^\pm)^{-1} - \Delta^\mp G_0^\mp \Delta^\pm \right]^{-1}, \quad (1.40)$$

$$\Xi^\pm = -G_0^\mp \Delta^\pm G^\pm. \quad (1.41)$$

In dense QCD, though the one gluon exchange interaction is the dominant one, it gets partially screened because of the surrounding dense medium. So the gluon propagator also gets modified because of the medium. The inverse gluon propagator in the medium can be written as

$$(\mathcal{D}^{-1})_{\mu\nu}^{AB} = (D_0^{-1})_{\mu\nu}^{AB} + \Pi_{\mu\nu}^{AB}, \quad (1.42)$$

where  $(D_0)_{\mu\nu}^{AB}$  is the gluon propagator in vacuum and  $\Pi_{\mu\nu}^{AB}$  is the gluon self-energy. The soft gluons play the key role in Cooper pairing. The dominant contribution to the soft gluon self energy comes from quark loops with hard internal momenta of the order of  $\mu$ . It is large compared to others because it is proportional to the density of states at Fermi surface and the running coupling,

$\alpha_S = g^2/4\pi$ , i.e.,  $\Pi_{\mu\nu}^{AB} \sim \alpha_S \mu^2$ . In case of asymptotically high densities, the bare quark-gluon vertices and the gluon propagator with the screening effects are used in the Schwinger-Dyson equation for the quark propagator which, for this case, can be written as

$$S^{-1}(k) = S_0^{-1}(k) + 4\pi\alpha_S \int \frac{d^4p}{(2\pi)^4} \Gamma_\mu^A S(p) \Gamma_\nu^B \mathcal{D}_{AB}^{\mu\nu}(k-p), \quad (1.43)$$

where the quark-gluon vertices to the leading order in the Nambu-Gorkov basis are given by

$$\Gamma_\mu^A = \gamma_\mu \begin{bmatrix} T^A & 0 \\ 0 & -(T^A)^T \end{bmatrix}. \quad (1.44)$$

In case of the quark propagator given in Eq.(1.37), the Schwinger-Dyson equation reduces to an equation for the diquark gap parameter  $\Delta$  in the weak coupling limit. Neglecting the dependence of the gap on the three-momentum and performing the momentum integration, the approximate form of the gap equation is obtained as [47, 48, 49],

$$\Delta(k_4) \simeq \frac{\alpha_S}{9\pi} \int \frac{dp_4 \Delta(p_4)}{\sqrt{p_4^2 + \Delta^2}} \ln \frac{c\mu}{|k_4 - p_4|}, \quad (1.45)$$

with  $k_4 \equiv ik_0$  and  $c = 2(4\pi)^{3/2} \alpha_S^{-5/2}$ . The extra coupling dependence ( $\alpha_S^{-5/2}$  in the logarithm) comes from the in medium gluon propagator within the hard dense loop (HDL) approximation [50]. The constant  $c$  is calculated by collecting the leading logarithms from both electric and magnetic gluon exchange. The gap equation, which is an integral equation, can be converted into a differential equation [47]. In the weak coupling limit, an approximate solution to Eq.(1.45) is given by [49],

$$\Delta(0) \simeq c\mu \exp\left(-\frac{3\pi^{3/2}}{2^{3/2}\sqrt{\alpha_S}}\right) = c\mu \exp\left(-\frac{3\pi^2}{\sqrt{2}g}\right). \quad (1.46)$$

The expression for the superconducting gap in Eq.(1.46) is valid only in the case of asymptotically high density. Careful analysis shows that the weak coupling approximation is valid only at  $\mu \gg 10^8$  MeV [50]! Below, this,

the higher order contributions of the coupling,  $g$  to the gap,  $\Delta$  can not be neglected. So in case of moderate density (few times  $\rho_0$ ), one has to depend on the effective models. One convenient choice is the NJL model. The Lagrangian for 2-flavor NJL model containing diquark term and which is invariant under global  $SU(2)_L \times SU(2)_R$  global chiral symmetry in the vanishing current quark mass limit is given as [51],

$$\mathcal{L}_{NJL} = \bar{\psi} (i\cancel{\partial} + \gamma^0 \mu) \psi + G_D (i\bar{\psi}^C \epsilon \epsilon^b \gamma^5 \psi) (i\bar{\psi} \epsilon \epsilon^b \gamma^5 \psi^C), \quad (1.47)$$

where  $(\varepsilon)^{ik} \equiv \varepsilon^{ik}$  and  $(\epsilon^b)^{ca} \equiv \epsilon^{cab}$  are the antisymmetric tensors in the flavor and color space respectively.  $G_D$  is the diquark four fermion coupling in the color flavor antisymmetric channel. The four fermion scalar and pseudo scalar terms of the Lagrangian in Eq.(1.10) are not included in Eq.(1.47) as this discussion is confined to densities where chiral symmetry gets restored. The interplay of both CSB and CSC has also been studied in NJL model. In the mean field approximation, an auxiliary field is introduced as

$$\Delta^b = -2G_D (i\bar{\psi}^C \epsilon \epsilon^b \gamma^5 \psi). \quad (1.48)$$

Using this auxiliary field, the Lagrangian of Eq.(1.47) can be rewritten as

$$\mathcal{L}_{MF} = \bar{\psi} (i\cancel{\partial} + \gamma^0 \mu) \psi - \frac{\Delta^{*b}}{2} (i\bar{\psi}^C \epsilon \epsilon^b \gamma^5 \psi) - \frac{\Delta^b}{2} (i\bar{\psi} \epsilon \epsilon^b \gamma^5 \psi^C) - \frac{\Delta^{*b} \Delta^b}{4G_D}, \quad (1.49)$$

with  $\Delta^{*b} = -2G_D (i\bar{\psi} \epsilon \epsilon^b \gamma^5 \psi^C)$ . In the mean field approximation, the expectation value of  $\Delta^b$  is taken to be a constant value  $\Delta$ , which is the diquark gap parameter. Here, it has been assumed conventionally that only red and green quarks form the condensates while the blue quarks remain free. Using the Lagrangian in Eq.(1.49), the partition function can be written as

$$\mathcal{Z} = N' \int [d\bar{\psi}][d\psi] \exp \left\{ \int_0^\beta d\tau \int d^3x \mathcal{L}_{MF} \right\}, \quad (1.50)$$

where  $\beta = 1/T$  is the inverse of temperature. In the mean field approximation,

the partition function reduces to a product of three terms as

$$\mathcal{Z} = \mathcal{Z}_c \mathcal{Z}_b \mathcal{Z}_{r,g}. \quad (1.51)$$

The constant term  $\mathcal{Z}_c$  is given by

$$\mathcal{Z}_c = N' \exp \left\{ - \int_0^\beta d\tau \int d^3x \frac{\Delta^* \Delta}{4G_D} \right\}. \quad (1.52)$$

$\mathcal{Z}_b$  denotes the contribution from the unpaired blue quarks and is given as

$$\mathcal{Z}_b = \int [d\bar{\psi}_b][d\psi_b] \exp \left\{ \int_0^\beta d\tau \int \frac{d^3x}{2} [\bar{\psi}_b(i\cancel{\partial} + \mu\gamma_0)\psi_b + \bar{\psi}_b^C(i\cancel{\partial} - \mu\gamma_0)\psi_b^C] \right\}. \quad (1.53)$$

Defining  $Q = \psi_{r,g}$  for the red and green quarks forming the Cooper pairs, the contribution from the paired quarks to the partition function can be written as

$$\begin{aligned} \mathcal{Z}_{r,g} &= \int [d\bar{Q}][dQ] \exp \left\{ \int_0^\beta d\tau \int \frac{d^3x}{2} [\bar{Q}(i\cancel{\partial} + \mu\gamma_0)Q \right. \\ &\quad \left. + \bar{Q}^C(i\cancel{\partial} - \mu\gamma_0)Q^C + \bar{Q}\Delta^- Q^C + \bar{Q}^C\Delta^+ Q] \right\}, \end{aligned} \quad (1.54)$$

where  $\Delta^- = -i\Delta\varepsilon\epsilon^b\gamma_5$  and  $\Delta^+ = -i\Delta^*\varepsilon\epsilon^b\gamma_5$  satisfy the relation  $\Delta^+ = \gamma^0(\Delta^-)^\dagger\gamma^0$ . Using the 8-component Nambu-Gorkov spinor in Eq.(1.36),  $\mathcal{Z}_b$  from Eq.(1.53) and  $\mathcal{Z}_{r,g}$  from Eq.(1.54) can be written as

$$\mathcal{Z}_b = [\text{Det}\{\beta(G_0^+)^{-1}\}\text{Det}\{\beta(G_0^-)^{-1}\}]^{1/2}, \quad (1.55)$$

$$\mathcal{Z}_{r,g} = [\text{Det}(\beta S^{-1})]^{1/2}, \quad (1.56)$$

where  $G_0^\pm$  are the free quark propagators in Eq.(1.38) and  $S$  is the dressed quark propagator in Eq.(1.39). The thermodynamic dynamic potential in terms of the partition function is given as

$$\Omega = -\frac{T}{V} \ln \mathcal{Z} = -\frac{T}{V} [\ln \mathcal{Z}_c + \ln \mathcal{Z}_b + \ln \mathcal{Z}_{r,g}]. \quad (1.57)$$

Using Eq.s(1.52,1.55,1.56), the logarithms of the three different contributions

can be written as

$$\begin{aligned}\ln \mathcal{Z}_c &= -\frac{V}{T} \frac{\Delta^2}{4G_D}, \\ \ln \mathcal{Z}_b &= \frac{N_f V}{T} \int \frac{d^3k}{(2\pi)^3} \left[ E_k^+ + 2T \ln\{1 + e^{-\beta E_k^+}\} + E_k^- + 2T \ln\{1 + e^{-\beta E_k^-}\} \right], \\ \ln \mathcal{Z}_{r,g} &= \frac{2N_f V}{T} \int \frac{d^3k}{(2\pi)^3} \left[ E_\Delta^+ + 2T \ln\{1 + e^{-\beta E_\Delta^+}\} + E_\Delta^- + 2T \ln\{1 + e^{-\beta E_\Delta^-}\} \right],\end{aligned}$$

where  $E_k^\pm = |\mathbf{k}| \pm \mu$  and  $E_\Delta^\pm = \sqrt{E_k^\pm{}^2 + \Delta^2}$ . Using these logarithms, the thermodynamic potential in Eq.(1.57) can explicitly be written as

$$\begin{aligned}\Omega &= \frac{\Delta^2}{4G_D} - 2N_f \int \frac{d^3k}{(2\pi)^3} \left[ |\mathbf{k}| + T \ln\{1 + e^{-\beta E_k^+}\} + T \ln\{1 + e^{-\beta E_k^-}\} \right. \\ &\quad \left. + E_\Delta^+ + 2T \ln\{1 + e^{-\beta E_\Delta^+}\} + E_\Delta^- + 2T \ln\{1 + e^{-\beta E_\Delta^-}\} \right].\end{aligned}\quad (1.58)$$

Minimizing  $\Omega$ , given in Eq.(1.58), with respect to  $\Delta$  gives the equation for the diquark gap parameter  $\Delta$  at  $T = 0$  as

$$1 = 8N_f G_D \int \frac{d^3k}{(2\pi)^3} \left[ \frac{1}{2E_\Delta^-} + \frac{1}{2E_\Delta^+} \right].\quad (1.59)$$

The approximate solution to the gap equation in Eq.(1.59) is given by

$$\Delta \simeq 2\sqrt{\Lambda^2 - \mu^2} \exp\left(-\frac{\pi^2}{8G_D\mu^2} + \frac{\Lambda^2 - 3\mu^2}{2\mu^2}\right),\quad (1.60)$$

where  $\Lambda$  is the three momentum cutoff. For  $\mu = 400$  MeV, which is relevant for the core of neutron stars, the gap turns out to be around 140 MeV for  $G_D = 3.5$  GeV<sup>-2</sup> and  $\Lambda = 600$  MeV [52]. This observation triggered interest in the field of CSC as such a large gap should be reflected in the observational data from the compact stars. This should affect the transport and thermodynamical properties as viscosity, conductivity, specific heat and equation of state.

Other than the lightest up and down quarks, strange quarks might also be present when the quark chemical potential,  $\mu_q$ , is much larger than the constituent mass of the strange quark. There have been speculations that strange quark matter may be the actual ground state of dense baryonic matter

[53]. If the density is so high that the current mass of strange quark becomes negligible compared to  $\mu_q$ , then all the three quarks can participate in Cooper pairing and the resulting phase will be a 3-flavor CSC phase. The condensate for such a state is antisymmetric in flavor and color and is given by [17],

$$\langle (\bar{\psi}^C)_i^a \gamma^5 \psi_j^b \rangle \sim \delta_i^a \delta_j^b + \delta_j^a \delta_i^b. \quad (1.61)$$

In this state, the left-handed condensates break the  $SU(3)_L$  chiral symmetry and  $SU(3)_C$  color symmetry but leave the  $SU(3)_{L+C}$  symmetry unbroken. Similarly the right-handed condensates break the  $SU(3)_R$  chiral symmetry and  $SU(3)_C$  color symmetry but leave the  $SU(3)_{R+C}$  symmetry unbroken. In presence of both types of condensates, the symmetry of the ground state is  $SU(3)_{L+R+C}$ . So the color-flavor orientations of the two condensates are locked to each other. This mechanism is called the color-flavor locking and so the 3-flavor CSC phase is called color-flavor locked (CFL) phase.

We have discussed about the 2SC phase which is the most widely studied phase at intermediate densities and whose essence is BCS type of superconductivity with Cooper pairs for weak interaction strength. But, as we mentioned while discussing the QCD phase diagram, a wide range of non BCS phases might appear at intermediate densities when the coupling is large. The expectation of this phase structure with non BCS phases is propelled mainly by two facts : the structural dependence of the Cooper pairs on the coupling strength and the relevance of charge neutrality condition in the context of neutron stars which implies a mismatch in chemical potential of different flavors of quarks. The structural change of Cooper pair alone can induce BEC phase in quark matter. This, coupled with the mismatch in chemical potential can induce more exotic phases like FFLO, interior gap superfluidity and breached pairing.

In the Cooper paired phase, the typical size of Cooper pairs is characterized by the coherence length,  $\xi_c$ , which is defined as [19],

$$\xi_c^2 = \frac{\int d^3r r^2 |\varphi(r)|^2}{\int d^3r |\varphi_+(r)|^2}, \quad (1.62)$$

where  $\varphi(r)$  is the diquark correlation function for the quarks related to the superfluid gap, defined as [19],

$$\varphi(r) = N \int \frac{d^3k}{(2\pi)^3} \frac{\Delta(k)}{2\sqrt{(|\mathbf{k}| - \mu)^2 + |\Delta(k)|^2}} e^{i\mathbf{k}\cdot\mathbf{r}}. \quad (1.63)$$

However, from  $\xi_c$  alone, it can not be concluded whether the Cooper pairs are tightly bound or loosely bound spatially. For that,  $\xi_c$  needs to be compared to the typical length scale of the system which in this case is the averaged inter quark quark distance  $d_q$ , given as

$$d_q = \frac{1}{\mu} \left[ \frac{\pi^2}{2} \right]^{1/3}. \quad (1.64)$$

The expression for  $d_q$  in Eq.(1.64) is obtained assuming the quarks to be free. For accurate estimation, the contributions from interaction should be included. However, for  $\Delta \gg \mu$ , the expression in Eq.(1.64) holds good as the corrections due to interaction are suppressed by powers of  $\Delta/\mu$ . The behavior of the ratio of  $\xi_c/d_q$  with  $\mu$  is shown in Fig.[1.2]

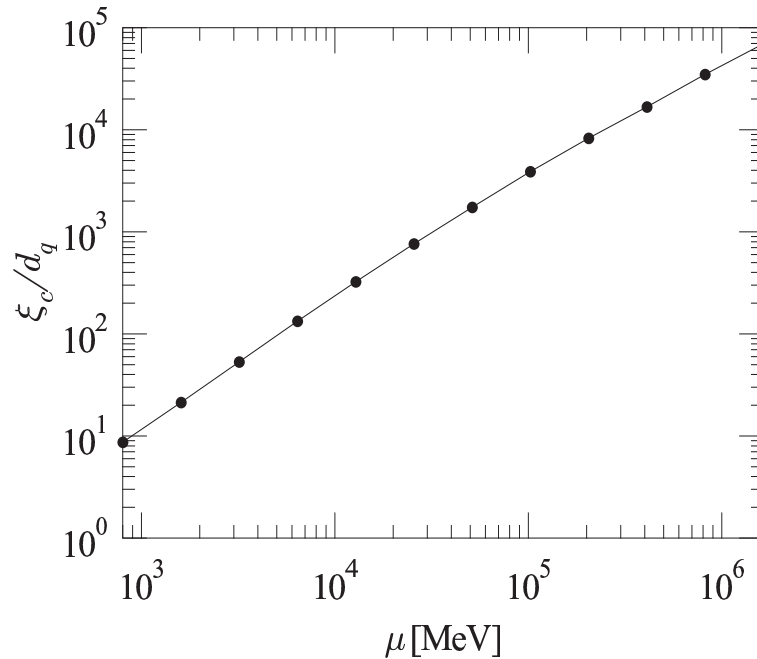


Figure 1.2: Ratio of the coherence length  $\xi_c$  and the average inter quark distance  $d_q$  as a function of the chemical potential. This figure is taken from Ref.[19]

As the chemical potential decreases, so does the ratio  $\xi_c/d_q$ . BCS phase is

characterized by  $\xi_c/d_q \gg 1$ , i.e, coherence length much larger than the inter quark separation. When the ratio becomes of the order of 1, the system might pass on to strongly coupled BEC with locally bound diquarks [19, 20]. Fig.[1.2] suggests that BEC might be the relevant phase at densities that exist in the neutron stars. The transition from BCS phase to BEC phase is expected to be a crossover similar to the case of cold atoms.

Now, in the context of neutron stars, one important constraint is the charge neutrality condition. Since different flavors of quarks have different charges, charge neutrality condition demands for unequal chemical potential for different species. This mismatch motivated the suggestion of FFLO condensates which was first proposed in the context of superconductivity in metals with magnetic impurity [21]. Unlike BCS superconductivity, the essence of FFLO is the formation of Cooper pairs with non zero momentum near the pairing-unpairing boundary which might be thermodynamically favorable when there is a mismatch in the chemical potential of different flavors of quarks. The FFLO condensates break translational and rotational invariance and consequently the gap varies periodically in a crystalline pattern. So FFLO is called the crystalline CSC phase.

There also have been suggestions of exotic non BCS phases with non zero effective Fermi surfaces induced by a mismatch in chemical potential in the strongly coupled CSC regime. These non zero effective Fermi surfaces imply the existence of non zero Fermi momenta of the quasi particles which correspond to the zeros of the respective energy dispersion relation. In these phases, there may exist one or more such Fermi surfaces for the quarks and this type of superfluidity is called gapless superfluidity. Phases with one non zero Fermi surface are known as the interior gap superfluid phase and phases with two such effective Fermi surfaces are called the breached pairing phase. Depending on the mismatch in chemical potential and the coupling strength, there may exist a mixed superfluid phase where particles and antiparticles of different flavors might exhibit different types of gapless superfluidity. In these mixed phases, usually one or more flavors show superfluidity without gapless modes

as all the species can not have gapless modes simultaneously. Gapless superfluidity has been studied in the context of quark matter [22] as well as in the case of cold atoms [54, 55].

We shall discuss BCS-BEC crossover and gapless superfluid phases for a general relativistic fermionic system in the context of quark matter in detail in chapter-2.

## 1.4 Outline of the thesis

This thesis has been organized in the following manner : In the second chapter, we shall discuss the BCS-BEC crossover in a system of two species of relativistic fermions. We shall consider a relativistic model with four fermion interaction for our purpose. First we shall discuss the BCS-BEC crossover within the mean field approximation. We shall compare our results to the results obtained in the non relativistic systems. Then we shall extend our model to include the quantum fluctuation of the condensate field to study the crossover beyond mean field approximation.

Chapter-3 is devoted to studying the effect of magnetic field on CSB at finite temperature and density. We use the 3-flavor NJL model with a KMT determinant interaction term to see the effect of flavor mixing. The effects of charge neutrality condition which is relevant for neutron stars have been studied and the equation of states for different values of magnetic field have also been obtained.

In chapter-4, we shall discuss the effect of finite temperature and density on strong  $CP$  violation and the interplay of CSB and strong  $CP$  violation in quark matter. Here also we have used the 3-flavor NJL model with the KMT term. The spontaneous  $CP$  violation at  $\theta = \pi$  has been discussed and the  $CP$  restoration at finite temperature and finite density is also discussed. Finally, in chapter-5, we shall summarize our studies.



# Chapter 2

## Relativistic BCS-BEC crossover

In this chapter, we shall discuss the BCS-BEC crossover in relativistic fermionic matter. At high density and low temperature, a system of fermions might form a degenerate Fermi gas with all the energy levels upto the Fermi level are completely filled. In presence of such a filled Fermi sea, even a arbitrarily small attractive interaction may lead to formation of Cooper pairs and consequently BCS type superconductivity as we have mentioned in Sec.[1.3.3]. But the scenario changes if the density decreases which means increase in coupling strength in the context of quark matter. As shown in Fig.[1.2], the ratio of the coherence length and the average inter particle separation becomes smaller as the density decreases. At some critical density before the quarks are confined the coherence length becomes of the order of the inter particle separation [19, 56]. At such situation, it is proper to treat the Cooper pairs as spatially localized bound states rather than pairs. At sufficiently low temperature, these bosonic bound states may condense to form a BEC of difermion molecules. If the density is decreased further, there might be a confinement phase transition from BEC to hadronic matter in the context of quarks [57].

The transition from BCS phase to BEC phase is likely to be a smooth crossover much similar to the case of cold fermionic atoms. Relativistic BCS-BEC crossover within four-fermion point interaction model has been studied using various approaches [56, 58, 59]. Effects of fluctuation of the condensate field on the crossover have also been examined [60, 61, 62]. Some exotic phases

other than BCS or BEC phases have been observed when charge neutrality or color neutrality conditions are imposed. These phases have been observed in quark matter [63] as well as polarized Fermi gas of atoms [64, 65]. This kind of stressed pairing implies a mismatch in the chemical potential of the two species of fermions. BCS-BEC crossover with such a mismatch has been studied in a boson-fermion model and a rich phase structure has been observed [59].

We shall study the BCS-BEC crossover with two species of fermions in a relativistic model. We restrict ourself to the pairing between particles and pairing between antiparticles. The variational method with an explicit construction of the ground state will be implemented. The ansatz functions will be determined from the minimization of the thermodynamic potential. The gap equation will also be determined from the minimization of the thermodynamic potential. Then the gap equation and the number density equation will be numerically solved and the thermodynamic stability of different phases at different coupling strength and mismatch in chemical potential will be checked by calculating the free energy and comparing the free energy of different states.

First, we study the BCS-BEC crossover within the mean field approximation with only fermionic degrees of freedom. The condensate field will be treated as a classical auxiliary field. Then we shall extend our model to treat the condensate field as a quantum field and there we shall study the effects of quantum fluctuation of the condensates on the crossover to study this beyond the mean field approximation.

## 2.1 BCS-BEC crossover in mean field approximation

In this section, we shall discuss the BCS-BEC crossover within the mean field approximation. We consider a general relativistic model with two species of fermions of equal mass and different chemical potential. The Lagrangian is given by

$$\mathcal{L} = \bar{\psi}^i (i\gamma^\mu \partial_\mu - m + \mu_i \gamma^0) \psi^i + \mathcal{L}_I \equiv \mathcal{L}_f + \mathcal{L}_I \quad (2.1)$$

where,  $\psi^i$  denotes the Dirac fields, the index  $i = 1, 2$  represents the fermion flavors and  $\mu_i$  denotes the chemical potentials of the two species of fermions.  $\mathcal{L}_f$  represents the free particle term and  $\mathcal{L}_I$  represents the interaction term of the Lagrangian. Here we take  $\mathcal{L}_I$  to be a four-fermion interaction term as

$$\mathcal{L}_I = -G(\bar{\psi}_c^i \gamma^5 \psi^j |\epsilon^{ij}|)(\bar{\psi}^k \gamma^5 \psi_c^l |\epsilon^{kl}|), \quad (2.2)$$

where  $G$  is the coupling constant and  $\psi_c$  is the charge conjugated spinor given by  $\psi_c = C\bar{\psi}^T$ ,  $\bar{\psi}_c = \psi^T C$ , with  $C = i\gamma^2\gamma^0$  being the charge conjugation matrix. The  $|\epsilon^{ij}|$  and  $|\epsilon^{kl}|$  terms ensure cross flavor, spin zero antisymmetric pairing. For mean field calculation we introduce a field  $\Phi$  which is a fermion bilinear. we can rewrite  $\mathcal{L}_I$  in terms of  $\Phi$  as

$$\mathcal{L}_I = g|\epsilon^{ij}| (\bar{\psi}^i \gamma^5 \psi_c^j \Phi + \bar{\psi}_c^i \gamma^5 \psi^j \Phi^*) - m_b^2 \Phi^* \Phi, \quad (2.3)$$

with  $G = g^2/m_b^2$ , which can be treated as a crossover parameter. The field  $\Phi$  here represents an auxiliary field as the Lagrangian does not have any kinetic term for  $\Phi$ . For mean field calculation, we shall consider  $\Phi$  as a classical field and take its expectation value  $\phi_0 = \langle \Phi \rangle$  a constant while retaining the quantum nature for the fermion field. This will enable us to calculate the effective potential as a function of  $\phi_0$ .

### 2.1.1 The ansatz for the ground state

We are now interested in choosing a suitable choice of ground state for the kind of interaction we have considered in Eq.(2.2). Since the dynamics is well understood when there is no interaction, it will be convenient for us to choose a ground state in terms of the free particle vacuum state. To do this, we need the creation and annihilation operator for the free vacuum. So we need the fermion field operator expansion which is given as

$$\psi(\mathbf{x}) = \frac{1}{(2\pi)^{3/2}} \int [U_0(\mathbf{k})q(\mathbf{k}) + V_0(-\mathbf{k})\tilde{q}(-\mathbf{k})] e^{i\mathbf{k}\cdot\mathbf{x}} d\mathbf{k} \quad (2.4)$$

The operators  $q$  and  $\tilde{q}$  are the two component particle annihilation and antiparticle creation operators respectively for the free vacuum  $|0\rangle$ . We can write them in terms of the two component spinors as

$$q(\mathbf{k}) = q_r(\mathbf{k})u_r \quad \text{and} \quad \tilde{q}(\mathbf{k}) = \tilde{q}_s(\mathbf{k})v_s$$

where both  $r$  and  $s$  can take values of  $\frac{1}{2}$  or  $-\frac{1}{2}$ .  $u_r$  and  $v_s$  are the two component spinors given by

$$\begin{aligned} u_{\frac{1}{2}} &= \begin{bmatrix} 1 \\ 0 \end{bmatrix} & \text{and} & u_{-\frac{1}{2}} &= \begin{bmatrix} 0 \\ 1 \end{bmatrix}, \\ v_{\frac{1}{2}} &= \begin{bmatrix} 0 \\ i \end{bmatrix} & \text{and} & v_{-\frac{1}{2}} &= \begin{bmatrix} -i \\ 0 \end{bmatrix}. \end{aligned}$$

Here we have suppressed the flavor indices of the fermion field operators. The fermionic spinors  $U_0(\mathbf{k})$  and  $V_0(-\mathbf{k})$  are given by

$$U_0(\mathbf{k}) = \begin{bmatrix} \cos \frac{\chi^0}{2} \\ \boldsymbol{\sigma} \cdot \hat{\mathbf{k}} \sin \frac{\chi^0}{2} \end{bmatrix} \quad \text{and} \quad V_0(-\mathbf{k}) = \begin{bmatrix} -\boldsymbol{\sigma} \cdot \hat{\mathbf{k}} \sin \frac{\chi^0}{2} \\ \cos \frac{\chi^0}{2} \end{bmatrix}. \quad (2.5)$$

The function  $\chi^0(\mathbf{k})$  in the spinors in Eq.(2.5) are given as  $\cot \chi_i^0 = m_i/|\mathbf{k}|$  for free massive fermion fields,  $i$  being the flavor index. For massless fields  $\chi^0(|\mathbf{k}|) = \pi/2$ . Now we can proceed to construct the ground state in terms of the vacuum state. We take it as a squeezed coherent state given as [66, 67],

$$|\Omega\rangle = \mathcal{U}_d|0\rangle = \exp(B_d^\dagger - B_d)|0\rangle. \quad (2.6)$$

$\mathcal{U}_d$  is a unitary operator which creates or annihilates fermion pairs and antifermion pairs.  $B_d^\dagger$  is the pair creation operator given by,

$$B_d^\dagger = \int [q_r^i(\mathbf{k})^\dagger r f(\mathbf{k}) q_{-r}^j(-\mathbf{k})^\dagger |\epsilon_{ij}|] d\mathbf{k} + \int [\tilde{q}_r^i(\mathbf{k}) r f_1(\mathbf{k}) \tilde{q}_{-r}^j(-\mathbf{k}) |\epsilon_{ij}|] d\mathbf{k}. \quad (2.7)$$

In the above,  $i, j$  are flavor indices, and  $r (= \pm 1/2)$  is the spin index. the

condensate functions for the fermion pairs and the antifermion pairs are represented by  $f(\mathbf{k})$  and  $f_1(\mathbf{k})$  respectively. These ansatz functions will be determined from the extremization of the thermodynamic potential. Since we assume isospin symmetry and we are not taking electric charge into account, we can assume that the condensate functions are independent of the flavor of the fermions. We shall see later that these condensate functions depend upon the average energy and average chemical potential of the fermions or antifermions consisting the condensates.

Now, to proceed further, we need the creation and annihilation operators for both particles and antiparticles for  $|\Omega\rangle$  which can be obtained through a Bogoliubov transformation of the creation and annihilation operators for  $|0\rangle$ ,

$$q_r^{\prime i}(\mathbf{k}) = \mathcal{U}_d q_r^i(\mathbf{k}) \mathcal{U}_d^{-1} \quad \text{and} \quad \tilde{q}_r^{\prime i}(\mathbf{k}) = \mathcal{U}_d \tilde{q}_r^i(\mathbf{k}) \mathcal{U}_d^{-1}, \quad (2.8)$$

where the primed operators correspond to  $|\Omega\rangle$  and the unprimed operators correspond to  $|0\rangle$ . Explicit calculation leads to the following inverse transformation matrices,

$$\begin{aligned} \begin{bmatrix} q_r^i(\mathbf{k}) \\ q_{-r}^{j\dagger}(-\mathbf{k}) \end{bmatrix} &= \begin{bmatrix} \cos f & 2r|\epsilon_{ij}|\sin f \\ -2r|\epsilon_{ij}|\sin f & \cos f \end{bmatrix} \begin{bmatrix} q_r^i(\mathbf{k}) \\ q_{-r}^{j\dagger}(-\mathbf{k}) \end{bmatrix} \\ \begin{bmatrix} \tilde{q}_r^i(\mathbf{k}) \\ \tilde{q}_{-r}^{j\dagger}(-\mathbf{k}) \end{bmatrix} &= \begin{bmatrix} \cos f_1 & 2r|\epsilon_{ij}|\sin f_1 \\ -2r|\epsilon_{ij}|\sin f_1 & \cos f_1 \end{bmatrix} \begin{bmatrix} \tilde{q}_r^i(\mathbf{k}) \\ \tilde{q}_{-r}^{j\dagger}(-\mathbf{k}) \end{bmatrix} \end{aligned} \quad (2.9)$$

The reason behind writing the inverse transformation matrices instead of the direct transformation matrices is that the Lagrangian we are considering is consisted of only the unprimed operators whereas  $|\Omega\rangle$  can identify the primed operators only. Finally, to include the effects of temperature and density we write down the state at finite temperature and density,  $|\Omega(\beta, \mu)\rangle$  taking a thermal Bogoliubov transformation over the state  $|\Omega\rangle$  using thermo field dynamics (TFD) [68]. We can write,

$$|\Omega_{\beta, \mu}\rangle = \mathcal{U}_{\beta, \mu} |\Omega\rangle = e^{\mathcal{B}^\dagger(\beta, \mu) - \mathcal{B}(\beta, \mu)} |\Omega\rangle, \quad (2.10)$$

with

$$\mathcal{B}^\dagger(\beta, \mu) = \int [q'(\mathbf{k})^\dagger \theta_-(\mathbf{k}, \beta, \mu) \underline{q}'(\mathbf{k})^\dagger + \tilde{q}'(\mathbf{k}) \theta_+(\mathbf{k}, \beta, \mu) \underline{\tilde{q}}'(\mathbf{k})] d\mathbf{k} \quad (2.11)$$

In Eq.(2.11), we have suppressed the flavor indices of the fermion operators and the ansatz functions  $\theta(\mathbf{k}, \beta, \mu)$ . The underlined operators in Eq.(2.11) are operators in the extended Hilbert space associated with thermal doubling in TFD method. We shall see later that the ansatz functions  $\theta_\pm(\mathbf{k}, \beta, \mu)$  will be related to the distribution functions for particles and antiparticles. Now we shall calculate the thermodynamic potential for  $|\Omega_{\beta, \mu}\rangle$  and carry out the minimization which will give us the ansatz functions in Eq.(2.10).

## 2.1.2 Evaluation of thermodynamic potential and gap equation

To calculate the thermodynamic potential for the state given in Eq.(2.10), we first write down the expectation values of the following Fermion bilinears.

$$\langle \Omega_{\beta, \mu} | \tilde{\psi}_\gamma^i(\mathbf{k}) \tilde{\psi}_\delta^j(\mathbf{k}')^\dagger | \Omega_{\beta, \mu} \rangle = \delta^{ij} \Lambda_{+\gamma\delta}^i(\mathbf{k}, \beta, \mu) \delta(\mathbf{k} - \mathbf{k}'), \quad (2.12)$$

$$\langle \Omega_{\beta, \mu} | \tilde{\psi}_\delta^{i\dagger}(\mathbf{k}) \tilde{\psi}_\gamma^j(\mathbf{k}') | \Omega_{\beta, \mu} \rangle = \delta^{ij} \Lambda_{-\gamma\delta}^i(\mathbf{k}, \beta, \mu) \delta(\mathbf{k} - \mathbf{k}'), \quad (2.13)$$

where,

$$\begin{aligned} \Lambda_{\pm\gamma\delta}^i(\mathbf{k}, \beta, \mu) &= \frac{1}{2} [1 \pm \{F_1^i(\mathbf{k}) - F^i(\mathbf{k})\} \pm \{\gamma^0 \cos \chi^i(\mathbf{k}) \\ &\quad + \boldsymbol{\alpha} \cdot \hat{\mathbf{k}} \sin \chi^i(\mathbf{k})\} \{1 - F^i(\mathbf{k}) - F_1^i(\mathbf{k})\}]_{\gamma\delta}. \end{aligned} \quad (2.14)$$

In the above,  $\tilde{\psi}(\mathbf{k})$  is the Fourier transform of  $\psi(\mathbf{x})$ . The effect of the fermion condensates and their temperature and density dependences are encoded in the functions  $F^i(\mathbf{k})$  and  $F_1^i(\mathbf{k})$ , respectively given as

$$F^i(\mathbf{k}) = \sin^2 \theta_-^i(\mathbf{k}) + \sin^2 f(\mathbf{k}) \cos 2\theta_-^{i,j}(\mathbf{k}), \quad (2.15)$$

$$F_1^i(\mathbf{k}) = \sin^2 \theta_+^i(\mathbf{k}) + \sin^2 f_1(\mathbf{k}) \cos 2\theta_+^{i,j}(\mathbf{k}), \quad (2.16)$$

where we have defined  $\cos 2\theta_{\pm}^{i,j} = 1 - \sin^2 \theta_{\pm}^i - \sin^2 \theta_{\pm}^j$ , with  $i \neq j$ .

For difermion operators, we have,

$$\langle \Omega_{\beta,\mu} | \psi_{\alpha}^i(\mathbf{x}) \psi_{\gamma}^j(\mathbf{0}) | \Omega_{\beta,\mu} \rangle = -\frac{1}{(2\pi)^3} \int e^{i\mathbf{k}\cdot\mathbf{x}} \mathcal{P}_{+\gamma\alpha}^{i,j}(\mathbf{k}, \beta, \mu) d\mathbf{k} \quad (2.17)$$

$$\langle \Omega_{\beta,\mu} | \psi_{\alpha}^{i\dagger}(\mathbf{x}) \psi_{\gamma}^{j\dagger}(\mathbf{0}) | \Omega_{\beta,\mu} \rangle = -\frac{1}{(2\pi)^3} \int e^{i\mathbf{k}\cdot\mathbf{x}} \mathcal{P}_{-\alpha\gamma}^{i,j}(\mathbf{k}, \beta, \mu) d\mathbf{k}, \quad (2.18)$$

where,

$$\begin{aligned} \mathcal{P}_{+}^{i,j} &= \frac{|\epsilon^{ij}|}{4} \left[ S^{i,j}(\mathbf{k}) \left\{ \cos\left(\frac{\chi_i - \chi_j}{2}\right) - \boldsymbol{\gamma} \cdot \hat{\mathbf{k}} \sin\left(\frac{\chi_i - \chi_j}{2}\right) \right\} \right. \\ &\quad \left. + \left\{ \gamma^0 \cos\left(\frac{\chi_i + \chi_j}{2}\right) - \boldsymbol{\alpha} \cdot \hat{\mathbf{k}} \sin\left(\frac{\chi_i + \chi_j}{2}\right) \right\} A^{i,j}(\mathbf{k}) \right] \gamma_5 C, \end{aligned} \quad (2.19)$$

$$\begin{aligned} \mathcal{P}_{-}^{i,j} &= \frac{|\epsilon^{ij}| C \gamma_5}{4} \left[ S^{i,j}(\mathbf{k}) \left\{ \cos\left(\frac{\chi_i - \chi_j}{2}\right) + \boldsymbol{\gamma} \cdot \hat{\mathbf{k}} \sin\left(\frac{\chi_i - \chi_j}{2}\right) \right\} \right. \\ &\quad \left. + \left\{ \gamma^0 \cos\left(\frac{\chi_i + \chi_j}{2}\right) - \boldsymbol{\alpha} \cdot \hat{\mathbf{k}} \sin\left(\frac{\chi_i + \chi_j}{2}\right) \right\} A^{i,j}(\mathbf{k}) \right]. \end{aligned} \quad (2.20)$$

In Eq.s(2.19,2.20) the functions  $S(\mathbf{k})$  and  $A(\mathbf{k})$  are given as

$$\begin{aligned} S^{i,j}(\mathbf{k}) &= \sin 2f(\mathbf{k}) \cos 2\theta_{-}^{i,j}(\mathbf{k}, \beta, \mu) + \sin 2f_1(\mathbf{k}) \cos 2\theta_{+}^{i,j}(\mathbf{k}, \beta, \mu), \\ A^{i,j}(\mathbf{k}) &= \sin 2f(\mathbf{k}) \cos 2\theta_{-}^{i,j}(\mathbf{k}, \beta, \mu) - \sin 2f_1(\mathbf{k}) \cos 2\theta_{+}^{i,j}(\mathbf{k}, \beta, \mu). \end{aligned}$$

The thermodynamic potential is given by

$$\Omega = \varepsilon - \mu^i \rho^i - \frac{1}{\beta} S, \quad (2.21)$$

where  $\varepsilon$  is the energy density and  $S$  is the entropy density and  $\rho^i = \langle \psi^{i\dagger} \psi^i \rangle$  ( $i = 1, 2$ ) is the number density of  $i$ -th species. It is now straightforward to calculate the expectation value of the Hamiltonian corresponding to the Lagrangian given in Eq.(2.1) as we have all the required expectation values. This can be written as

$$\varepsilon - \mu^i \rho^i = \langle H - \mu^i \psi^{i\dagger} \psi^i \rangle = T + V_D \quad (2.22)$$

Explicitly, the kinetic energy minus the  $\mu^i \rho^i = \mu^i \langle \psi^{i\dagger} \psi^i \rangle$  part is given as

$$\begin{aligned} T &\equiv \langle \Omega_{\beta,\mu} | \psi_i^\dagger (-i\boldsymbol{\alpha} \cdot \nabla + \gamma^0 m - \mu^i) \psi_i | \Omega_{\beta,\mu} \rangle \\ &= \frac{2}{(2\pi)^3} \sum_{i=1}^2 \int d\mathbf{k} \left[ \sqrt{\mathbf{k}^2 + m^2} (F^i + F_1^i) - \mu^i (F^i - F_1^i) \right], \end{aligned} \quad (2.23)$$

where,  $F^i$  and  $F_1^i$  are given by Eq.(2.15,2.16). Here we have subtracted out the vacuum contributions. Similarly, the contribution from the interaction term in Eq.(2.3) to the energy density can be written as

$$V_D = -\langle \Omega_{\beta,\mu} | \mathcal{L}_I | \Omega_{\beta,\mu} \rangle = -4gI_D\phi_0 + m_b^2\phi_0^2, \quad (2.24)$$

where we have taken  $\phi_0$  to be real. In the above,

$$\begin{aligned} I_D &= \frac{1}{2} \langle \bar{\psi}_c^i \gamma^5 | \epsilon^{ij} | \psi^j \rangle = \frac{1}{(2\pi)^3} \int d\mathbf{k} \left[ \sin 2f(\mathbf{k})(1 - \sin^2 \theta_-^1 - \sin^2 \theta_-^2) \right. \\ &\quad \left. + \sin 2f_1(\mathbf{k})(1 - \sin^2 \theta_+^1 - \sin^2 \theta_+^2) \right], \end{aligned} \quad (2.25)$$

which is proportional to the fermion condensate. Finally, to calculate the thermodynamic potential we have to include the entropy density for the fermions. This is given as [68],

$$\begin{aligned} S &= -\frac{2}{(2\pi)^3} \sum_i \int d\mathbf{k} \left[ \sin^2 \theta_-^i \ln \sin^2 \theta_-^i + \cos^2 \theta_-^i \ln \cos^2 \theta_-^i \right. \\ &\quad \left. + \sin^2 \theta_+^i \ln \sin^2 \theta_+^i + \cos^2 \theta_+^i \ln \cos^2 \theta_+^i \right]. \end{aligned} \quad (2.26)$$

The extremization of the thermodynamic potential Eq. (2.21) with respect to the condensate functions  $f(\mathbf{k})$  and  $f_1(\mathbf{k})$  respectively yields

$$\tan 2f(\mathbf{k}) = \frac{2g\phi_0}{\bar{\epsilon} - \bar{\mu}} \equiv \frac{\Delta}{\bar{\epsilon} - \bar{\mu}}, \quad (2.27)$$

$$\tan 2f_1(\mathbf{k}) = \frac{2g\phi_0}{\bar{\epsilon} + \bar{\mu}} \equiv \frac{\Delta}{\bar{\epsilon} + \bar{\mu}}, \quad (2.28)$$

where, we have defined the superconducting gap  $\Delta = 2g\phi_0$ . In the above  $\bar{\epsilon} = (\epsilon_1 + \epsilon_2)/2$  and  $\bar{\mu} = (\mu_1 + \mu_2)/2$  with  $\epsilon_i = \sqrt{\mathbf{k}^2 + m_i^2}$  being the free particle

energy. So we can see the condensate functions depend on the average energy and the average chemical potential of the particles or antiparticles that condense. Finally, the minimization of the thermodynamic potential with respect to the thermal functions  $\theta_{\pm}(\mathbf{k})$  gives

$$\sin^2 \theta_{\pm}^i(\mathbf{k}) = \frac{1}{\exp(\beta\omega_{\pm}^i) + 1}, \quad (2.29)$$

where  $\omega_{\pm}^i$  are the energy dispersion relations for the particles and antiparticles of the two species and are given as

$$\omega_{\pm}^1 = \bar{\omega}_{\pm} + \delta_{\epsilon} \pm \delta_{\mu}, \quad (2.30)$$

$$\omega_{\pm}^2 = \bar{\omega}_{\pm} - \delta_{\epsilon} \mp \delta_{\mu}, \quad (2.31)$$

with  $\bar{\omega}_{\pm} = \sqrt{\Delta^2 + \bar{\xi}_{\pm}^2}$ , where  $\bar{\xi}_{\pm} = (\xi_{1\pm} + \xi_{2\pm})/2$  and  $\xi_{i\pm} = \epsilon_i \pm \mu_i$ . The average chemical potential difference and the average free particle energy difference are respectively given by,  $\delta_{\mu} = (\mu_1 - \mu_2)/2$  and  $\delta_{\epsilon} = (\epsilon_1 - \epsilon_2)/2$ . Since we have assumed equal masses for the two species, we can see from Eq.s(2.30,2.31) that, for  $\delta_{\mu} > 0$ , we may have gapless modes for  $\omega_{-}^1$  or  $\omega_{+}^2$ , which means one or more non zero values of momentum will correspond to zeros of the energy dispersion relation. Using these dispersion relations, condensate functions and distribution functions, the thermodynamic potential given by Eq.(2.21) can be written as

$$\begin{aligned} \Omega = & \frac{2}{(2\pi)^3} \int d\mathbf{k} [2\epsilon - \bar{\omega}_{-} - \bar{\omega}_{+}] - \frac{2}{(2\pi)^3\beta} \sum_i \int d\mathbf{k} \left[ \ln \left\{ 1 + e^{-\beta\omega_{-}^i} \right\} \right. \\ & \left. + \ln \left\{ 1 + e^{-\beta\omega_{+}^i} \right\} \right] + m_b^2 \phi_0^2. \end{aligned} \quad (2.32)$$

Extremization of Eq.(2.32) with respect to  $\phi_0$  leads to the gap equation

$$\frac{m_b^2}{4g^2} = \int \frac{d\mathbf{k}}{(2\pi)^3} \left[ \frac{\cos 2\theta_{-}^{1,2}}{\bar{\omega}_{-}} + \frac{\cos 2\theta_{+}^{1,2}}{\bar{\omega}_{+}} \right], \quad (2.33)$$

The gap equation in Eq.(2.33) is quadratically divergent which is regularized in the NJL model by introducing a momentum cut off  $\Lambda$ . In the non relativistic

case this is rendered finite by subtracting out the vacuum contribution and relating the four fermion coupling to the s-wave scattering length [55, 69]. A similar approach here leads to the regularized gap equation [58],

$$-\frac{m}{4\pi a} = \int \frac{d\mathbf{k}}{(2\pi)^3} \left[ \frac{\cos 2\theta_-^{1,2}}{\bar{\omega}_-} + \frac{\cos 2\theta_+^{1,2}}{\bar{\omega}_+} - \frac{1}{\epsilon - m} - \frac{1}{\epsilon + m} \right]. \quad (2.34)$$

However, after this regularization, unlike the non relativistic case, dependence on ultraviolet cutoff still remains in the above gap equation, although the dependence is milder. The gap equation can also be regularized by defining a renormalized boson mass  $m_{b,r}$  with  $m_{b,r}^2 = \partial\Omega/\partial\phi_0^2|_{\phi_0=T=0,\mu=m}$  which will also result into the same gap equation [59]. In our analysis, we shall treat the renormalized coupling in Eq.(2.34) as the crossover parameter. As a function of this coupling, the gap parameter  $\Delta$  for different densities of the fermions of the two species will be calculated. The average number density is given as

$$\bar{\rho} = \frac{\rho_1 + \rho_2}{2} = \rho_- - \rho_+, \quad (2.35)$$

where, the fermionic and antifermionic components are given as

$$\rho_{\mp} = -\frac{1}{(2\pi)^3} \int \frac{\xi_{\mp}}{\bar{\omega}_{\mp}} \cos 2\theta_{\mp}^{1,2} d\mathbf{k} \quad (2.36)$$

The difference in the number densities is given as

$$\delta_{\rho} = \frac{\rho_1 - \rho_2}{2} = \frac{1}{(2\pi)^3} \int [(\sin^2 \theta_-^1 - \sin^2 \theta_+^1) - (\sin^2 \theta_-^2 - \sin^2 \theta_+^2)] d\mathbf{k} \quad (2.37)$$

Using the gap equation Eq.(2.33), the thermodynamic potential in Eq.(2.32) can be rewritten as

$$\begin{aligned} \Omega(\Delta, \bar{\mu}, \delta_{\mu}, \beta) &= \frac{2}{(2\pi)^3 \beta} \int d\mathbf{k} \left[ \left\{ \bar{\xi}_- - \bar{\omega}_- + \frac{\Delta^2}{2\bar{\omega}_-} + \bar{\xi}_+ - \bar{\omega}_+ + \frac{\Delta^2}{2\bar{\omega}_+} \right\} \right. \\ &\quad \left. - \sum_i \left\{ \ln \left( 1 + e^{-\beta\omega_-^i} \right) + \ln \left( 1 + e^{-\beta\omega_+^i} \right) \right\} \right]. \quad (2.38) \end{aligned}$$

To compare the stability of various phases we compare the thermodynamic

potentials of these phases with respect to that of normal matter. This can be obtained from Eq.(2.38) in the limit of gap  $\Delta \rightarrow 0$ . We consider the difference in the thermodynamic potentials between condensed phase and the normal matter as given by

$$\begin{aligned}
\tilde{\Omega}(\Delta, \bar{\mu}, \delta_\mu, \beta) &= \Omega(\Delta, \bar{\mu}, \delta_\mu, \beta) - \Omega(\Delta = 0, \bar{\mu}, \delta_\mu, \beta) \\
&= \frac{2}{(2\pi)^3} \int \left\{ |\bar{\xi}_-| - \bar{\omega}_- + \frac{\Delta^2}{2\bar{\omega}_-} \cos 2\theta_-^{1,2} \right. \\
&\quad \left. + |\bar{\xi}_+| - \bar{\omega}_+ + \frac{\Delta^2}{2\bar{\omega}_+} \cos 2\theta_+^{1,2} \right\} d\mathbf{k} \\
&\quad - \frac{2}{(2\pi)^3 \beta} \sum_{i=1,2} \int \left[ \ln \left\{ 1 + e^{-\beta\omega_-^i} \right\} + \ln \left\{ 1 + e^{-\beta\omega_+^i} \right\} \right. \\
&\quad \left. - \ln \left\{ 1 + e^{-\beta\omega_{0-}^i} \right\} - \ln \left\{ 1 + e^{-\beta\omega_{0+}^i} \right\} \right] d\mathbf{k} \quad (2.39)
\end{aligned}$$

In the above,  $\omega_{0\mp}^1 = |\bar{\xi}_\mp| \mp \delta_\mu$  and  $\omega_{0\mp}^2 = |\bar{\xi}_\mp| \pm \delta_\mu$ , correspond to the normal matter dispersion relations for the two species. For stability of the condensed phase,  $\tilde{\Omega}$  has to be negative with  $\Delta$  and  $\bar{\mu}$  determined from the gap equation Eq.(2.34) and the number density equation Eq.(2.35). Further, it has to be ensured that the extremized solution corresponds to a minimum and not a maximum. Here, we shall restrict ourselves to the case of zero temperature only but, we shall consider  $\delta_\mu > 0$ . This leads to the possibility of quasi particle energy for species ‘1’,  $\omega_-^1$  or the quasi antiparticle energy for species ‘2’,  $\omega_+^2$  becoming negative. In that case the distribution functions given by Eq.(2.29), become Heaviside  $\Theta$  functions, i.e.  $\sin^2 \theta^a = \Theta(-\omega^a)$ . Further, using the identity  $\lim_{a \rightarrow \infty} \ln(1 + e^{-ax})/a = -x\Theta(-x)$ , in Eq.(2.39), the zero temperature thermodynamic potential can be calculated as

$$\begin{aligned}
\tilde{\Omega}_0(\Delta, \bar{\mu}, \delta_\mu) &= \frac{2}{(2\pi)^3} \int \left\{ |\bar{\xi}_-| - \bar{\omega}_- + \frac{\Delta^2}{2\bar{\omega}_-} + |\bar{\xi}_+| - \bar{\omega}_+ + \frac{\Delta^2}{2\bar{\omega}_+} \right\} d\mathbf{k} \\
&\quad + \frac{2}{(2\pi)^3} \int \left[ \left\{ \omega_-^1 - \frac{\Delta^2}{2\bar{\omega}_-} \right\} \theta(-\omega_-^1) + \left\{ \omega_+^2 - \frac{\Delta^2}{2\bar{\omega}_+} \right\} \theta(-\omega_+^2) \right. \\
&\quad \left. - \omega_{0-}^1 \theta(-\omega_{0-}^1) - \omega_{0+}^2 \theta(-\omega_{0+}^2) \right] d\mathbf{k} \quad (2.40)
\end{aligned}$$

The Eq.(2.34) and Eq.(2.35) need to be solved self consistently to determine

the gap as a function of the coupling. BEC is usually discussed using the canonical ensemble where the particle number density is fixed. BCS-BEC crossover with fixed number density has been discussed in the relativistic regime [59, 60]. However, we might note that, to discuss quark matter, usually grand canonical ensemble with a fixed quark chemical potential is employed to explore the QCD phase diagram in the chemical potential and temperature plane. In the numerical analysis, we keep the average number density fixed and consider the solutions as a function of the coupling and the difference in chemical potentials. Sometimes we find multiple solutions for the gap and average chemical potential satisfying Eq.s(2.34,2.35), which correspond to multiple extrema of the thermodynamic potential. In such cases, the solution with least thermodynamic potential is chosen. The positivity of the second derivative of the thermodynamic potential is checked in such cases. Next we discuss the detailed numerical calculations for the present investigation.

### 2.1.3 Numerical analysis and the phase structure

For convenience in numerical analysis, we introduce dimensionless quantities in terms of Fermi momentum  $k_f$  or Fermi energy  $\epsilon_f = \sqrt{k_f^2 + m^2}$ , defined as  $|\mathbf{k}| = k_f x$ ,  $\eta = 1/(k_f a)$ ,  $m = k_f \hat{m}$ ,  $\Delta = \epsilon_f z$ ,  $\mu = \epsilon_f \hat{\mu}$ . Then the gap equation in Eq.(2.34) can be written in terms of these dimensionless variables at zero temperature as

$$-\frac{\eta}{2} = \int_0^{x_{max}} \frac{dx x^2}{\hat{m}\pi} \left[ \frac{1}{\hat{\omega}_-} + \frac{1}{\hat{\omega}_+} - \frac{2\epsilon(x)}{x^2} - \frac{1}{\hat{\omega}_-^1} \Theta(-\hat{\omega}_-^1) - \frac{1}{\hat{\omega}_-^2} \Theta(-\hat{\omega}_-^2) \right]. \quad (2.41)$$

Similarly, the equation for the average number density in Eq.(2.35) can be rewritten in terms of these dimensionless variables as

$$1 = 1.5 \int_0^{x_{max}} dx x^2 \left[ \frac{\hat{\xi}_+(x)}{\hat{\omega}_+(x)} \{1 - \Theta(-\hat{\omega}_+^2)\} - \frac{\hat{\xi}_-(x)}{\hat{\omega}_-(x)} \{1 - \Theta(-\hat{\omega}_-^1)\} \right]. \quad (2.42)$$

Here,  $\hat{\omega}_\pm = \sqrt{\hat{\xi}_\pm^2 + z^2(1 + \hat{m}^2)}$  and  $\hat{\xi}_\pm(x) = \hat{\epsilon}(x) \pm \bar{\mu} \sqrt{1 + \hat{m}^2}$  with  $\hat{\epsilon}(x) = \sqrt{x^2 + \hat{m}^2}$ . The upper cut-off for momentum in units of Fermi momentum  $k_f$

is given by  $x_{max} = \Lambda/k_f$ . Here  $\bar{\mu}$  is the average chemical potentials of the two species in units of Fermi energy. Essentially we have three dimensional quantities here : the cutoff  $\Lambda$ , the mass of the fermion  $m$  and the scattering length  $a$ . The dimensional coupling  $G$  is bounded above with a critical value  $G_c \Lambda^2 > 2\pi^2$ , beyond which the zero density vacuum itself is unstable to form fermion pairs leading to a Majorana mass for the fermions.

To analyze the crossover, let us first consider the symmetric case, i.e,  $\delta_\mu = 0$ . In this limit,  $\Theta(-\omega_-^i)$  become zero in Eq.s(2.41,2.42). At zero density, the minimum excitation energy for the fermion is its mass  $m$ . For normal matter with finite chemical potential it is  $(m - \mu)$ . In the BEC state, the decay mode is the bound state going to two fermions. So the threshold energy for this is  $2(m - \mu)$ . The BEC state should therefore be stable if this threshold energy is positive, implying  $m > \mu$ . This we shall take as our working definition for distinguishing BEC phase from BEC phase as we increase the coupling parameter  $\eta$  from weak coupling BCS (large negative  $\eta$ ) to strong coupling BEC phase (large positive  $\eta$ ) through unitary regime ( $\eta=0$ ).

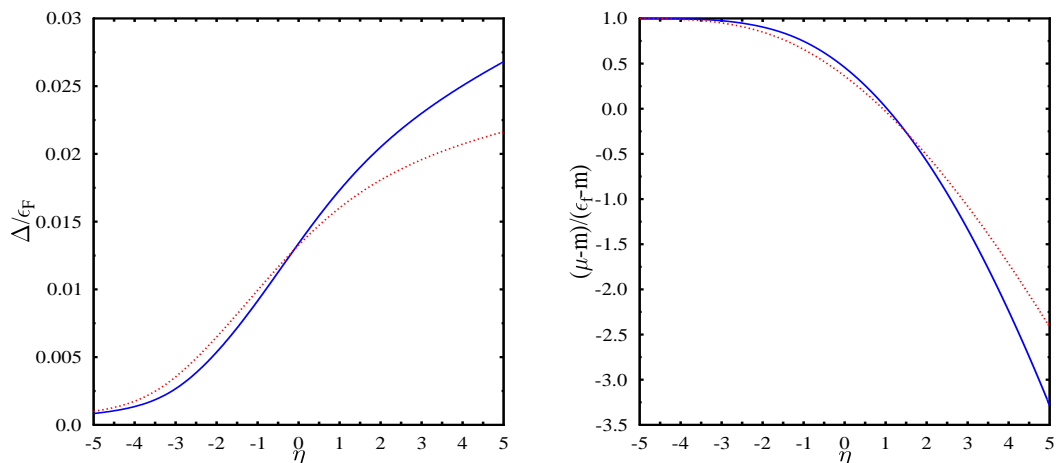


Figure 2.1: Gap parameter (left panel) and the scaled chemical potential  $(\mu - m)/(\epsilon_f - m)$  (right panel) in units of Fermi energy as a function of the coupling. The dotted line corresponds to the case where antiparticle contributions are not included and the solid line corresponds to inclusion of the antiparticle contributions.

To test the non relativistic limit of our calculations we choose the parameters  $x_{max} = \Lambda/k_f = 50$  and  $\hat{m} = m/k_f = 5$ . The resulting gap and chemical

potential are shown in Fig.[2.1]. To show the contribution from antiparticles we have plotted the results obtained by solving Eq.s(2.41,2.42), with and without the antiparticle contributions.

We might naively expect that the antiparticle channel is suppressed in the non relativistic limit. But Fig.[2.1] shows that, while such an expectation might be satisfied to a reasonable extent for weak coupling BCS regime, the antiparticle contributions become increasingly important as the coupling increases. As the coupling increases, the chemical potential  $\tilde{\mu} = \mu - m$  decreases and changes sign at coupling  $\eta \approx 1.04$  signaling the BEC regime.

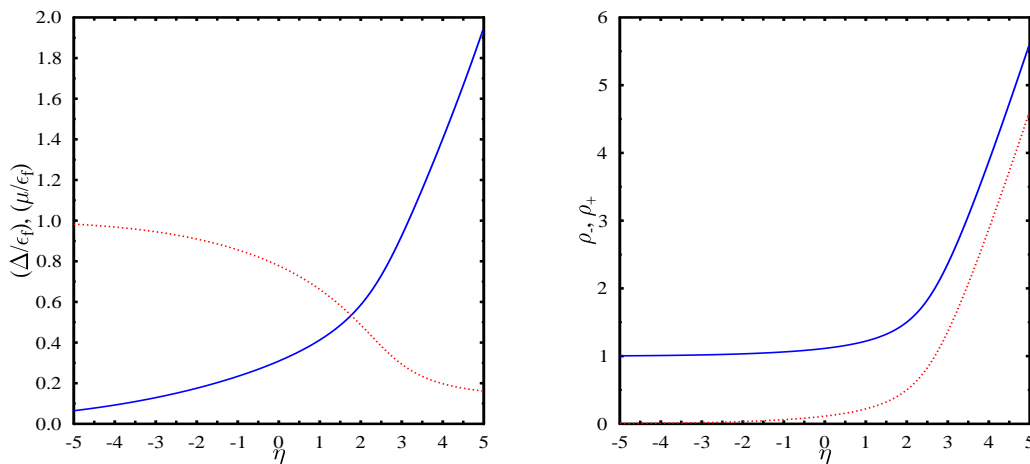


Figure 2.2: (Left panel) Superfluid gap (solid line) and chemical potential (dotted line) in units of Fermi energy as functions of the coupling. (Right panel) Number densities of particles,  $\rho_-$  (solid line) and antiparticles,  $\rho_+$  (dotted line) in units of  $k_f^3/3\pi^2$  as functions of the coupling.

To investigate the relativistic effects we choose  $m/k_f = 0.67$  and  $\Lambda/k_f = 3.3$  [59] and the resulting gap and the chemical potential are shown in the left panel of Fig.[2.2]. In the weak coupling BCS limit, the chemical potential is given by the Fermi energy. But it decreases with increasing coupling and becomes negligible as compared to the Fermi energy in deep BEC regime. The gap is negligible as compared to the Fermi energy in the weak coupling regime as expected from BCS theory and rises monotonically as the coupling increases. At  $\eta = 0$ , the gap and the chemical potential turn out to be  $\Delta = 0.3\epsilon_f$  and  $\mu = 0.78\epsilon_f$  respectively in our analysis whereas  $\mu = 0.37\epsilon_f$  at  $\eta = 0$  in Ref.[59]. This discrepancy arises from the different regularization of the

gap equation. To compare with the non relativistic systems, we consider the ratio  $\tilde{\mu}/\tilde{\epsilon}_f = (\mu - m)/(\epsilon - m)$ . In our model,  $\tilde{\mu}/\tilde{\epsilon}_f \approx 0.5$  at  $\eta = 0$ . In the non relativistic fermionic models this value is about 0.4 to 0.5 [64, 70]. As  $\eta$  increases, at about  $\eta = 1.68$ , the chemical potential becomes smaller than the mass of the fermion and the system enters the BEC regime.

As the coupling approaches the unitary regime, the antiparticle contributions become important. In the right panel of Fig.[2.2], the number densities of the particles,  $\rho_-$  and the antiparticles  $\rho_+$  as defined in Eq.(2.36), are shown. The particle number density remains almost constant in the BEC regime and starts increasing monotonically from near the unitary regime. In the weak coupling BCS regime the antiparticle contribution to the number density is almost zero but near the unitary regime it starts increasing and as the coupling increases, the antiparticle contribution becomes larger and larger. At very large values of  $\eta$ , the chemical potential becomes negligible, signaling very little preference of particles over antiparticles. The difference in the contributions from particles and antiparticles produces a conserved net density [58].

Now, we consider the case of superfluidity with a mismatch in the chemical potentials, i.e.  $\delta_\mu \neq 0$ . Here, we keep the average density fixed and calculate the average chemical potential and the superfluid gap using Eq.(2.35) and Eq.(2.34) respectively. In this case, sometimes we get multiple solutions of the gap and number density equations near the transition region. As mentioned earlier, we choose the solution with the least thermodynamic potential in such instances.

Without loss of generality, we take  $\delta_\mu > 0$ . It is possible then that the quasi particle energy for species ‘1’,  $\omega_-^1(\mathbf{k}) = \bar{\omega}_-(\mathbf{k}) - \delta_\mu$ , and the quasi antiparticle energy for species ‘2’,  $\bar{\omega}_+^2(\mathbf{k}) = \bar{\omega}_+(\mathbf{k}) - \delta_\mu$ , may become negative. The contributions of the  $\Theta$  functions in Eq.s(2.41,2.42) will be non vanishing at zero temperature in that case. The  $\Theta$  functions will limit the range of the momentum integrations.  $\omega_-^1$ , vanishes at momenta  $\mathbf{k}_{min/max}^2 = (\bar{\mu} \pm \sqrt{\delta_\mu^2 - \Delta^2})^2 - m^2$  and  $\omega_+^2$  vanishes at momenta  $\mathbf{k}_{min/max}^2 = (-\bar{\mu} \pm \sqrt{\delta_\mu^2 - \Delta^2})^2 - m^2$ . These momenta are imaginary if  $\delta_\mu$  is smaller than the gap  $\Delta$ . But for  $\delta_\mu > \Delta$ , the

zeros of the dispersion relations correspond to real effective Fermi surfaces. In general there can be two such Fermi surfaces for species ‘1’ and one for species ‘2’ along with the gapped ones. So we can have the interesting possibility of interior gap solutions, which means the existence of one effective Fermi surface, for both species [59]. When there exist two effective Fermi surfaces, the corresponding phase is called the breached pairing phase. Here, it is possible for quasi particle of species ‘1’ to have breached pairing solutions but it is not a possibility for species ‘2’ since there can be only one effective Fermi surface.

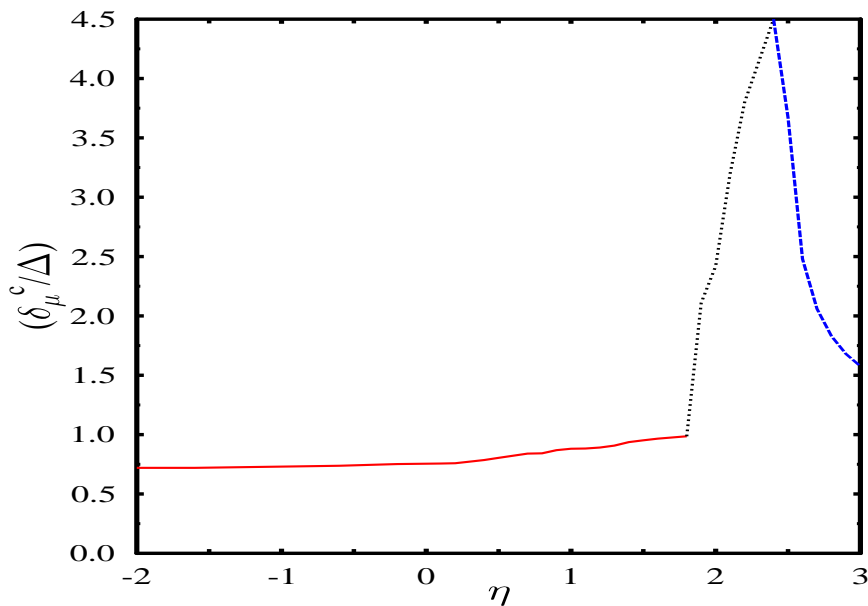


Figure 2.3: *Ratio of critical chemical potential difference to the gap as a function of the coupling strength  $\eta$ . Gapless phase appear for  $\eta > 1.9$ . Solid line denotes absence of gapless modes. The dotted line corresponds to gapless modes for quasi particles of species ‘1’ and the dashed line indicates the regime where quasi antiparticles of species ‘2’ also become gapless.*

In Fig.[2.3], we have shown  $\delta_\mu^c/\Delta$ , the ratio of maximum chemical potential difference to the superfluid gap, that can sustain pairing, as a function of  $\eta$ . Here, we have taken the parameters  $\Lambda/k_f = 3.3$  and  $m/k_f = 0.67$  which is same as that corresponding to Fig.[2.2]. For weak coupling BCS limit, the ratio approaches the Clogston-Chandrasekhar limit,  $\delta_\mu^c/\Delta \simeq 0.72$ . As the coupling increases,  $\delta_\mu^c/\Delta$  increases slowly as shown by the solid line in Fig.[2.3]. There is no gapless mode upto  $\eta \simeq 1.9$ . So we can see that BCS phase does not correspond to any gapless mode as we have seen in the left panel of Fig.[2.2],

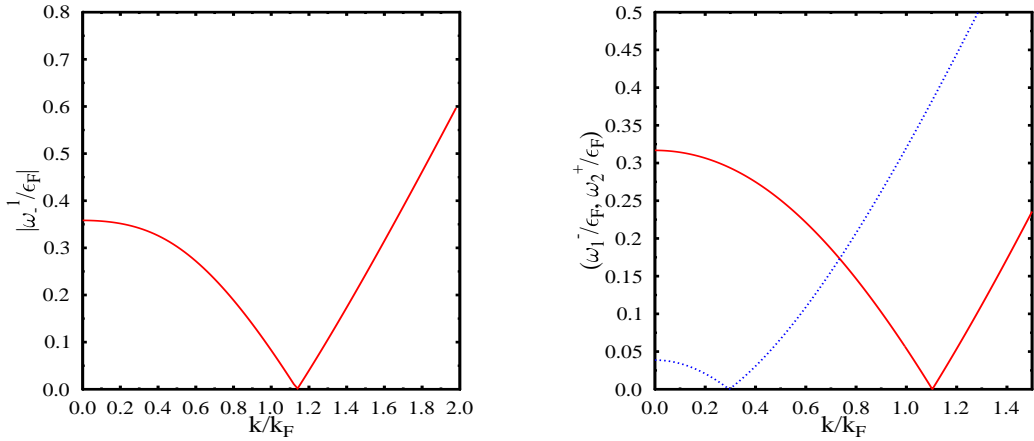


Figure 2.4: (Left panel) Quasi particle dispersion relation for species ‘1’ for  $\eta = 2.1$  and  $\delta_\mu/\Delta_0 = 1.125$ ,  $\Delta_0$  being the gap at  $\delta_\mu = 0$ . (Right panel) Dispersion relations for quasi particle of species ‘1’ (solid line) and for quasi antiparticle of species ‘2’ (dotted line) for  $\eta = 3$  and  $\delta_\mu/\Delta_0 = 1.195$ .

that the crossover from BCS phase to BEC phase occurs at  $\eta = 1.68$ . From,  $\eta \simeq 1.9$ ,  $\delta_\mu^c/\Delta$  increases sharply until  $\eta \simeq 2.38$  as  $\omega_-^1$  corresponds to one gapless mode in this regime while all other modes are gapped. This phase is shown by the dotted line in Fig.[2.3]. The energy dispersion relation corresponding to the gapless mode,  $\omega_-^1(\mathbf{k})$  in this region is shown in the left panel of Fig.[2.4] for  $\eta = 2.1$  and  $\delta_\mu/\Delta_0 = 1.125$ . Here  $\Delta_0$  is the gap at  $\delta_\mu = 0$  and turns out to be  $\Delta_0 = 0.637\epsilon_f$ . The average chemical potential turns out to be  $\bar{\mu} = 0.47\epsilon_f$  and the gap is  $\Delta = 0.35\epsilon_f$  corresponding to the left panel of Fig.[2.4].

Beyond  $\eta \simeq 2.38$ ,  $\omega_+^2$  also corresponds to one gapless mode along with  $\omega_-^1$ . The dashed line in Fig.[2.3] represents this regime. In the right panel of Fig.[2.4], we show the dispersion relations for these gapless modes for  $\eta = 3$  and  $\delta_\mu/\Delta_0 = 1.195$ . The gap and the average chemical potential are  $\Delta = 0.72\epsilon_f$  and  $\bar{\mu} = 0.23\epsilon_f$  respectively corresponding to the right panel of Fig.[2.4].

$(\bar{\mu} - m) < 0$  for all the gapless phases shown in Fig.[2.3]. Which implies the stability criteria for BEC is satisfied in the gapless phases. We have not observed any breached pairing phenomena for any value of the coupling  $\eta$ .

The density difference between the two species is non zero for the gapless phases which can be realized from Eq.(2.37). In left panel of Fig.[2.5], the dependence of the gap on the density difference,  $\delta_\rho$  is shown for cou-

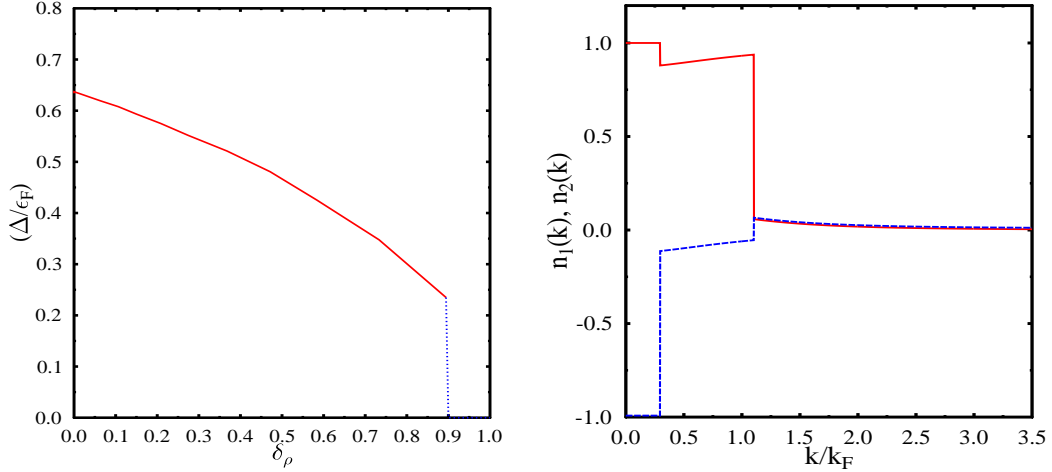


Figure 2.5: (Left panel) Superfluid gap as a function of difference in number densities of the condensing species. This is plotted for  $\eta = 2.1$ . (Right panel) Number density distribution for the two species. Solid line corresponds to species ‘1’ and the dashed line corresponds to species ‘2’. This plot corresponds to  $\eta = 3$  and  $\delta_\mu/\Delta_0 = 1.195$ .

pling  $\eta = 2.1$ . Superfluidity is supported for a maximum density difference of  $\delta_\rho \simeq 0.9(k_f^3/3\pi^2)$  beyond which the system goes over to unpaired matter phase with zero gap. For coupling  $\eta < 1.9$ , we do not find any superfluid phase energetically favorable with any non zero value of density difference  $\delta_\rho$ .

Next, we consider the number density distribution of the two species in the momentum space when gapless modes exist. The number densities at zero temperature for the two species are given by

$$\begin{aligned} \rho_1 &= \frac{2}{(2\pi)^3} \int d\mathbf{k} [\sin^2 f(\mathbf{k}) + \Theta(-\omega_-^1) \cos^2 f(\mathbf{k}) - \sin^2 f_1(\mathbf{k}) \{1 - \theta(-\omega_+^2)\}] \\ &= \frac{2}{(2\pi)^3} \int d\mathbf{k} n_1(\mathbf{k}), \end{aligned} \quad (2.43)$$

$$\begin{aligned} \rho_2 &= \frac{2}{(2\pi)^3} \int d\mathbf{k} [\sin^2 f(\mathbf{k}) \{1 - \Theta(-\omega_-^1)\} - \sin^2 f_1(\mathbf{k}) + \cos^2 f_1(\mathbf{k}) \theta(-\omega_+^2)] \\ &= \frac{2}{(2\pi)^3} \int d\mathbf{k} n_2(\mathbf{k}). \end{aligned} \quad (2.44)$$

In the right panel of Fig.[2.5], we have shown the momentum space density distributions  $n_1(\mathbf{k})$  and  $n_2(\mathbf{k})$  for  $\eta = 3$  and  $\delta_\mu/\Delta_0 = 1.195$ . In this case both  $\omega_-^1$  and  $\omega_+^2$  can become gapless. In the region where both  $\omega_-^1$  and  $\omega_+^2$  are negative,  $n_1(k) = 1$  and  $n_2(k) = -1$  from Eq.(2.43,2.44). In the region, where

only  $\omega_-^1$  is negative,  $n_1(k) = (1 + \bar{\xi}_+/\bar{\omega}_+)/2$  and  $n_2(k) = -(1 + \bar{\xi}_+/\bar{\omega}_+)/2$ . Finally, when both  $\omega_-^1$  and  $\omega_+^2$  are positive, both  $n_1(k)$  and  $n_2(\mathbf{k})$  are identical and are given by the relativistic BCS distribution function  $n(\mathbf{k}) = (\bar{\xi}_+/\bar{\omega}_+ - \bar{\xi}_-/\bar{\omega}_-)$ . This behavior is depicted the right panel of Fig.[2.5]. Although the individual distribution functions in the momentum space for the two species can be negative, the average occupation number densities  $\bar{n}(\mathbf{k}) = [n_1(\mathbf{k}) + n_2(\mathbf{k})]/2$  as well as the difference in occupation number densities  $\delta_n(\mathbf{k}) = [n_1(\mathbf{k}) - n_2(\mathbf{k})]/2$  are always positive definite.

The phase structure obtained in this section with a four-fermion interaction is similar to the mean field results obtained in a boson-fermion model [59]. It is nice to see the similarity to the mean field results of Ref.[59] which in our investigation arises with a simple ansatz for the ground state given by Eq.(2.10) determined through an extremization of  $\Omega$ . As emphasized in the beginning of Sec.[2.1], the scalar condensate field was considered as a classical auxiliary field. In the following section we shall treat them as dynamical fields and generalize the ansatz of Eq.(2.10) to include the quanta of this field along with those of the fermions. We shall illustrate this for the symmetric case, i.e, when there is no mismatch in chemical potential for the two species of fermions.

## 2.2 BCS-BEC crossover with condensate fluctuations

In this section, we shall treat the condensate field introduced in Eq.(2.3) as a dynamical field rather than as an auxiliary field as considered in the previous section. Here, we generalize the BCS ansatz to include quanta of the scalar field. We shall see that this modified ansatz for the ground state leads to a mass gap equation for the scalar field and the corresponding thermodynamic potential can be obtained by resummation of bubble diagrams of perturbation theory similar to the Cornwall-Jackiw-Tomboulis (CJT) composite operator formalism [71]. Treating the condensate field  $\Phi$  as a dynamical field, we can

write the Lagrangian as

$$\mathcal{L} = \mathcal{L}_f + \mathcal{L}_b + \mathcal{L}_{bf} \quad (2.45)$$

where,

$$\begin{aligned} \mathcal{L}_f &= \bar{\psi}^i (i\gamma^\mu \partial_\mu - m + \mu\gamma^0) \psi^i \\ \mathcal{L}_b &= (\partial_0 - i\mu_B)\Phi^\dagger (\partial_0 + i\mu_B)\Phi - m_b^2 \Phi^\dagger \Phi - (\nabla\Phi^\dagger)(\nabla\Phi) - \lambda(\Phi^\dagger\Phi)^2 \\ \mathcal{L}_{bf} &= g|\epsilon^{ij}| (\bar{\psi}^i \gamma^5 \psi_c^j \Phi + \bar{\psi}_c^i \gamma^5 \psi^j \Phi^*). \end{aligned} \quad (2.46)$$

We shall illustrate the effect of the dynamical bosonic field on the BCS-BEC crossover physics and will consider the case where there is no mismatch in the chemical potentials of the two condensing fermionic species with a common chemical potential  $\mu$ . For the dynamical bosonic field we have introduced the chemical potential  $\mu_B$  which is twice the fermionic chemical potential  $\mu$  in equilibrium.  $\mathcal{L}_B$  has a quartic term in the scalar field which, as we shall see later, leads to non perturbative corrections to the thermodynamic potential. In absence of the kinetic term and quartic interaction term of  $\Phi$ , this Lagrangian reduces to the one considered in section [2.1].

We consider a state such that  $\langle\Phi\rangle = \phi_0 = \langle\Phi^\dagger\rangle$  and investigate the fluctuations of the condensate field by defining the quantum fields  $\Phi' = \Phi - \phi_0$ , and  $\Phi'^\dagger = \Phi^\dagger - \phi_0$ . If we neglect odd powers in  $\Phi'$ s  $\mathcal{L}_b$  then reduces to

$$\begin{aligned} \mathcal{L}_b &\simeq (\partial_0 - i\mu_B)\Phi'^\dagger (\partial_0 + i\mu_B)\Phi' - m_b^2 \Phi'^\dagger \Phi' - (\nabla\Phi'^\dagger)(\nabla\Phi') \\ &\quad - \lambda(\Phi'^\dagger\Phi')^2 - 4\lambda\phi_0^2(\Phi'^\dagger\Phi') - V_0(\phi_0), \end{aligned} \quad (2.47)$$

where  $V_0(\phi_0)$  is the tree level potential given as

$$V_0(\phi_0) = (m_b^2 - \mu_B^2)\phi_0^2 + \lambda\phi_0^4 \quad (2.48)$$

The corresponding Hamiltonian density can be written as

$$\mathcal{H} = \mathcal{H}_f + \mathcal{H}_b + \mathcal{H}_{bf} \quad (2.49)$$

with

$$\begin{aligned}
\mathcal{H}_f &= \sum_i \psi_i^\dagger (-i\alpha \cdot \nabla + \beta m) \psi_i \\
\mathcal{H}_b &= \Pi_{\Phi'^\dagger} \Pi_{\Phi'} + i\mu_b (\Pi_{\Phi'} \Phi' - \Pi_{\Phi'^\dagger} \Phi'^\dagger) + \Phi'^\dagger (-\nabla^2 + m_b^2) \Phi' \\
&\quad + \lambda (\Phi'^\dagger \Phi')^2 + 4\lambda \phi_0^2 (\Phi'^\dagger \Phi') + V_0(\phi_0) \\
\mathcal{H}_{bf} &= -\mathcal{L}_{bf} = -g |\epsilon^{ij}| (\bar{\psi}^i \gamma^5 \psi_c^j \Phi + \bar{\psi}_c^i \gamma^5 \psi^j \Phi^*)
\end{aligned} \tag{2.50}$$

Here,  $\Pi_{\Phi'}$  ( $\Pi_{\Phi'^\dagger}$ ) is the conjugate momentum of the field  $\Phi'$  ( $\Phi'^\dagger$ ).

### 2.2.1 The new improved ground state

To construct the ground state for the Lagrangian in Eq.(2.45), we write down the field operator expansions of the boson field  $\Phi'$  ( $\Phi'^\dagger$ ) and the conjugate momentum  $\Pi_{\Phi'}$  ( $\Pi_{\Phi'^\dagger}$ ) in terms of the creation and annihilation operators,

$$\Phi'(\mathbf{x}, t=0) = \frac{1}{(2\pi)^{3/2}} \int d\mathbf{k} \frac{1}{\sqrt{2\omega(k)}} \{a(\mathbf{k}) + b^\dagger(-\mathbf{k})\} e^{i\mathbf{k}\cdot\mathbf{x}} \tag{2.51}$$

$$\Pi_{\Phi'}(\mathbf{x}, t=0) = \frac{i}{(2\pi)^{3/2}} \int d\mathbf{k} \sqrt{\frac{\omega(k)}{2}} \{-b(\mathbf{k}) + a^\dagger(-\mathbf{k})\} e^{i\mathbf{k}\cdot\mathbf{x}} \tag{2.52}$$

The above expansion for  $\Pi_{\Phi'}$  satisfying the quantum algebra  $[\Phi'(\mathbf{x}), \Pi_{\Phi'}(\mathbf{y})] = i\delta(\mathbf{x} - \mathbf{y})$  leads to the usual commutation relations  $[a(\mathbf{k}), a^\dagger(\mathbf{k}')] = \delta(\mathbf{k} - \mathbf{k}') = [b(\mathbf{k}), b^\dagger(\mathbf{k}')]$ , for bosons for any arbitrary function  $\omega(\mathbf{k})$ .

With the operators for the scalar fields defined, we now generalize the ground state  $|\Omega_{\beta,\mu}\rangle$ , given in Eq.(2.10), to include the effects of boson field and write down the new ansatz  $|\Omega_{\beta,\mu}^B\rangle$  as

$$|\Omega_{\beta,\mu}^B\rangle = \mathcal{U}_{\beta,\mu}^B U^B |\Omega_{\beta,\mu}\rangle. \tag{2.53}$$

Here, similar to Eq.s(2.7,2.11) the operator  $U^B$  and  $\mathcal{U}_{\beta,\mu}^B$  are given as

$$U^B = \exp \left[ \int d\mathbf{k} g(\mathbf{k}) a^\dagger(\mathbf{k}) b^\dagger(-\mathbf{k}) - h.c. \right], \tag{2.54}$$

$$\mathcal{U}_{\beta,\mu}^B = \exp \left[ \int d\mathbf{k} \{ a^\dagger(\mathbf{k}) \underline{a}(-\mathbf{k}) \theta_a(\mathbf{k}) + b^\dagger(\mathbf{k}) \underline{b}(-\mathbf{k}) \theta_b(\mathbf{k}) \} - h.c. \right]. \tag{2.55}$$

Here,  $g(\mathbf{k})$  is the condensate function and  $\theta_{a,b}(\mathbf{k}) = \theta_{a,b}(\mathbf{k}, \beta, \mu)$  is the thermal ansatz function corresponding to bosonic degrees of freedom. Similar to the fermionic case, here also we shall see later that this thermal function is related to the bosonic distribution functions.

## 2.2.2 Thermodynamic potential and gap equation

To calculate the thermodynamic potential for the state  $|\Omega_{\beta,\mu}^B\rangle$ , we require the following expectation value,

$$\begin{aligned} \langle \Omega_{\beta,\mu}^B | \Phi'(\mathbf{x}) \Phi'(\mathbf{y}) | \Omega_{\beta,\mu}^B \rangle &= \frac{1}{(2\pi)^3} \int \frac{d\mathbf{k}}{2\omega(\mathbf{k})} e^{i\mathbf{k}\cdot(\mathbf{x}-\mathbf{y})} [\{\cosh 2g(\mathbf{k}) \\ &+ \sinh 2g(\mathbf{k})\} (\cos h^2\theta^a + \sin h^2\theta^b)] \\ &\equiv I(\mathbf{x} - \mathbf{y}, \beta). \end{aligned} \quad (2.56)$$

Now we can proceed to calculate the thermodynamic potential which, for the boson fermion system can be written as

$$\Omega_{tot} = \Omega + \Omega_B = \Omega + \epsilon_B - \mu_B \rho_B - \frac{1}{\beta} S_B. \quad (2.57)$$

Here, the fermionic contribution  $\Omega$  has already been evaluated in Eq.(2.21). The contribution of the first two terms of  $\Omega_B$  is the expectation value of the Hamiltonian in Eq.(2.49) with respect to the state in Eq.(2.53). The bosonic entropy density  $S_B$  is given similar to their fermionic counterpart in Eq.(2.26), as [68],

$$S_B = \frac{1}{(2\pi)^3} \sum_i \int d\mathbf{k} [\cosh^2 \theta_a \ln \cosh^2 \theta_a - \sinh^2 \theta_a \ln \sinh^2 \theta_a + a \rightarrow b]. \quad (2.58)$$

Minimization of  $\Omega_{tot}$  with respect to the fermionic functions  $f(\mathbf{k})$ ,  $f_1(\mathbf{k})$  and  $\theta_{\mp}^i(\mathbf{k})$  leads to the same solutions for them as given in subsection [2.1.2]. Minimization with respect to the bosonic function  $g(\mathbf{k})$  leads to

$$\tanh 2g(k) = \frac{\omega^2 - \mathbf{k}^2 - M^2}{\omega^2 - \mathbf{k}^2 + M^2}, \quad (2.59)$$

with the quantity  $M^2$  satisfying the temperature dependent mass gap equation given as

$$\begin{aligned} M^2 &= m^2 + 4\lambda\phi_0^2 + \frac{4\lambda}{(2\pi)^3} \int \frac{d\mathbf{k}}{2\sqrt{\mathbf{k}^2 + M^2}} (\cosh^2 \theta_a + \sinh^2 \theta_b) \\ &= m^2 + 4\lambda(\phi_0^2 + I(\beta)). \end{aligned} \quad (2.60)$$

Here,  $I(\beta) = I(\mathbf{0}, \beta)$ , as given in Eq.(2.56). Minimization of  $\Omega_{tot}$  with respect to the bosonic thermal functions yields the distribution function for respectively the bosonic particles and the bosonic antiparticles.

$$\sinh^2 \theta_a = \frac{1}{\exp(E_B - \mu_B) - 1} \equiv n_B^a(\mathbf{k}), \quad (2.61)$$

$$\sinh^2 \theta_b = \frac{1}{\exp(E_B + \mu_B) - 1} \equiv n_B^b(\mathbf{k}). \quad (2.62)$$

Here  $E_B = \sqrt{\mathbf{k}^2 + M^2}$ , with the temperature dependent mass  $M$  satisfying the self consistent mass gap equation in Eq.(2.60).

With all the ansatz functions in Eq.(2.53) determined, we can now write the thermodynamic potential in a more elaborated form. For our convenience, we choose to split it into fermionic and bosonic parts using Eq.(2.32,2.57),

$$\Omega_{tot} = \Omega_f + \Omega_B, \quad (2.63)$$

where, the fermionic part of the thermodynamic potential is given by

$$\begin{aligned} \Omega_f &= \frac{2}{(2\pi)^3} \int [2\epsilon - \bar{\omega}_- - \bar{\omega}_+] d\mathbf{k} \\ &- \frac{2}{(2\pi)^3 \beta} \sum_i \int d\mathbf{k} \left[ \ln\{1 + e^{-\beta\omega_-^i}\} + \ln\{1 + e^{-\beta\omega_+^i}\} \right]. \end{aligned} \quad (2.64)$$

the only difference of Eq.(2.64) from Eq.(2.32) is the mass term  $m_b^2\phi_0^2$  which is absorbed in the bosonic part  $\Omega_B$  in Eq.(2.63).  $\Omega_B$  can be written as

$$\Omega_B = \int \frac{d\mathbf{k}}{(2\pi)^3} \left[ \sqrt{\mathbf{k}^2 + M^2} + \frac{1}{\beta} \sum_{i=1}^2 \ln\{1 - e^{E_i}\} \right] - 2\lambda I^2(\beta) + V_0, \quad (2.65)$$

where  $V_0$  is the tree level potential given in Eq.(2.48). The summation is over the bosons and antibosons with  $E_1 = E_B - \mu_B$  and  $E_2 = E_B + \mu_B$ . Finally, the minimization of  $\Omega_{tot}$  with respect to  $\phi_0$  leads to the superfluid gap equation,

$$M^2 - \mu_B^2 = 2\lambda\phi_0^2 + 4g^2 \int \frac{d\mathbf{k}}{(2\pi)^3} \left[ \frac{\cos 2\theta_-^{1,2}}{\bar{\omega}_-} + \frac{\cos 2\theta_+^{1,2}}{\bar{\omega}_+} \right], \quad (2.66)$$

with, the mass  $M$  satisfying the mass gap equation Eq.(2.60) and  $\cos 2\theta_{\mp}^{1,2} = 1 - \sin^2 \theta_{\mp}^1(\mathbf{k}) - \sin^2 \theta_{\mp}^2(\mathbf{k})$  with  $\sin^2 \theta_{\pm}^i(\mathbf{k})$  being the thermal distribution functions for the fermions defined in Eq.(2.29). This is the parallel of Eq.(2.33) where the condensate field was considered as an auxiliary field.

However the bosonic part of the thermodynamic potential,  $\Omega_B$ , given in Eq.(2.65) is affected by two types of divergences, one arising from the divergent integrals as vacuum terms ( $\phi_0 = 0$  at  $T = 0, \mu = 0$ ), and the other arising from the logarithmic divergence in the mass parameter  $M^2$ , given in the mass gap equation Eq.(2.60). This can be taken care of by defining the renormalized quartic coupling and the renormalized boson mass as [71],

$$\frac{1}{\lambda_R} = \frac{1}{\lambda} + 4I_2(\Lambda, \mu_{sc}) \quad (2.67)$$

$$\frac{m_R^2}{\lambda_R} = \frac{m_b^2}{\lambda} + 4I_1(\Lambda) \quad (2.68)$$

where,  $I_1$  and  $I_2$  are divergent integrals which are rendered finite by introducing a three momentum cutoff  $|\mathbf{k}| < \Lambda$ ,

$$I_1 = \frac{1}{(2\pi)^3} \int \frac{d\mathbf{k}}{2|\mathbf{k}|} = \lim_{\Lambda \rightarrow \infty} \frac{\Lambda^2}{8\pi^2}, \quad (2.69)$$

$$I_2 = \frac{1}{(2\pi)^3} \int \frac{d\mathbf{k}}{2\mu_{sc}^2} \left[ \frac{1}{|\mathbf{k}|} - \frac{1}{\sqrt{\mu_{sc}^2 + \mathbf{k}^2}} \right] = \frac{1}{16\pi^2} \left[ \ln \frac{4\Lambda^2}{\mu_{sc}^2} - 1 \right], \quad (2.70)$$

where,  $\mu_{sc}$  is the renormalization scale and  $\Lambda$  is the three momentum cutoff. We can see from Eq.(2.67), that the difference between the bare and the renormalized quartic coupling is given by

$$\lambda - \lambda_R = \frac{4\lambda_R I_2(\Lambda, \mu_{sc})}{1 - 4\lambda_R I_2(\Lambda, \mu_{sc})} \lambda_R. \quad (2.71)$$

In terms of the renormalization parameters, the mass gap equation can be written as

$$M^2 = m_R^2 + 4\lambda_R\{\phi_0^2 + I_f(\beta)\}, \quad (2.72)$$

with  $I_f(\beta)$  given as

$$I_f(\beta) = \frac{M^2}{16\pi^2} \left[ \ln \frac{M^2}{\mu_{sc}^2} + 1 \right] + \int \frac{d\mathbf{k}}{(2\pi)^3} \frac{1}{2E} \{n_B(\mathbf{k}) + n_{\bar{B}}(\mathbf{k})\}. \quad (2.73)$$

Now, since the mass parameter  $M^2$  is renormalized, the bosonic part of the effective potential,  $\Omega_B$ , can be rendered finite by subtracting out the vacuum contribution. We can write the finite  $\Omega_B$  as

$$\Omega_B = V_0 + V_1 + V_2, \quad (2.74)$$

with

$$V_0 = m_R^2\phi_0^2 + \lambda_R\phi_0^4 - \mu_B^2\phi_0^2 + (\lambda_R - \lambda)\phi_0^4, \quad (2.75)$$

$$V_1 = \frac{1}{\beta(2\pi)^3} \int d\mathbf{k} \sum_{i=1}^2 \ln\{1 - e^{E_i}\} + \frac{M^4}{32\pi^2} \ln \frac{M^2}{\mu_{sc}^2}, \quad (2.76)$$

$$V_2 = -2\lambda_R I_f(\beta)^2. \quad (2.77)$$

However, the cut off dependence is still there in the last term of Eq.(2.75) which vanishes in the limit  $\Lambda \rightarrow \infty$ . In the present calculations, however, we keep the cut off finite. Still we can take care of the cut off dependence by choosing  $4\lambda_R I_2 \ll 1$ . We can see from Eq.(2.71), that this choice would make the contribution of the last term in Eq.(2.75) negligible.

Due to the presence of dynamical condensate fields having a chemical potential twice as that of the fermions, the number density equation described in Eq.(2.35) gets modified,

$$\bar{\rho} = 8\mu\phi_0^2 + \int \frac{d\mathbf{k}}{(2\pi)^3} \left[ 2\{n_B^a(\mathbf{k}) - n_B^b(\mathbf{k})\} + \frac{\xi_+}{\bar{\omega}_+} \cos 2\theta_+^{1,2} - \frac{\xi_-}{\bar{\omega}_-} \cos 2\theta_-^{1,2} \right]. \quad (2.78)$$

To discuss the crossover, we define the mass parameter  $m_1$  as [59],

$$m_1^2 = m_R^2 - 4g^2 \int \frac{d\mathbf{k}}{(2\pi)^3} \frac{2}{\sqrt{\mathbf{k}^2 + m^2}}, \quad (2.79)$$

and define the crossover parameter as

$$x = -\frac{m_1^2 - \mu_B^2}{4g^2}. \quad (2.80)$$

The gap equation in Eq.(2.66) can be written as

$$\begin{aligned} m_1^2 - \mu_B^2 &= 4g^2 \int \frac{d\mathbf{k}}{(2\pi)^3} \left[ \frac{\cos 2\theta_-^{1,2}}{\bar{\omega}_-} + \frac{\cos 2\theta_+^{1,2}}{\bar{\omega}_+} - \frac{2}{\sqrt{\mathbf{k}^2 + m^2}} \right] \\ &+ 2(\lambda - \lambda_R)\phi_0^2 - 2\lambda_R\phi_0^2 - 4\lambda_R I_f(\beta). \end{aligned} \quad (2.81)$$

The contributions from bosonic fluctuations comes into the gap equation through  $I_f(\beta)$  which is given in Eq.(2.73). Now, since we have the gap equation and the number density equation, we are in a position to analyze the crossover by solving them numerically. Next, we shall discuss this numerical analysis.

### 2.2.3 Numerical analysis of the crossover

For numerical analysis, we solve the number density equation, Eq.(2.78), and the gap equation, Eq.(2.81), for chemical potential and superfluid gap for a given value of the renormalized boson mass,  $m_R$ . At each stage of evaluation, the boson mass parameter  $M^2$  is calculated self consistently solving Eq.(2.72). This way we obtain the superfluid gap and the chemical potential for a given value of  $m_R$  or equivalently, for a given value of the crossover parameter  $x$  obtained through Eq.s(2.79,2.80). These values are then used to calculate the thermodynamical potential. Throughout our analysis we have chosen  $g = 2\sqrt{2}$  and the cut off scale  $\mu_{sc}^2 = m_R^2$ .

In the left panel of Fig.[2.6], we show the gap and chemical potential as a function of the dimensionless order parameter  $x/x_0$  with  $x_0 = \Lambda^2/(4\pi^2)$  for three values of the quartic coupling  $\lambda_R=0, 0.5$  and  $2.0$  at zero temperature.

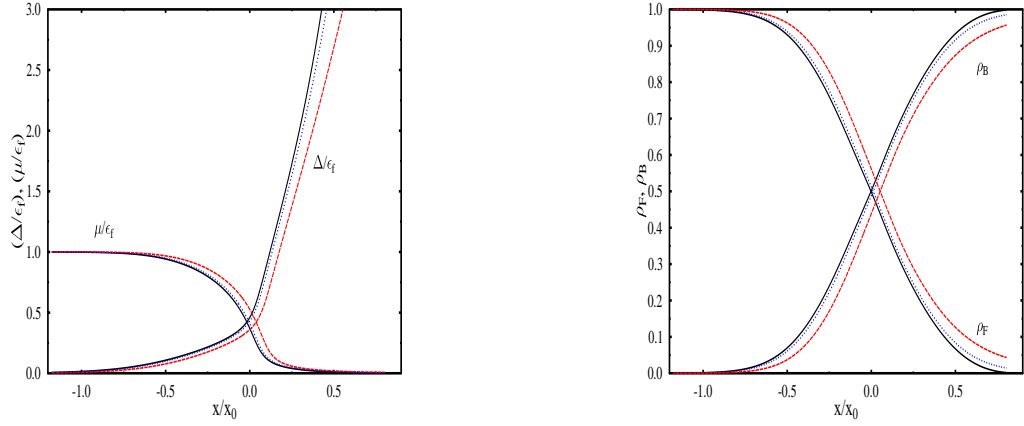


Figure 2.6: (Left panel) Fermion chemical potential and gap in units of Fermi energy as functions of the crossover parameter. (Right panel) Number densities of fermions and bosons in units of total number density as functions of the crossover parameter. In both the plots, The solid (black), dotted (blue) and dashed (red) curves correspond to  $\lambda_R=0, 0.5$  and  $2$  respectively.

$\lambda = 0$  corresponds to the mean field results. Effects of the bosonic fluctuations are almost negligible in the BCS regime ( $x/x_0 < 0$ ) as well as near the unitary regime ( $x/x_0 \sim 0$ ). However, these effects manifest a small reduction of the superfluid gap at large positive values of  $x/x_0$  and a small increase of chemical potential near the unitary regime from their corresponding mean field values. Magnitudes of these changes increase with the quartic coupling,  $\lambda_R$ . This can be understood from Eq.(2.81), which implies an increase in  $\mu_B$  with increasing  $\lambda_R$  for a given value of the gap. This leads to an increase in the corresponding value of the crossover parameter  $x$  as it can be seen from Eq.(2.80). However, the chemical potential approaches zero in the deep BEC regime for any values of  $\lambda_R$ , similar to the mean field case. These effects of fluctuations are reflected in the number densities of the fermions and bosons also, which are shown in the right panel of Fig.[2.6].

The behavior of critical temperature,  $T_C$  and the chemical potential at  $T = T_C$  as a function of the crossover parameter is shown in the left panel of Fig.[2.7]. These results are obtained by setting  $\Delta = 0 = \phi_0$  in all the equations to be solved. The chemical potential behaves in a qualitatively similar manner to the  $T = 0$  case and  $T_C$  behaves similar to the gap at  $T = 0$  with the crossover parameter. The correction to the critical temperature is significant

in the BEC regime only and increases with  $\lambda_R$ . Here also, the reduction of  $T_C$  is due to the increase in chemical potential due to thermal and vacuum fluctuations which can be realized from Eq.(2.81).

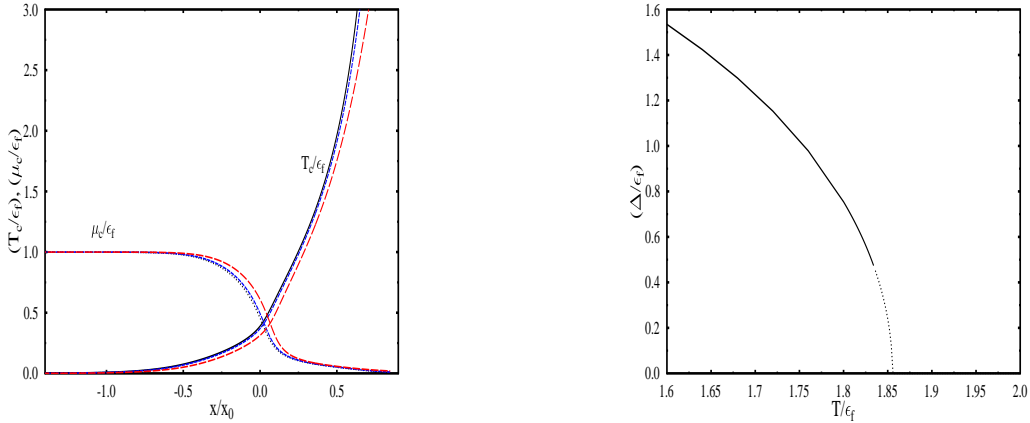


Figure 2.7: (Left panel) Critical temperature  $T_c$  and the chemical potential at  $T = T_c$  in units of Fermi energy as a function of the crossover parameter. The solid (black), dotted (blue) and dashed (red) curves correspond to  $\lambda_R = 0, 0.5$  and  $2$  respectively. (Right panel) Superfluid gap as a function of temperature for quartic coupling  $\lambda_R = 5$ . The dotted line corresponds to unstable solutions with higher thermodynamic potential as compared to  $\Delta = 0$ .

We have also studied the effect of thermal fluctuations of the condensate field for different values of  $\lambda_R$ . As  $\lambda_R$  is increased, we observed that the order parameter  $\Delta$  changes discontinuously at  $T_C$ . A typical behavior is shown in the right panel of Fig.[2.7] where we have taken  $\lambda_R = 5$ . Near  $T_C$  there are solutions with finite  $\Delta$  but larger thermodynamic potential as compared to the solution with  $\Delta = 0$ . These unstable solutions are indicated by the dotted line in the right panel of Fig.[2.7]. This suggests a first order phase transition when the effect of thermal fluctuations becomes large. However it is difficult to draw conclusions from extrapolation for such a large value of  $\lambda_R$ , because, although the result here is non perturbative, it is limited by the ansatz for the ground state in Eq.(2.53). In this context we might remark here that the gauge field fluctuations in color superconductors change the superconducting phase transition to a first order transition [72]. Similar observations were also made in a boson-fermion model where the fluctuations were treated within a CJT formalism [61].

## 2.3 Summary

We have considered here a variational approach to discuss the BCS-BEC crossover in a system with two species of relativistic fermions with a mismatch in their Fermi momenta. An explicit construct for the ground state is considered to describe the difermion condensates. The ansatz functions are determined by minimizing the thermodynamic potential.

In section[2.1], the BCS-BEC crossover is described within the mean field approximation by considering the condensate field to be a classical auxiliary field. We constructed the ground state in terms of particle-particle and antiparticle-antiparticle pairs corresponding to a crossed flavor four fermion interaction term. Using the thermofield dynamics, we extended our ground state to include the effect of temperature. Minimizing  $\Omega$  with respect to the thermal function gives us the distribution functions and the gap equation is obtained by minimizing  $\Omega$  with respect to the expectation value of the condensate field.

The quadratically divergent gap equation is made logarithmically divergent by subtracting out the vacuum contribution and by relating the four fermion coupling to the s-wave scattering length [55, 58, 69]. Unlike the usual non relativistic case, the antiparticle degrees of freedom become important even for the case  $k_f/m \ll 1$ , particularly for large values of  $\eta \equiv 1/k_f a$ .

We have not observed any gapless modes in the BCS regime when the Fermi momenta of the two species are different. Breached pairing solutions with two Fermi surfaces are also not observed. However, in the BEC region with  $\bar{\mu} < m$ , stable gapless modes are observed. The quasi particle of type ‘1’ becomes gapless for  $\eta > 1.9$  and beyond  $\eta = 2.38$ , quasi antiparticle of type ‘2’ also becomes gapless. In the deep BEC region, the phase transition from gapped phase to gapless phase is a second order phase transition with the order parameter decreasing continuously, while the transition from the gapless phase to the normal matter phase is a first order transition as the difference in the densities of the two condensing species is increased. Such gapless modes is relevant for the transport coefficients of the fermionic system. The phase

structure for this fermionic theory turns out to be similar to that of the boson-fermion model treated within a mean field approximation [59].

We have not calculated here the Meissner masses, or the number susceptibility to discuss the stability of different phases by ruling out regions in the parameter space of gap and chemical potential difference. Instead, we have solved the gap equation and the number density equation self consistently and have compared  $\Omega$ . In certain regions of the chemical potential difference and the coupling, we have multiple solutions for the gap equation. In such cases, we have taken the solution which has the least  $\Omega$ .

We have also considered the effects of quantum fluctuations by treating the condensate field as a dynamical bosonic field in a model with quartic self interactions of the boson field. The BCS ansatz was modified to include the quanta of the fluctuating field along with the usual fermion pairs. In the evaluation of the superconducting gap the scalar field mass gap was also calculated self consistently. This leads to a decrease of the critical temperature in the BEC regime. We also observed that the superfluid transition can be first order for larger quartic coupling with the effect of the condensate fluctuations becoming larger. The present ansatz for the ground state leads to the result arising from a summation of an infinite series of bubble diagrams for the scalar field. However, this does not include the effect of 'sunset' type diagram. Inclusion of such diagrams has been successfully done recently within a CJT formulation [61].

The results obtained here are of course limited by the choice of the ansatz. Here, we have not considered other non uniform ansatz leading to the FFLO phase [64, 65, 73]. Nevertheless, the results obtained here might be regarded as a reference solution with which other numerical or analytical results obtained from more involved ansatz for the ground state may be compared.

## Chapter 3

# Chiral symmetry breaking in a magnetic background

This chapter is devoted to the discussion on the effects of strong magnetic fields on chiral symmetry breaking (CSB) in the context of hot and dense quark matter. The importance of this study lies in the fact that the natural sources where we can find quark matter or the laboratory experiments where we can produce quark matter are usually associated with very strong magnetic fields and recent calculations, both analytic and lattice simulations, indicate that the QCD phase diagram gets significantly affected by strong magnetic fields [74, 75]. Studies on effects of magnetic fields on chiral symmetry breaking (CSB) also suggest that strong magnetic fields act as catalyzer of CSB [25, 26, 27].

The strength of the magnetic fields is of the order of  $eB \sim 2m_\pi^2$  ( $m_\pi^2 \simeq 10^{18}$  Gauss) at RHIC [11, 12] to  $eB \sim 15m_\pi^2$  at LHC [12]. Study of CSB in presence of a strong magnetic field has led to one interesting finding, known as the chiral magnetic effect (CME), in the context of heavy ion collision experiments [29]. There an electric current is generated along the magnetic field axis if the densities of left and right handed quarks are not equal. The phase structure of dense matter in presence of magnetic field along with a non zero chiral density has been investigated for two flavor Polyakov loop extended NJL (PNJL) model for high temperatures relevant for RHIC and LHC [76].

Neutron stars usually posses magnetic fields of the order of  $10^{13}$  Gauss at

the surface of ordinary pulsars [9] to  $10^{16}$  Gauss at the pole of magnetars [10]. Physical upper limit on the magnetic field in a gravitationally bound star is  $10^{18}$  Gauss that is obtained by using virial theorem [9]. This limit can be higher for self bound objects like quark stars [77]. Since the magnetic field strengths are of the order of QCD scale, this can affect both the thermodynamics and hydrodynamics [78]. The effects of magnetic fields on the equation of state for cold dense matter have also been studied using NJL model for both two and three flavors [79].

Here, we shall consider 3-flavor NJL model with a KMT determinant interaction term. First, the Dirac spinors in presence of magnetic field will be derived and then, we shall consider explicit variational construct for the ground state in terms of quark-antiquark pairs. The ansatz functions will be determined from the minimization of the thermodynamic potential and we shall obtain the mass gap equation in the similar manner. The gap equation will be solved at different chemical potential and temperature for various strengths of the magnetic field. The thermodynamic stability of different phases will be checked by comparing the free energy.

### 3.1 Dirac spinors in a magnetic field

We consider a constant magnetic field  $\mathbf{B}$  in the  $z$ - direction. We choose the gauge such that the electromagnetic vector potential is given as  $A_\mu(\mathbf{x}) = (0, 0, Bx, 0)$ . The Dirac equation in presence of the uniform magnetic field can be written as

$$i\frac{\partial\psi}{\partial t} = (\boldsymbol{\alpha} \cdot \boldsymbol{\Pi} + \beta m)\psi, \quad (3.1)$$

where,  $\boldsymbol{\Pi} = \mathbf{p} - q\mathbf{A}$  is the kinetic momentum of the particle with electric charge  $q$  in presence of the magnetic field. We choose the stationary solution of Eq.(3.1) for positive energy,  $E$  as

$$U(\mathbf{x}, t) = \begin{bmatrix} \phi(\mathbf{x}) \\ \chi(\mathbf{x}) \end{bmatrix} e^{-iEt}, \quad (3.2)$$

where  $\phi(\mathbf{x})$  and  $\chi(\mathbf{x})$  are the two component spinors. Substitution this in Eq.(3.1) leads to

$$\chi(\mathbf{x}) = \frac{\boldsymbol{\sigma} \cdot \boldsymbol{\Pi}}{E + m} \phi(\mathbf{x}), \quad (3.3)$$

So using Eq.(3.3) and  $(\boldsymbol{\sigma} \cdot \boldsymbol{\Pi})^2 = \boldsymbol{\Pi}^2 - q\boldsymbol{\sigma} \cdot \mathbf{B}$ , Eq.(3.1) and using can be reduced into an equation of  $\phi$ ,

$$(E^2 - m^2)\phi(\mathbf{x}) = [-\nabla^2 + (qBx)^2 - qB(\sigma_3 + 2xp_y)]\phi(\mathbf{x}). \quad (3.4)$$

Noticing that the coordinates  $y$  and  $z$  do not occur explicitly except for in the derivatives, we assume the solution to be of the form

$$\phi(\mathbf{x}) = e^{i(p_y y + p_z z)} f(x) \quad (3.5)$$

where,  $f(x) = f_\alpha u_\alpha$ ,  $\alpha = \pm 1$  for spin up and spin down respectively with

$$u_1 = \begin{bmatrix} 1 \\ 0 \end{bmatrix} \quad \text{and} \quad u_{-1} = \begin{bmatrix} 0 \\ 1 \end{bmatrix},$$

so that  $\sigma_3 f = \alpha f$ . Using Eq.(3.5) in Eq.(3.4) we have,

$$\left[ \frac{\partial^2}{\partial \xi^2} - \xi^2 + a_\alpha \right] f_\alpha(\xi) = 0, \quad (3.6)$$

where, we have introduced the dimensionless variables  $\xi = \sqrt{|q|B}(x - p_y/qB)$  and  $a_\alpha = (E^2 - m^2 - p_z^2 + qB\alpha)/|q|B$ . Eq.(3.6) is a special form of Hermite differential equation, whose solutions exist for  $a_\alpha = 2n + 1$ ,  $n = 0, 1, 2, \dots$ . This condition gives the energy levels,  $E_{n\alpha}^2 = m^2 + p_z^2 + (2n + 1)|q|B - qB\alpha$ . The solution of Eq.(3.6) is

$$f_\alpha(\xi) = c_n e^{-\frac{\xi^2}{2}} H_n(\xi) = I_n(\xi), \quad (3.7)$$

where  $H_n(\xi)$  is the Hermite polynomial of the  $n$ -th order, with the normalization constant  $c_n = (\sqrt{|q|B}/n!2^n\sqrt{\pi})^{1/2}$ . The functions  $I_n(\xi)$ 's satisfy the

following completeness relation and the orthonormality condition respectively

$$\sum_n I_n(\xi) I_n(\xi') = |q|B\delta(\xi - \xi'). \quad (3.8)$$

$$\int d\xi I_n(\xi) I_m(\xi) = \sqrt{|q|B}\delta_{n,m}, \quad (3.9)$$

Using Eq.s(3.5,3.7,3.3), we can write the positive energy spinors as  $U(\mathbf{x}, t) = U(n, \mathbf{p}_x, x) \exp(i\mathbf{p}_x \cdot \mathbf{x}_x - i\epsilon_n t)$  with

$$U_\uparrow(x, \mathbf{p}_x, n) = N_n \begin{bmatrix} (\epsilon_n + m) \{ \Theta(q)I_n + \Theta(-q)I_{n-1} \} \\ 0 \\ p_z \{ \Theta(q)I_n + \Theta(-q)I_{n-1} \} \\ -i\sqrt{2n|q|B} \{ \Theta(q)I_{n-1} + \Theta(-q)I_n \} \end{bmatrix} \quad (3.10a)$$

$$U_\downarrow(x, \mathbf{p}_x, n) = N_n \begin{bmatrix} 0 \\ (\epsilon_n + m) \{ \Theta(q)I_{n-1} + \Theta(-q)I_n \} \\ i\sqrt{2n|q|B} \{ \Theta(q)I_n - \Theta(-q)I_{n-1} \} \\ -p_z \{ \Theta(q)I_n - \Theta(-q)I_{n-1} \} \end{bmatrix}. \quad (3.10b)$$

We have defined the normalization constant as  $N_n = 1/\sqrt{2\epsilon_n(\epsilon_n + m)}$  with,  $\epsilon_n = \sqrt{m^2 + p_z^2 + 2n|q|B} \equiv \sqrt{m^2 + |\mathbf{p}|^2}$  being the Landau levels. We have also defined  $I_{-1} = 0$ .

In an identical manner, we can obtain the solutions for the antiparticles as  $V(\mathbf{x}, t) = V(x, \mathbf{p}_x, n) \exp(-i\mathbf{p}_x \cdot \mathbf{x}_x + i\epsilon_n t)$  with

$$V_\uparrow(x, -\mathbf{p}_x, n) = N_n \begin{bmatrix} \sqrt{2n|q|B} \{ \Theta(q)I_n - \Theta(-q)I_{n-1} \} \\ ip_z \{ \Theta(q)I_{n-1} + \Theta(-q)I_n \} \\ 0 \\ i(\epsilon_n + m) \{ \Theta(q)I_{n-1} + \Theta(-q)I_n \} \end{bmatrix}, \quad (3.11a)$$

$$V_\downarrow(x, -\mathbf{p}_x, n) = N_n \begin{bmatrix} ip_z \{ \Theta(q)I_n + \Theta(-q)I_{n-1} \} \\ \sqrt{2n|q|B} \{ \Theta(q)I_{n-1} - \Theta(-q)I_n \} \\ -i(\epsilon_n + m) \{ \Theta(q)I_n + \Theta(-q)I_{n-1} \} \\ 0 \end{bmatrix}. \quad (3.11b)$$

The spinors are normalized as

$$\int dx U_r(x, \mathbf{p}_x, n)^\dagger U_s(x, \mathbf{p}_x, m) = \delta_{n,m} \delta_{r,s} = \int dx V_r(x, \mathbf{p}_x, n)^\dagger V_s(x, \mathbf{p}_x, m). \quad (3.12)$$

In terms of these normalized spinors, the Dirac field operator expansion for a particle in a magnetic field can be written as [80],

$$\psi(\mathbf{x}) = \sum_{n,r} \frac{1}{2\pi} \int d\mathbf{p}_x \left[ q_r(n, \mathbf{p}_x) U_r(x, \mathbf{p}_x, n) + \tilde{q}_r(n, -\mathbf{p}_x) V_r(x, -\mathbf{p}_x, n) \right] e^{i\mathbf{p}_x \cdot \mathbf{x}_x}. \quad (3.13)$$

The sum over  $n$  in the above expansion runs from 0 to infinity. In the above,  $\mathbf{p}_x \equiv (p_y, p_z)$ , and,  $r = \pm 1$  denotes the up and down spins. We have suppressed the color and flavor indices of the quark field operators. The quark annihilation and antiquark creation operators,  $q_r$  and  $\tilde{q}_r$ , respectively, satisfy the quantum algebra

$$\{q_r(n, \mathbf{p}_x), q_{r'}^\dagger(n', \mathbf{p}'_x)\} = \{\tilde{q}_r(n, \mathbf{p}_x), \tilde{q}_{r'}^\dagger(n', \mathbf{p}'_x)\} = \delta_{rr'} \delta_{nn'} \delta(\mathbf{p}_x - \mathbf{p}'_x). \quad (3.14)$$

## 3.2 Ground state and chiral order parameter

Now, we shall construct a variational ground state in a constant magnetic field. We are in a position to do so because we have obtained the Dirac field operator in terms of the spinors in a magnetic field. To incorporate CSB, we choose the ground state as a squeezed coherent state with quark-antiquarks pairs as [66, 67],

$$|\Omega\rangle = \mathcal{U}_Q |0\rangle. \quad (3.15)$$

Here,  $\mathcal{U}_Q$  is an unitary operator which creates quark-antiquark pairs from the vacuum  $|0\rangle$ . Explicitly, the operator,  $\mathcal{U}_Q$  is given as

$$\mathcal{U}_Q = \exp \left[ \sum_{n=0}^{\infty} \int d\mathbf{p}_x q_r^{i\dagger}(n, \mathbf{p}_x) a_{r,s}^i(n, p_z) f^i(n, \mathbf{p}_x) \tilde{q}_s^i(n, -\mathbf{p}_x) - h.c. \right]. \quad (3.16)$$

In Eq.(3.16), We have retained the flavor index  $i$  for the quark field opera-

tors.  $f^i(n, p_z)$  is a real function describing the quark-antiquark condensates related to the vacuum realignment for chiral symmetry breaking. In the above equation, the spin dependent structure  $a_{r,s}^i$  is given by

$$a_{r,s}^i = \frac{1}{|\mathbf{p}_i|} \left[ -\sqrt{2n|q_i|B}\delta_{r,s} - ip_z\delta_{r,-s} \right], \quad (3.17)$$

with  $|\mathbf{p}_i| = \sqrt{p_z^2 + 2n|q_i|B}$  denoting the magnitude of the three momentum of the quarks (antiquarks) of  $i$ -th flavor with electric charge  $q_i$  ( $-q_i$ ). in presence of magnetic field. It can be shown that,  $aa^\dagger = I$ , where  $I$  is the identity matrix in two dimensions. The ansatz functions  $f_i(n, p_z)$  are determined from the minimization of thermodynamic potential. This particular choice of ground state in Eq.(3.15) is a generalization of the ansatz considered earlier [81], to include the effects of magnetic field. Clearly, a nontrivial  $f_i(n, p_z)$  breaks the chiral symmetry. Summation over three colors is assumed in the exponent of  $\mathcal{U}_Q$  in Eq. (3.16).

The creation and annihilation operators for  $|\Omega\rangle$  can be expressed in terms of the operators in Eq.(3.13) through a Bogoliubov transformation as

$$\begin{bmatrix} q'_r(n, \mathbf{p}_x) \\ \tilde{q}'_s(n, -\mathbf{p}_x) \end{bmatrix} = \begin{bmatrix} \cos |f| & -a_{r,s} \sin |f| \\ a_{s,r}^\dagger \sin |f| & \cos |f| \end{bmatrix} \begin{bmatrix} q_r(n, \mathbf{p}_x) \\ \tilde{q}_s(n, -\mathbf{p}_x) \end{bmatrix} \quad (3.18)$$

The ‘primed’ operators satisfy the same anticommutation relations as the ‘unprimed’ ones as in Eq.(3.14). Using Eq.(3.18), we can expand the quark field operator  $\psi(\mathbf{x})$  in terms of the primed operators,

$$\psi(\mathbf{x}) = \sum_n \sum_r \frac{1}{2\pi} \int d\mathbf{p}_x \left[ q'_r(n, \mathbf{p}_x) U'_r(x, n, \mathbf{p}_x) + \tilde{q}'_r(n, -\mathbf{p}_x) V'_r(x, n, -\mathbf{p}_x) \right] e^{i\mathbf{p}_x \cdot \mathbf{x}}, \quad (3.19)$$

where we have suppressed the flavor and color indices. It is easy to see that the ‘primed’ spinors are given as

$$U'_r(x, n, p_x) = \cos |f| U_r(x, n, p_x) - a_{r,s}^\dagger \sin |f| V_s(x, n, -p_x) \quad (3.20a)$$

$$V'_r(x, n, -p_x) = \cos |f| V_r(x, n, -p_x) + a_{s,r} \sin |f| U_s(x, n, p_x). \quad (3.20b)$$

For positive charges,  $U'_r$ 's can be explicitly written as

$$U'_\uparrow(\mathbf{p}_x, n) = \frac{1}{\sqrt{2\epsilon_n(\epsilon_n + m)}} \begin{bmatrix} a_1 I_n \\ 0 \\ a_2 p_z I_n \\ -ia_2 \sqrt{2n|q|B} I_{n-1} \end{bmatrix}, \quad (3.21a)$$

$$U'_\downarrow(\mathbf{p}_x, n) = \frac{1}{\sqrt{2\epsilon_n(\epsilon_n + m)}} \begin{bmatrix} 0 \\ a_1 I_{n-1} \\ ia_2 \sqrt{2n|q|B} I_n \\ -a_2 p_z I_{n-1} \end{bmatrix}. \quad (3.21b)$$

Similarly,  $V'_r$ 's can be explicitly written for positive charges as

$$V'_\uparrow(-\mathbf{p}_x, n) = \frac{1}{\sqrt{2\epsilon_n(\epsilon_n + m)}} \begin{bmatrix} a_2 \sqrt{2n|q|B} I_n \\ ia_2 p_z I_{n-1} \\ 0 \\ ia_1 I_{n-1} \end{bmatrix} \quad (3.22a)$$

$$V'_\downarrow(-\mathbf{p}_x, n) = \frac{1}{\sqrt{2\epsilon_n(\epsilon_n + m)}} \begin{bmatrix} ia_2 p_z I_n \\ a_2 \sqrt{2n|q|B} I_{n-1} \\ -ia_1 I_n \\ 0 \end{bmatrix}, \quad (3.22b)$$

where the functions,  $a_1$  and  $a_2$ , are given in terms of the condensate function  $f(p_z, n)$  as

$$a_1 = (\epsilon_n + m) \cos |f(n, p_z)| + |\mathbf{p}_i| \sin |f(n, p_z)|, \quad (3.23)$$

$$a_2 = \cos |f(n, p_z)| - \frac{\epsilon_n + m}{|\mathbf{p}_i|} \sin |f(n, p_z)|. \quad (3.24)$$

So through Eq.(3.19), we have defined the quark field operator in terms of operators which induce CSB in presence of magnetic field. Now, to include the effects of temperature and density, we write down the state at finite temperature and density  $|\Omega_{\beta, \mu}\rangle$  through a thermal Bogoliubov transformation over

the state  $|\Omega\rangle$  using the thermofield dynamics (TFD) method as [68],

$$|\Omega_{\beta,\mu}\rangle = \mathcal{U}_{\beta,\mu}|\Omega\rangle = e^{\mathcal{B}^\dagger(\beta,\mu) - \mathcal{B}(\beta,\mu)}|\Omega\rangle \quad (3.25)$$

with

$$\mathcal{B}^\dagger(\beta,\mu) = \sum_{n=0}^{\infty} \int d\mathbf{k}_x \left[ \underline{q}'_r(n, k_z)^\dagger \theta_- \underline{q}'_r(n, k_z)^\dagger + \tilde{q}'_r(n, k_z) \theta_+ \tilde{q}'_r(n, k_z) \right]. \quad (3.26)$$

We have suppressed the color and flavor indices in Eq.(3.26). The underlined operators in Eq.(3.26) are the operators in the extended Hilbert space associated with thermal doubling in TFD method and  $\theta_\pm = \theta_\pm(n, k_z, \beta, \mu)$  are thermal the ansatz functions and, as we shall see, are related to the quark and antiquark distribution functions. The ansatz functions in Eq.(3.25) are obtained by minimizing the thermodynamic potential which we shall carry out in the next section.

Now, to test the reliability of the ansatz, considered in Eq.(3.25), we shall calculate the expectation values of the chiral and axial current densities with respect to  $|\Omega_{\beta,\mu}\rangle$  and check whether they reduce to the already known results in the respective limits. We use the following relation which transforms three dimensional integrals into one dimensional integrals in presence of quantizing magnetic field with discrete Landau levels [82],

$$\int \frac{d\mathbf{p}}{(2\pi)^3} \rightarrow \frac{|qB|}{(2\pi)^2} \sum_{n=0}^{\infty} \alpha_n \int dp_z.$$

For the  $i$ -th flavor, the chiral order parameter, i.e, the expectation value of the chiral current density,  $\langle \Omega_{\beta,\mu} | \bar{\psi}_i \psi_i | \Omega_{\beta,\mu} \rangle \equiv -I_i$  is given as

$$I_i = \sum_{n=0}^{\infty} \frac{N_c |q_i| B \alpha_n}{(2\pi)^2} \int \frac{dp_z}{\epsilon_{ni}} [m_i \cos 2f_i + |\mathbf{p}_i| \sin 2f_i] \cos 2\theta_{\mp}^i, \quad (3.27)$$

where  $\cos 2\theta_{\mp}^i = 1 - \sin^2 \theta_-^i - \sin^2 \theta_+^i$  and  $\alpha_n = (2 - \delta_{n,0})$  is the degeneracy factor of the  $n$ -th Landau level (all levels are doubly degenerate except the lowest Landau level). We shall see later that, the functions  $\sin^2 \theta_{\mp}$  are related

to the distribution functions for the quarks and antiquarks. It is useful to define  $\phi^i = \phi_0^i - 2f_i$  with  $\cos \phi_0^i = m_i/\epsilon_{ni}$  and  $\sin \phi_0^i = |\mathbf{p}_i|/\epsilon_{ni}$  and rewrite the order parameter  $I_i$  as

$$I_i = \sum_{n=0}^{\infty} \frac{N_c |q_i| B \alpha_n}{(2\pi)^2} \int dp_z \cos \phi^i \cos 2\theta_{\mp}^i. \quad (3.28)$$

In the limit of vanishing condensates ( $f_i=0$ ),  $I_i$  in Eq.(3.28) reduces to the expression derived in Ref.[80]. In the absence of the magnetic field at zero temperature and zero density,  $I_i$  becomes

$$\langle \bar{\psi}^i \psi^i \rangle = -I_i = -\frac{6}{(2\pi)^3} \int d\mathbf{p} \cos \phi^i, \quad (3.29)$$

which is the same as derived earlier [67].

Now, let us consider the axial current density. The expectation value of the axial current density is given by

$$\langle j_5^3 \rangle \equiv \langle \bar{\psi}_i^a \gamma^3 \gamma^5 \psi_j^a \rangle = \sum_n \frac{N_c}{(2\pi)^2} \int dp_x (I_n^2 - I_{n-1}^2) (\sin^2 \theta_-^i - \sin^2 \theta_+^i). \quad (3.30)$$

Integrating over  $dp_y$  using the orthonormal condition of Eq.(3.9), all the terms in the above sum for the Landau levels cancel out except for the zeroth level so that,

$$\langle j_5^3 \rangle = \frac{N_c |q_i| B}{(2\pi)^2} \int dp_z [\sin^2 \theta_-^{i0} - \sin^2 \theta_+^{i0}]. \quad (3.31)$$

which is identical to that in Ref.[83] once we identify the functions  $\sin^2 \theta_{\mp}^{i0}$  as the particle and the antiparticle distribution functions for the zero modes (see e.g.Eq.(3.42) in the next section).

So with our ansatz, taking the appropriate limits, we have reproduced the results obtained in previous works. So we can say that our ansatz is valid in the previously tested limits. Now, we can proceed to calculate the thermodynamic potential with a suitable choice of effective model and to determine the mass gap equation from the minimization of the thermodynamic potential.

### 3.3 Thermodynamic potential and gap equation

In the present work, we shall consider 3-flavor NJL model with KMT determinant interaction term. The corresponding Hamiltonian density is given as

$$\begin{aligned} \mathcal{H} = & \psi^\dagger(-i\boldsymbol{\alpha} \cdot \boldsymbol{\nabla} - qBx\alpha_2 + \gamma^0\hat{m})\psi - G_s \sum_{A=0}^8 [(\bar{\psi}\lambda^A\psi)^2 - (\bar{\psi}\gamma^5\lambda^A\psi)^2] \\ & + K [det_f[\bar{\psi}(1 + \gamma_5)\psi] + det_f[\bar{\psi}(1 - \gamma_5)\psi]] \end{aligned} \quad (3.32)$$

Here also, we have suppressed the color and flavor indices. With the color and flavor indices, the field operator is denoted by  $\psi^{i,a}$  with color ‘ $a$ ’ ( $a = r, g, b$ ), and flavor ‘ $i$ ’ ( $i = u, d, s$ ), indices.  $\hat{m} = \text{diag}_f(m_u, m_d, m_s)$  is the current quark mass matrix in the flavor space. We shall assume isospin symmetry for  $u$  and  $d$  quarks. This is an approximate symmetry because, when the electromagnetic effects are taken into account, the current quark masses of  $u$  and  $d$  quarks will not be the same due to the difference in their electrical charge. However, because of the smallness of the electromagnetic coupling, we shall ignore this tiny effect and continue with  $m_u = m_d$  in the present investigation of CSB. In Eq.(3.32),  $\lambda^A$ ,  $A = 1, \dots, 8$  denotes the Gell-Mann matrices acting in the flavor space and  $\lambda^0 = \sqrt{\frac{2}{3}} \mathbb{1}_f$  with  $\mathbb{1}_f$  being the unit matrix in the flavor space. The four point interaction term  $\sim G_s$  is symmetric in  $SU(3)_V \times SU(3)_A \times U(1)_V \times U(1)_A$ . In contrast, the determinant term  $\sim K$  which generates a six point interaction term for 3 flavors, breaks  $U(1)_A$  symmetry. In the absence of the magnetic field and the mass term, the overall symmetry in the flavor space is  $SU(3)_V \times SU(3)_A \times U(1)_V$ . This spontaneously breaks to  $SU(3)_V \times U(1)_V$  implying conservation of the baryon number and the flavor number. The current quark mass term introduces additional explicit breaking of chiral symmetry leading to partial conservation of the axial current. On the other hand, due to the presence of magnetic field, the  $SU(3)_V$  symmetry in flavor space reduces to  $SU(2)_V \times SU(2)_A$  since the  $u$  quark has different electric charge compared to  $d$  and  $s$  quarks [84].

Now, the thermodynamic potential is given by,

$$\Omega = \varepsilon - \sum_{i=1}^3 \mu_i \rho_i - \frac{S}{\beta} = T + V_S + V_D - \sum_{i=1}^3 \mu_i \rho_i - \frac{S}{\beta}, \quad (3.33)$$

where  $\varepsilon = T + V_S + V_D$  is the expectation value of the Hamiltonian given in Eq.(3.32) with  $T$  being the expectation value of the kinetic term,  $V_s$  being the expectation value of the four point interaction term  $G_S$  and  $V_D$  being the expectation value of the six point interaction term  $\sim K$ .  $\mu_i$  and  $\rho_i$  are respectively the chemical potential and number density for the  $i$ -th flavor.  $S$  denotes the entropy density.

Evaluation of the kinetic term requires the spatial derivatives of the function  $I_n(\xi)$  which, from Eq.(3.7), can be written as

$$\frac{\partial I_n}{\partial x} = \sqrt{|q_i|B} \left[ -\xi I_n + \sqrt{2n} I_{n-1} \right]. \quad (3.34)$$

Using Eq.(3.34) and the field operator described in Eq.(3.19), a straightforward calculation gives the expectation value of the kinetic term as

$$\begin{aligned} T &= \langle \Omega_{\beta,\mu} | \psi_i^{\alpha\dagger} (-i\boldsymbol{\alpha} \cdot \boldsymbol{\nabla} - q_i B x \alpha_2) \psi_i^a | \Omega_{\beta,\mu} \rangle \\ &= - \sum_{n=0}^{\infty} \sum_i \frac{N_c \alpha_n |q_i B|}{(2\pi)^2} \int dp_z (m_i \cos \phi_i + |\mathbf{p}_i| \sin \phi_i) \cos 2\theta_{\mp}^i. \end{aligned} \quad (3.35)$$

Using Eq.(3.27) and the properties of the Gell-Mann matrices,  $\sum_{A=0}^8 \lambda_{ij}^A \lambda_{kl}^A = 2\delta_{il}\delta_{jk}$ , the contribution from the quartic interaction term in Eq.(3.32) to the energy expectation value turns out to be

$$V_S \equiv -G_s \langle \Omega_{\beta,\mu} | \sum_{A=0}^8 [(\bar{\psi} \lambda^A \psi)^2 - (\bar{\psi} \gamma^5 \lambda^A \psi)^2] | \Omega_{\beta,\mu} \rangle = -2G_s \sum_{i=1,3} I^{i^2}. \quad (3.36)$$

Finally, the expectation value of the six quark interaction term is given as

$$V_D = K \langle \det_f [\bar{\psi}(1 + \gamma_5)\psi] + \det_f [\bar{\psi}(1 - \gamma_5)\psi] \rangle = -2K I_1 I_2 I_3. \quad (3.37)$$

So we have the expectation value of the Hamiltonian given in Eq.(3.32). Now,

The number density of the  $i$ -th flavor is given by

$$\rho_i = \langle \psi_i^\dagger \psi_i \rangle = \sum_{n=0}^{\infty} \frac{N_c \alpha_n |q_i B|}{(2\pi)^2} \int dp_z [\sin^2 \theta_-^i - \sin^2 \theta_+^i]. \quad (3.38)$$

Finally, the entropy density for the quarks is given as

$$S = - \sum_{i,n} \frac{N_c \alpha_n |q_i B|}{(2\pi)^2} \int dp_z \{ (\sin^2 \theta_-^i \ln \sin^2 \theta_-^i + \cos^2 \theta_-^i \ln \cos^2 \theta_-^i) + (- \rightarrow +) \}. \quad (3.39)$$

Now, as we have the expressions for all the terms of the thermodynamic potential  $\Omega$  given in Eq.(3.33), we can carry out the minimization of  $\Omega$ . Minimization of  $\Omega$  with respect to the chiral condensate function  $\phi_i(p_z)$  gives

$$\cot \phi_i = \frac{m_i + 4G_s I_i + 2K |\epsilon_{ijk}| I_j I_k}{|\mathbf{p}_i|} = \frac{M_i}{|\mathbf{p}_i|}, \quad (3.40)$$

where we have defined  $M_i$  as the constituent quark mass for the  $i$ -th flavor as

$$M_i = m_i + 4G_s I_i + 2K |\epsilon_{ijk}| I_j I_k. \quad (3.41)$$

Minimisation of  $\Omega$  with respect to the thermal functions  $\theta_{\pm}(\mathbf{k})$  leads to the distribution functions of the quarks,

$$\sin^2 \theta_{\pm}^{i,n} = \frac{1}{e^{\beta(\omega_{i,n} \pm \mu_i)} + 1}, \quad (3.42)$$

where,  $\omega_{i,n} = \sqrt{M_i^2 + p_z^2 + 2n|q_i|B}$  is the excitation energy of the  $i$ -th flavor with constituent quark mass  $M_i$ .

Substituting the solution for the condensate function in Eq.(3.40) and the thermal function in Eq.(3.42) back in Eq.(3.28) yields the chiral condensate as

$$-\langle \bar{\psi}_i \psi_i \rangle \equiv I_i = \sum_{n=0}^{\infty} \frac{N_c |q_i| B \alpha_n}{(2\pi)^2} \int dp_z \frac{M_i}{\omega_i} (1 - \sin^2 \theta_-^i - \sin^2 \theta_+^i). \quad (3.43)$$

Eq.s(3.41,3.43) describe the self consistent mass gap equation for the  $i$ -th quark flavor. Using the solutions for the condensate functions in Eq.s(3.40,3.42)

and the chiral condensate in Eq.(3.43), the thermodynamic potential given in Eq.(3.33) reduces to

$$\begin{aligned} \Omega = & - \sum_{n,i} \frac{N_c \alpha_n |q_i B|}{(2\pi)^2} \int dp_z \omega_i + 2G_s \sum_i I_i^2 + 4K I_1 I_2 I_3 \\ & - \sum_{n,i} \frac{N_c \alpha_n |q_i B|}{(2\pi)^2 \beta} \int dp_z [\ln \sin^2 \theta_-^i + \ln \sin^2 \theta_+^i]. \end{aligned} \quad (3.44)$$

In the limit,  $T = \mu = 0$ , the first term of  $\Omega$  in Eq.(3.44) suffers from ultraviolet divergence which is also transmitted to the gap equation in Eq.(3.41) through  $I_i$  in Eq.(3.43). In absence of magnetic field, such terms are usually regularized either by a sharp momentum cutoff [24, 85] or by a smooth regulator [86, 87] in effective theories like NJL model. But in presence of magnetic field, a sharp cutoff suffers from cutoff artifact as the continuous momentum dependence in two spatial dimensions gets replaced by a sum over discretized Landau level. A smooth parametrization can still be used and it has been successfully used in the context of chiral magnetic effect in PNJL model [76]. Here, however, we shall adopt the regularization scheme of adding and subtracting a vacuum ( $T = \mu = B = 0$ ) term which is also divergent [79]. This makes the first term of Eq.(3.44) acquire a more convenient form by separating terms with explicit field dependence and terms without explicit field dependence and can be written in terms of Riemann-Hurwitz  $\zeta$  function as

$$\begin{aligned} \sum_{n,i} \frac{N_c \alpha_n |q_i B|}{(2\pi)^2} \int dp_z \omega_i &= \frac{N_c}{2\pi^2} \sum_{i=1}^3 |q_i B|^2 \left[ \zeta'(-1, x_i) - \frac{1}{2}(x_i^2 - x_i) \ln x_i + \frac{x_i^2}{4} \right] \\ &+ \frac{2N_c}{(2\pi)^3} \sum_{i=1}^3 \int d\mathbf{p} \sqrt{\mathbf{p}^2 + M_i^2}, \end{aligned} \quad (3.45)$$

where  $x_i = M_i^2/2|q_i B|$  is a dimensionless quantity and  $\zeta'(-1, x) = d\zeta(z, x)/dz|_{z=1}$  is the derivative of the Riemann-Hurwitz  $\zeta$  function which is given by [88],

$$\zeta'(-1, x) = \frac{\ln x}{2} \left[ x^2 - x + \frac{1}{6} \right] - \frac{x^2}{4} + x^2 \int_0^\infty \frac{2 \tan^{-1} y + y \ln(1 + y^2)}{e^{2\pi xy} - 1} dy. \quad (3.46)$$

Using Eq.s(3.44,3.45), the thermodynamic potential can be rewritten as

$$\Omega(\beta, \mu, B, M_i) = \Omega_{vac} + \Omega_{field} + \Omega_{med} + 2G_s \sum_{i=1}^3 I_i^2 + 4KI_1I_2I_3, \quad (3.47)$$

where  $\Omega_{vac}$  denotes the vacuum term with no explicit dependence on  $T$ ,  $\mu$  or  $B$ .  $\Omega_{field}$  denotes the field contribution which explicitly depends only on  $B$  and  $\Omega_{med}$  represents the medium contribution which explicitly depends on  $T$ ,  $\mu$  and  $B$ . Explicitly they are given as

$$\Omega_{vac} = -\frac{2N_c}{(2\pi)^3} \sum_i \int d\mathbf{p} \sqrt{\mathbf{p}^2 + M_i^2}, \quad (3.48)$$

$$\Omega_{field} = -\frac{N_c}{2\pi^2} \sum_i |q_i B|^2 \left[ \zeta'(-1, x_i) - \frac{1}{2}(x_i^2 - x_i) \ln x_i + \frac{x_i^2}{4} \right], \quad (3.49)$$

$$\Omega_{med} = \sum_{n,i} \frac{N_c \alpha_n |q_i B|}{(2\pi)^2 \beta} \int dp_z [\ln \sin^2 \theta_-^i + \ln \sin^2 \theta_+^i]. \quad (3.50)$$

Similar to the thermodynamic potential, we can split the chiral condensate,  $I_i$  into different terms according to dependence on  $T$ ,  $\mu$  and  $B$  using Eq.(3.45) as

$$\begin{aligned} I_i &= \frac{2N_c}{(2\pi)^3} \int d\mathbf{p} \frac{M_i}{\sqrt{\mathbf{p}^2 + M_i^2}} + \frac{N_c M_i |q_i B|}{(2\pi)^2} \left[ x_i(1 - \ln x_i) + \ln \Gamma(x_i) + \frac{1}{2} \ln \frac{x_i}{2\pi} \right] \\ &- \sum_{n=0}^{\infty} \frac{N_c |q_i B| \alpha_n}{(2\pi)^2} \int dp_z \frac{M_i}{\sqrt{M_i^2 + |\mathbf{p}_i|^2}} [\sin^2 \theta_-^i + \sin^2 \theta_+^i] \\ &= I_{vac}^i + I_{field}^i + I_{med}^i. \end{aligned} \quad (3.51)$$

The field contribution  $\Omega_{field}$ , given in Eq.(3.49) to the thermodynamic potential has the simplest form that we can have since we have the derivative of Riemann-Hurwitz  $\zeta$  function in Eq.(3.46). The  $\ln \Gamma(x_i)$  term in the field contribution  $I_{field}^i$  to the chiral condensate in Eq.(3.51) has to be calculated numerically and rest of the terms in  $I_{field}^i$  are simple enough. The integrals in the vacuum contributions to both the chiral condensate and thermodynamic potential,  $I_{vac}^i$  and  $\Omega_{vac}$ , given in Eq.(3.51) and Eq.(3.48), can be analytically solved and since there is no explicit magnetic field dependence in the vacuum contributions, a three momentum cutoff can safely be imposed as is usually

done in NJL model [24, 85]. Solving the integrals with a three momentum cutoff  $\Lambda$ , the vacuum terms can be written as

$$I_{vac}^i = \frac{N_c M_i}{2\pi^2} \left[ \Lambda \sqrt{\Lambda^2 + M_i^2} - M_i^2 \ln \frac{\Lambda + \sqrt{\Lambda^2 + M_i^2}}{M_i} \right], \quad (3.52)$$

$$\Omega_{vac} = \frac{N_c}{8\pi^2} \sum_i \left[ M_i^4 \ln \frac{\Lambda + \sqrt{\Lambda^2 + M_i^2}}{M_i} - \sqrt{\Lambda^2 + M_i^2} (2\Lambda^2 + M_i^2) \right] \quad (3.53)$$

However, since in presence of magnetic field,  $|\mathbf{p}|^2 = p_z^2 + 2n|q_i B|$ , the condition of sharp three momentum cutoff translates to a summation over finite number of Landau levels in  $\Omega_{vac}$  or in  $I_{vac}^i$  with the maximum number of Landau levels that are filled up being given as  $n_{max} = \text{Int} \left[ \frac{\Lambda^2}{2|q_i B|} \right]$  for  $p_z = 0$ . For the medium contribution  $I_{med}$ , this also leads to a cut off for the magnitude of  $|p_z|$  as  $\Lambda' = \sqrt{\Lambda^2 - 2n|q_i B|}$  for a given value of  $n$ . At finite temperature the medium contributions  $\Omega_{med}$  and  $I_{med}^i$  can not be calculated analytically. However, in the zero temperature limit, the integrals in  $\Omega_{med}$  and  $I_{med}^i$  can be solved analytically. At  $T = 0$  the particle distribution function  $\sin^2 \theta_-^i = \Theta(\mu_i - \omega_n^i)$  while the antiparticle distribution function  $\sin^2 \theta_+^i = 0$ . The  $\theta$  function restricts the magnitude of  $|p_z|$  to be less than  $p_{zmax}^i = \sqrt{p_f^i{}^2 - 2n|q_i B|}$ , where,  $p_f^i = \sqrt{\mu_i^2 - M_i^2}$  is the Fermi momentum of the  $i$ -th flavor. This also restricts maximum number of Landau levels to  $n_{max}^i = \text{Int} \left[ \frac{p_f^i{}^2}{2|q_i B|} \right]$ . Solving the integrals and setting the upper limit of  $p_z$  as  $p_{zmax}^i$ , the medium contributions  $I_{med}^i$  and  $\Omega_{med}$  at  $T = 0$  can be written as

$$I_{med}^i(T = 0) = \frac{N_c}{2\pi^2} \sum_{n=0}^{n_{max}^i} \alpha_n |q_i| B M_i \ln \left[ \frac{p_{zmax}^i + \mu_i}{\sqrt{M_i^2 + 2n|q_i B|}} \right], \quad (3.54)$$

$$\begin{aligned} \Omega_{med}(T = 0) = & \sum_i \frac{N_c}{4\pi^2} \sum_{n=0}^{n_{max}^i} \alpha_n |q_i| B M_i \left[ \mu_i p_{zmax}^i \right. \\ & \left. - (M_i^2 + 2n|q_i B|) \ln \left\{ \frac{p_{zmax}^i + \mu_i}{\sqrt{M_i^2 + 2n|q_i B|}} \right\} \right]. \quad (3.55) \end{aligned}$$

So, we have complete expressions for the thermodynamic potential and the chiral condensate for  $T = 0$ . This situation is relevant for neutron stars.

However, in the context of neutron star matter, the presence of electrons should also be considered along with  $u$ ,  $d$  and  $s$  quarks. The following processes can take place in weak equilibrium with three quarks,

$$d \rightarrow u + e^- + \bar{\nu}_{e-}, \quad s \rightarrow u + e^- + \bar{\nu}_{e-} \quad \text{and} \quad s + u \rightarrow d + u,$$

which leads to the following relation between the chemical potentials  $\mu_u$ ,  $\mu_d$ ,  $\mu_s$  and  $\mu_E$  as

$$\mu_s = \mu_d = \mu_u + \mu_e. \quad (3.56)$$

The neutrino chemical potentials are taken to be zero as they can diffuse out of the star. So two independent chemical potentials are needed in the context of neutron star matter which we take to be the quark chemical potential  $\mu_q = \mu_B/3$  and the electric charge chemical potential,  $\mu_E$  in terms of which the chemical potentials are given by  $\mu_s = \mu_q - \frac{1}{3}\mu_E = \mu_d$ ,  $\mu_u = \mu_q + \frac{2}{3}\mu_E$  and  $\mu_e = -\mu_E$ . In addition, for description of the charge neutral matter, there is another constraint for the chemical potentials through the following relation for the particle densities given by

$$\frac{2}{3}\rho_u - \frac{1}{3}\rho_d - \frac{1}{3}\rho_s - \rho_e = 0. \quad (3.57)$$

The quark number densities  $\rho_i$  for each flavor are already defined in Eq.(3.38).

The electron number density is given by

$$\rho_e = \sum_{n=0}^{\infty} \frac{\alpha_n |eB|}{(2\pi)^2} \int dp_z [\sin^2 \theta_-^e - \sin^2 \theta_+^e], \quad (3.58)$$

where  $\sin^2 \theta_{\mp} = 1/\{\exp(\omega_e \mp \mu_e) + 1\}$  are the distribution functions for electrons and positrons with  $\omega_e = \sqrt{p_z^2 + 2n|e|B}$ . To calculate the total thermodynamic potential relevant for neutron star, the contribution of the electrons,  $\Omega_e$  must be added to  $\Omega$  in Eq.(3.47), which is given by

$$\Omega_e = \sum_{n,i} \frac{\alpha_n |eB|}{(2\pi)^2 \beta} \int dp_z [\ln \{1 + e^{-\beta(\omega_e - \mu_e)}\} + \ln \{1 + e^{-\beta(\omega_i + \mu_e)}\}] \quad (3.59)$$

Now, as we have the complete expressions for the mass gap and thermodynamic potential, we can proceed to evaluate them numerically by solving Eq.(3.41) for the mass gap and Eq.(3.47) for the thermodynamic potential. In the context of neutron star matter, we shall use Eq.s(3.57,3.59) for incorporating charge neutrality and electronic contribution. We shall discuss the numerical analysis for various physical situations in the next section.

### 3.4 Results and discussions

For numerical evaluations, we need to choose fixed values for some parameters in the NJL model. If we take the masses of  $u$  and  $d$  quarks to be equal, then, we have to fix five parameters in total. They are the four-fermion coupling  $G_s$  which has the dimension of  $[\text{Mass}]^{-2}$ , the six fermion coupling  $K$  with dimension  $[\text{Mass}]^{-5}$ , the sharp three momentum cutoff  $\Lambda$  and the current quark masses for the non strange and strange quarks,  $m_q$  and  $m_s$  respectively. After choosing  $m_q$  MeV, the remaining four parameters are fixed by fitting to the pion decay constant and the masses of pion, kaon and  $\eta'$ . Here, we have chosen  $m_q = 5.5$  MeV and  $m_s = 0.1407$  GeV,  $\Lambda = 0.6023$  GeV,  $G_s\Lambda^2 = 1.835$  and  $K\Lambda^5 = 12.36$  [89]. With this set of parameters the mass of  $\eta'$  is underestimated by about six percent and the constituent masses of the light quarks turn out to be  $M_q = 0.368$  GeV for  $u$  and  $d$  quarks and  $M_s = 0.549$  GeV for strange quark at  $T = \mu = B = 0$ .

For 3-flavor NJL model, different values of the parameters have also been used although the principle there is same as above [85, 90]. This discrepancy lies in the different treatments of the  $\eta'$  meson. Since NJL model does not confine, and because of the large mass of  $\eta'$  ( $m_{\eta'} = 958$  MeV), it lies above the threshold for  $q\bar{q}$  decay with an unphysical imaginary part for the corresponding polarization diagram. This is an unavoidable feature of NJL model and leaves an uncertainty which is reflected in the choice of different values of the parameters. Within this limitation, however, we shall proceed with the above set of parameters which has been used in the study of the phase diagram of

dense matter [91] and in the context of equation of state of neutron star [92].

Let us start our analysis by considering the case when the charge neutrality condition is not imposed. In this case  $\mu_E = 0$  and all the quark flavors have equal chemical potential  $\mu_q$ . For given values of  $\mu_q$ ,  $T$  and  $eB$ , we solve Eq.(3.41) self consistently for the mass gap  $M$  using Eq.(3.51) for the chiral order parameter  $I_i$ . We then evaluate the thermodynamic potential  $\Omega$  using Eq.(3.47) to examine whether the chiral condensate is energetically favored or not. In the evaluation of  $I_{med}^i$  of Eq.(3.51), while considering  $T = 0$ , the Landau levels are filled upto a maximum value,  $n_{max} = \text{Int} \left[ \frac{\Lambda^2}{2|q_i|B} \right]$  as already mentioned in the previous section. On the other hand, for  $T \neq 0$ , the levels are filled upto the maximum Landau level. But the error in neglecting the higher Landau levels is less than  $10^{-5}$ . Near the crossover transition temperature, there may be multiple solutions for  $M$  corresponding to multiple extrema of  $\Omega$ . In such cases, as we have mentioned in the previous chapter, we have chosen the solution with least  $\Omega$ . This is verified by checking the positivity of the second derivative of  $\Omega$  with respect to  $M$ .

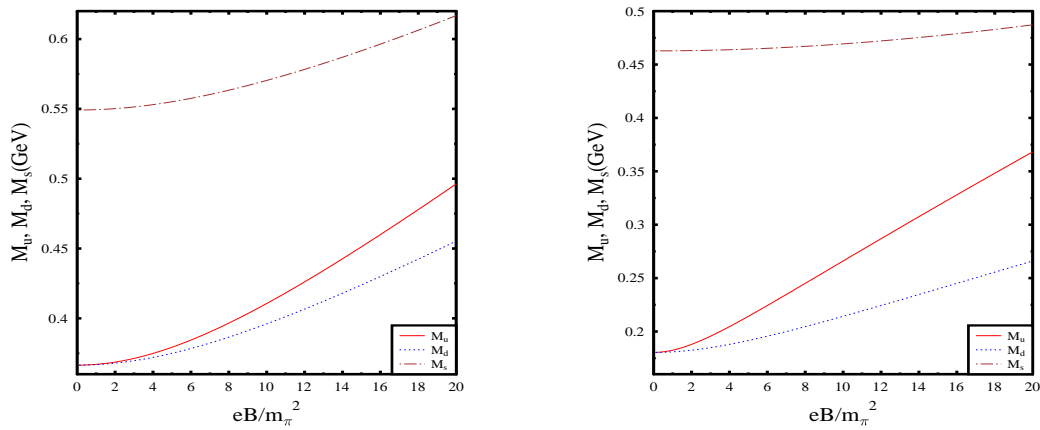


Figure 3.1: *Constituent quark masses as functions of magnetic field at  $T = \mu = 0$ . (Left panel) Effect of the KMT determinant interaction term is included. (Right Panel) The KMT term is ignored, i.e.  $K = 0$ . The solid curves, the dotted curves and the dash-dotted curves represent the constituent masses of  $u$ ,  $d$  and  $s$  quarks respectively in both the plots.*

In the left panel of Fig.[3.1], we show the effect of magnetic field on the constituent masses of the three quark flavors for  $T = \mu = 0$  including the KMT term. It is evident that magnetic field enhances the order parameters though,

because of difference in electric charge, the enhancement is not the same for different flavors. For  $eB = 20m_\pi^2$ , the enhancement factors,  $[M(B) - M(B = 0)]/M(B = 0)$ , are about 35%, 24% and 12% for  $u$ ,  $d$  and  $s$  quarks respectively. The effect of magnetic field on CSB has been studied in NJL model without the KMT term also [93]. For comparing the effects of magnetic field with and without the KMT term, we have shown the constituent quark masses as functions of magnetic field at  $T = \mu = 0$  in the right panel of Fig.[3.1]. The mass splitting between  $u$  and  $d$  quarks is much larger when the KMT term is not taken in to account, i.e,  $K = 0$ . For  $eB = 20m_\pi^2$ , the ratio  $[M_u(B) - M_d(B)]/M_u(B = 0) = 57\%$  when  $K = 0$  while the same ratio is about 11% when  $K\Lambda^5 = 12.36$ . This difference is due to the flavor mixing through the KMT term. Whereas the magnetic field tends to differentiate among different flavors depending on electric charges, the KMT term tends to bring the constituent quark masses together through mixing of different flavors. So the splitting between the constituent masses of different flavors in presence of magnetic field become smaller when  $K \neq 0$ . This behavior has also been observed in 2-flavor NJL model [27]. The effect of the KMT term is prominent in the  $s$  quark mass also. For  $K = 0$ , the  $s$  quark mass experiences little enhancement compared to  $u$  and  $d$  quarks whereas, because of the flavor mixing, the enhancement is significant in presence of the KMT term.

The temperature dependence of the constituent quark masses for different strengths of magnetic field at  $\mu = 0$  is shown in Fig.[3.2]. The left panel corresponds to the constituent mass of  $u$  quark and the right panel corresponds to the constituent mass of the  $s$  quark. The magnetic catalysis is evident as the constituent quark masses increase with higher magnetic field for a given temperature. In this calculation, instead of assuming the lowest Landau level approximation, we have considered the maximum number of Landau levels as appropriate for a given magnetic field. For both the quarks, the transition from chiral symmetry broken phase to chiral symmetry restored phase remains a crossover for finite strengths of magnetic field as is the case for zero magnetic field. Here, the restoration of chiral symmetry is approximate as we have taken

the current quark masses to be non zero for all flavors. In the chiral symmetry restored phase, the constituent quark masses approach the current quark mass values of the respective flavors. Similar feature has been observed in 2-flavor NJL model also [27] but this is in contrast with the linear sigma model results where the usual crossover becomes a first order phase transition for strong magnetic fields [75].

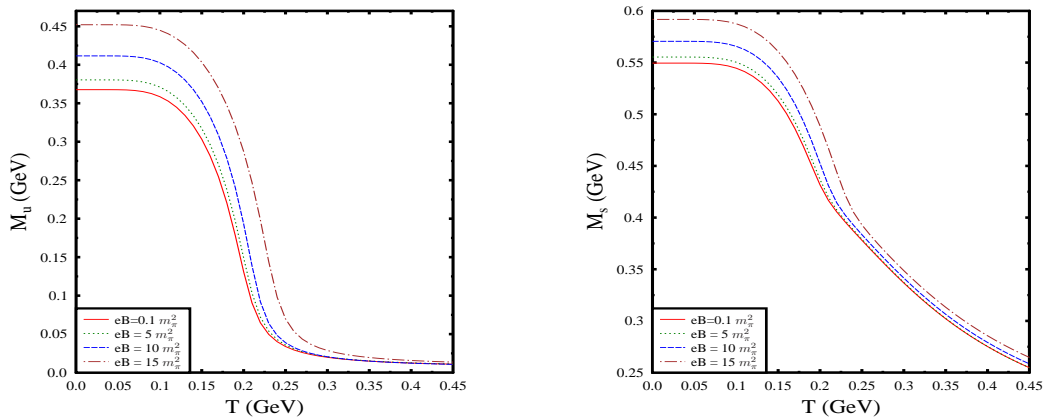


Figure 3.2: *Constituent masses of the  $u$  quark,  $M_u$  (left panel) and the  $s$  quark,  $M_s$  (right panel) as functions of temperature for different strengths of magnetic field at  $\mu = 0$ .*

Now, we shall discuss the behavior of constituent quark masses and baryon number density as functions of the quark chemical potential,  $\mu_q$  for different strengths of magnetic field at  $T = 0$ . In Fig.[3.3], we show the variations constituent quark masses for  $u$  quark,  $M_u$  (left panel) and  $d$  quark,  $M_d$  (right panel). Fig.[3.4] shows the variation of the constituent mass of the  $s$  quark,  $M_s$  (left panel) and the ratio of the baryon number density,  $\rho$  to the normal nuclear matter density,  $\rho_0 = 0.17/fm^3$  (right panel).

For  $eB = 0$ , as  $\mu_q$  increases, a first order transition is observed to take place for all flavors at a critical value  $\mu_c = 362$  MeV. Prior to that ( $\mu < \mu_c$ ), the quark masses stay at their vacuum values and  $\rho/\rho_0$  remains zero. At  $\mu = \mu_c$ , the light quarks experience a drop in their masses from their vacuum values of  $\sim 367$  MeV to  $\sim 52$  MeV. The  $s$  quark mass also experiences a first order transition and drops from its vacuum value of  $\sim 549$  MeV to  $\sim 464$  MeV due to flavor mixing through the KMT term.  $\rho/\rho_0$  also jumps from zero to 2.37.

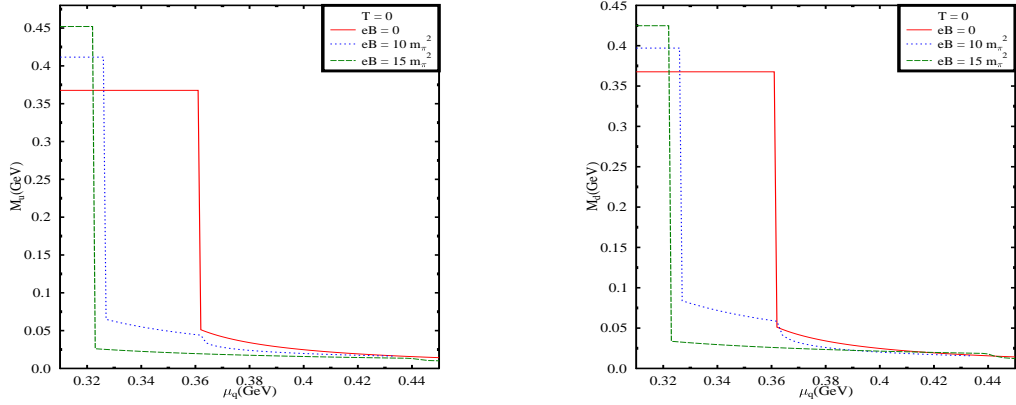


Figure 3.3: Constituent masses of  $u$  quark (left panel) and  $d$  quark (right panel) as functions of  $\mu_q$  for different strengths of magnetic field at  $T = 0$ .

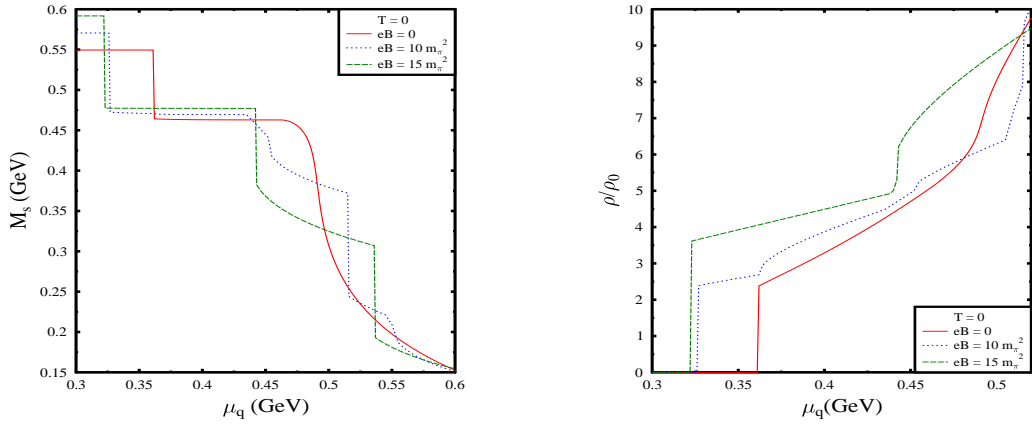


Figure 3.4: Constituent mass of  $s$  quark (left panel) and baryon density (right panel) as functions of  $\mu_q$  for different strengths of magnetic field at  $T = 0$ .

As the magnetic field is increased, the  $\mu_c$  for the first order transition consistently decreases. For  $eB = 10m_\pi^2$  and  $eB = 15m_\pi^2$ , the corresponding values of  $\mu_c$  are 327 MeV and 323 MeV respectively. This decrease of  $\mu_c$  with the increase in magnetic field has also been observed in the context of dense holographic matter and it has been termed as inverse magnetic catalysis of CSB [28]. For  $\mu < \mu_c$ , the constituent quark masses increase with the magnetic field for all flavors. For  $eB = 10m_\pi^2$ , the increase in  $M_u$  and  $M_d$  are  $\sim 45$  MeV and  $\sim 30$  MeV respectively while  $M_s$  experiences an increase of about  $\sim 21$  MeV as compared to  $eB = 0$ .

Since the  $\mu_c$  decreases with increase in magnetic field, there are windows in the range of  $\mu_q$  where the quark masses apparently decrease with the magnetic

field in the range  $\mu = 323$  MeV to  $\mu = 362$  MeV. In this regime however, the chiral transition has already taken place for  $eB = 15m_\pi^2$  and it is yet to happen for  $eB = 0$ . For  $eB = 10m_\pi^2$ , though the chiral transition takes place in this regime, the transition is weaker compared to the case of  $eB = 15m_\pi^2$ . This is because of the kinks that appear in the quark masses after the transition due to filling of different Landau levels for  $eB \neq 0$  and these kinks change the ordering of the quark masses after the transition. Expectedly, no kinks appear for  $eB = 0$  and the quark masses smoothly approach the respective values of the current quark masses.

Although  $\mu_c$  decreases with magnetic field, the corresponding baryon density increases as it can be seen in the right panel of Fig.[3.4]. For  $eB = 10m_\pi^2$ , the critical density  $\rho_c/\rho_0 = 2.39$  is almost similar to  $eB = 0$  case where  $\rho_c/\rho_0 = 2.38$  but it is substantially larger for  $eB = 15m_\pi^2$  with  $\rho_c/\rho_0 = 3.62$ . Similar qualitative feature has been observed in Ref.[79].

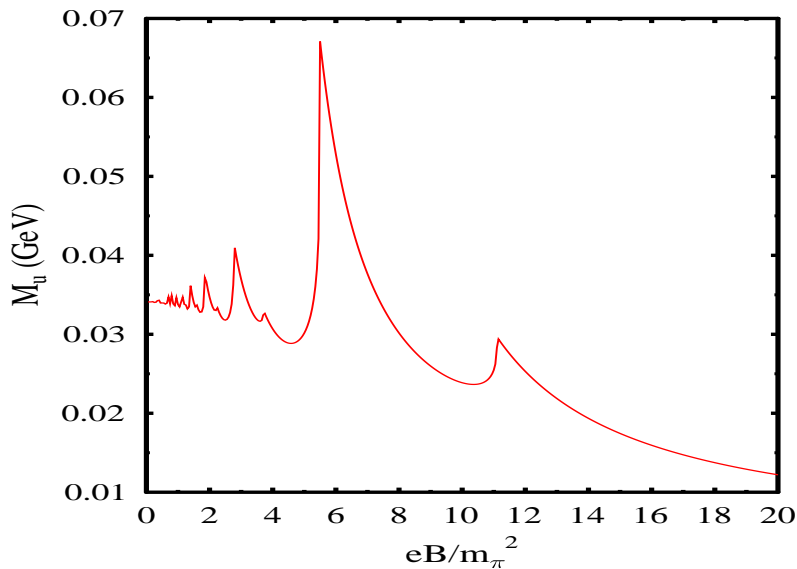


Figure 3.5: *Oscillation of  $u$  quark mass with magnetic field. We have taken  $\mu_q = 380$  MeV and  $T = 0$ .*

For  $\mu_q > \mu_c$ , the quark masses exhibit de Haas van Alphen oscillation similar to the oscillation of the magnetization of a metal in presence of magnetic field [94]. This oscillation is shown for  $u$  quark in Fig.[3.5]. Here we have taken  $\mu_q = 380$  MeV and  $T = 0$ . This phenomenon is a consequence of oscillation of the density of states at Fermi surface due to Landau quantization. The

oscillation continues as long as  $2|q|B < \sqrt{\mu_q^2 - M_q^2}$  and ceases when the first Landau level lies above the Fermi surface [87, 95].

Now, let us focus our attention on the effects of magnetic field on charge neutral dense matter which is relevant in the context of neutron star matter. Here, we take the value of the electric charge chemical potential  $\mu_E$  to be non zero along with  $T$ ,  $\mu_q$  and  $eB$ . The mass gap is calculated by self consistently solving Eq.(3.41) for given values of  $T$ ,  $\mu_q$ ,  $\mu_E$  and  $eB$ .  $\mu_E$  is varied so that the charge neutrality condition in Eq.(3.57) is satisfied. The resulting solutions are then used in Eq.(3.47) to compute  $\Omega$ .

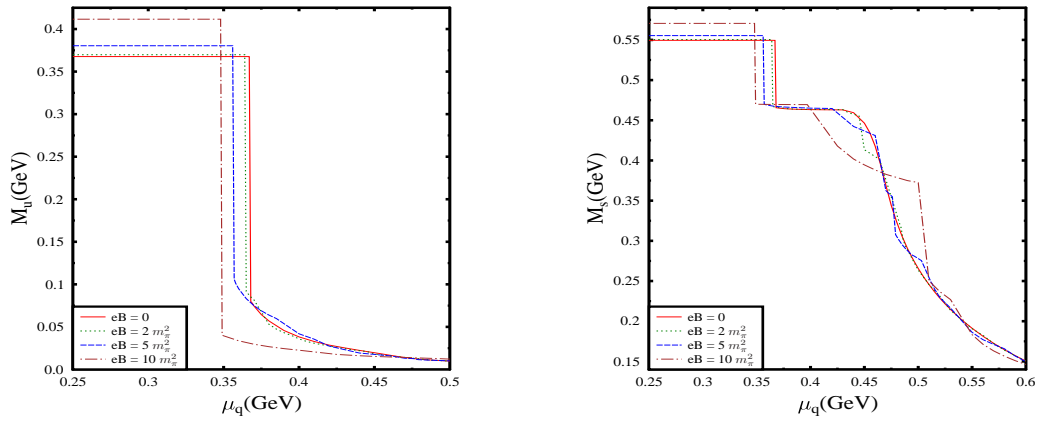


Figure 3.6: *Constituent masses of  $u$  quarks (left panel) and  $s$  quarks (right panel) as functions of  $\mu_q$  at  $T = 0$  for different strengths of magnetic field for charge neutral matter.*

Fig.[3.6], shows  $M_u$  (left panel) and  $M_s$  (right panel) as functions of  $\mu_q$  for charge neutral matter at  $T = 0$  for different strengths of magnetic field. Similar to the case without charge neutrality condition, here also we observe a first order transition at a critical quark chemical potential  $\mu_c$ . To maintain the charge neutrality condition, the  $d$  quark number density should be almost twice that of  $u$  quark number density at the transition point as  $M_s$  is much too large to contribute to the charge density. To realize this,  $M_d$  should be sufficiently smaller as compared to  $M_u$ . This implies that  $\mu_d$  should be larger than  $\mu_u$  unlike case without charge neutrality where the chemical potential of all the flavors were the same and equal to  $\mu_q$ . Numerically, it turns out for  $eB = 0$  that  $\mu_d = 393$  MeV,  $\mu_u = 318$  MeV and  $\mu_q = \mu_c = 368$  MeV which is

slightly higher as compared to the common chemical potential  $\mu_c = 362$  MeV when charge neutrality condition were not imposed. At the transition point,  $M_u = 80$  MeV and  $M_d = 61$  MeV whereas both the quarks had a common mass of 52 MeV at the transition point when the charge neutrality condition were not imposed. These values of  $\mu_u = 318$  MeV and  $\mu_d = 393$  MeV at the transition point correspond to  $\mu_e = 75$  MeV. At  $\mu_c$ , the electron number density turns out to be three orders of magnitude lower than the number densities of both  $u$  and  $d$  quarks. As the magnetic field is increased, the constituent masses of all three flavors increase for  $\mu_q < \mu_c$ . The first drop in  $M_s$  is related to the drops in  $M_u$  and  $M_d$  through the KMT term. The kink structure in  $M_s$  for higher magnetic fields is due to the filling of different Landau levels. Similar to the case without charge neutrality, here also we observed that higher magnetic field induces smaller  $\mu_c$ . However, the critical density increases for increase in magnetic field. This behavior is shown in Fig.[3.7], where  $M_u$  (left panel) and  $M_s$  (right panel) are shown as functions of baryon density at  $T = 0$  for different strengths of magnetic field.

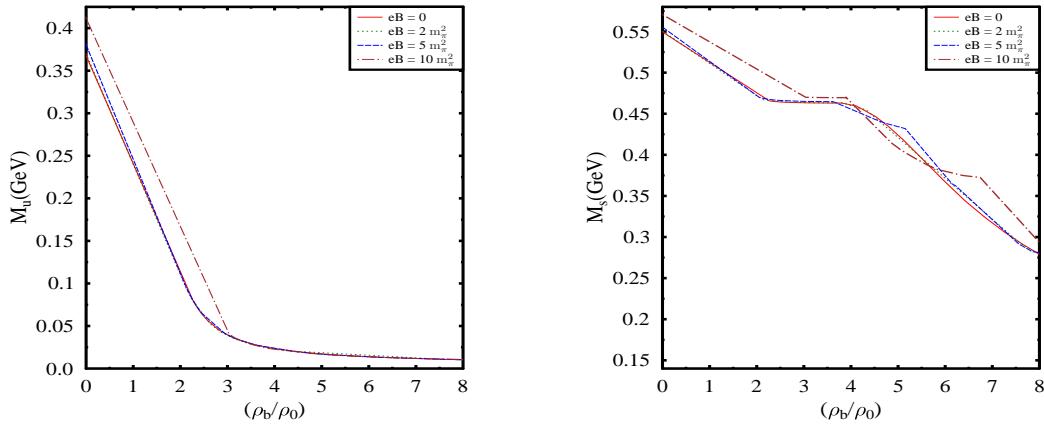


Figure 3.7: *Constituent masses of  $u$  and  $s$  quarks as functions of baryon density in units of nuclear matter density  $\rho_0$  for different strengths of magnetic field at  $T = 0$ .*

Next, we discuss the effects of magnetic field on hot neutral quark matter. Such a condition is relevant for the matter in the interior of the proto-neutron stars where the temperature can be about few tens of MeV. In Fig.[3.8], we show the effects of magnetic field on  $M_u$  (left panel) and  $M_s$  (right panel) in magnetized charge neutral matter at  $T = 40$  MeV. Here also, the chiral

symmetry restoration happens through a first order transition similar to the  $T = 0$  case although the transition is smoother. Here also,  $\mu_c$  decreases for increase in magnetic field and the constituent masses increase with magnetic field for  $\mu_q < \mu_c$  reflecting the magnetic catalysis of CSB.

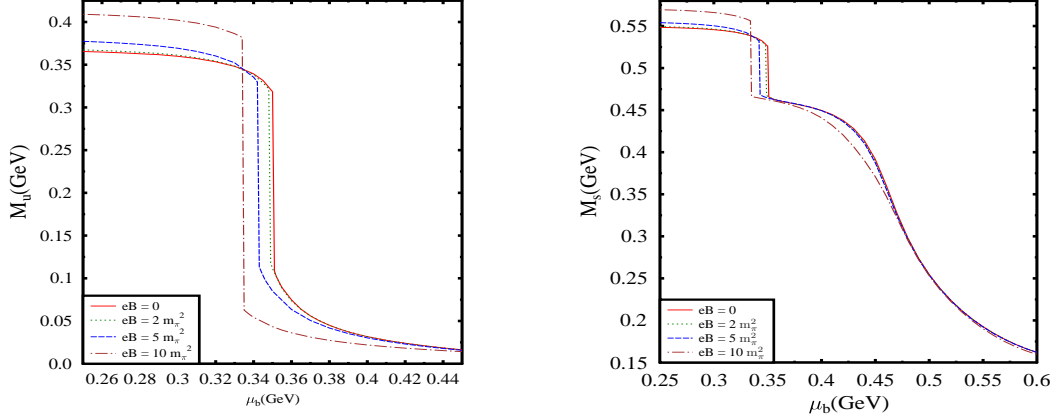


Figure 3.8: *Constituent masses of  $u$  and  $s$  quarks as functions of  $\mu_q$  for charge neutral matter for different strengths of magnetic field at  $T = 40$  MeV.*

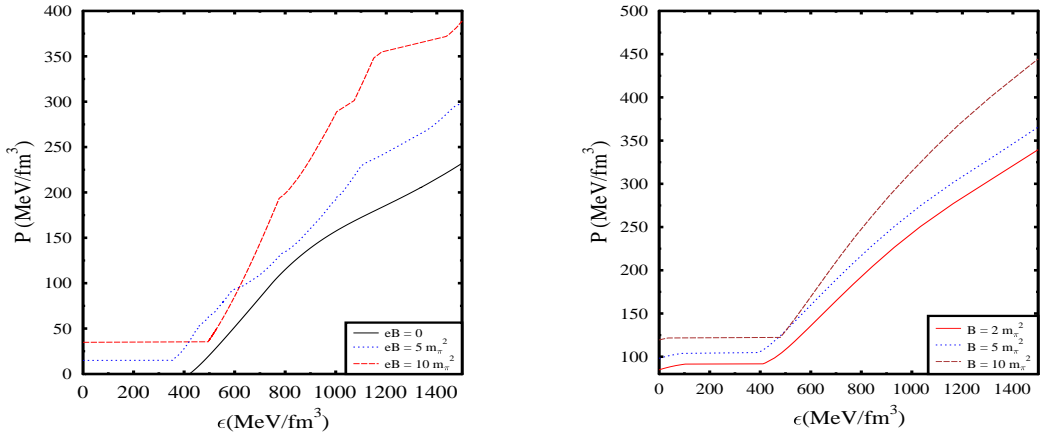


Figure 3.9: *Equations of state for charge neutral matter at  $T = 0$  (left panel) and  $T = 40$  MeV (right panel) for different strengths of magnetic field.*

Now, let us study the effect of magnetic field on the equation of state, i.e, pressure as a function of energy for the charge neutral matter. This is shown in Fig.[3.9] for  $T = 0$  (left panel) and  $T = 40$  MeV (right panel). For  $T = 0$ , the effect of Landau quantization shows up in the kink structure of the equations of state. For smaller magnetic fields, this effect is less visible as the number of filled Landau levels are quite large. For both  $T = 0$  and  $T = 40$  MeV, the equation of state becomes steeper as the magnetic field increases. Since the

zero density constituent quark masses increase with magnetic field, the vacuum energy density decreases with increasing magnetic field. Therefore the starting value of pressure is lowest for  $eB = 0$  and increases with the magnetic field as seen in Fig.[3.9]. For higher densities when chiral symmetry is restored, the magnetic field contribution to the  $\Omega$  as given in Eq.(3.49) increases with magnetic field. This means that the chemical potential must be larger for lower magnetic field as compared to higher field to have the same energy density. So we might naively expect the pressure ( $P = \mu\rho - \epsilon$ ) to be higher for lower field which is in contrast with what we see in Fig.[3.9]. The explanation to this lies in the fact that higher magnetic field induces lower  $\mu_c$  as observed in Fig.[3.6] and Fig.[3.8]. So for a given energy density, the number density can be higher for higher magnetic field leading to a higher pressure and consequently, the equation of state becomes steeper with higher magnetic field.

The pressure that we have considered to show the equations of state in Fig.[3.9] is the thermodynamic pressure, i.e, negative of  $\Omega$  given in Eq.(3.47). However, in presence of strong magnetic fields, the hydrodynamic pressure can be highly anisotropic when there is significant magnetization of the matter [77, 78, 96]. The hydrodynamic pressure in the direction of the field is given by the thermodynamic pressure,  $P_{\parallel} = P = -\Omega$  as defined in Eq.(3.47). On the other hand, the pressure in the transverse direction of the magnetic field is given by  $P_{\perp} = P - MB$  [78]. Here,  $M = -\partial\Omega/\partial B$  is the magnetization of the system. Using the expression for  $\Omega$  in Eq.(3.47), we can write the magnetization as

$$M = M_{med} + M_{field} + M_c \quad (3.60)$$

where  $M_{med} = -\partial\Omega_{med}/\partial B$  is the medium contribution to the magnetization at  $T = 0$  and is given by

$$M_{med} = \frac{N_c}{4\pi^2} \sum_{n,i} \alpha_n |q_i| \left[ \mu_i p_{zmax}^i - (A_{n,i}^2 + 2n|q_i|B) \ln \frac{\mu_i + p_{zmax}^i}{A_{n,i}} \right], \quad (3.61)$$

where  $A_{n,i} = \sqrt{M_i^2 + 2n|q_i|B}$ . The field contribution to the magnetization is

given as

$$M_{field} = -\frac{\partial \Omega_{field}}{\partial B} = \sum_i q_i^2 B \left[ \frac{\ln x_i}{12} - \frac{1}{24} + x_i^3 I_1(x_i) \right], \quad (3.62)$$

where  $x_i = (M_i^2/2|q_i|B)$  as we have defined earlier and  $I_1(x_i)$  is defined as

$$I_1(x_i) = \frac{1}{\pi} \int y \frac{2 \arctan(y) + y \ln(1+y^2)}{\{\exp(2\pi x_i y) - 1\} \{1 - \exp(-2\pi y)\}} dy. \quad (3.63)$$

Since the  $\Omega_{field}$  term originates from the effect of magnetic field on Dirac sea so  $M_{field}$  can be recognized as the contribution arising because of the magnetization of the Dirac sea. Finally,  $M_c$  in Eq.(3.60) is the contribution to the magnetization arising from the last two terms of the thermodynamic potential in Eq.(3.47) and is given as

$$M_c = -4G \sum_i I_i \frac{\partial I_i}{\partial B} - 2K \sum_{i \neq j \neq k} I_i I_j \frac{\partial I_k}{\partial B}. \quad (3.64)$$

Here,  $\partial I_i / \partial B$  is the derivative of the chiral condensate ( $-\langle \bar{\psi} \psi \rangle_i$ ) with respect to the magnetic field and using Eq.(3.51), we can write this derivative as a sum of the contribution from the medium and contribution from field as

$$\frac{\partial I_i}{\partial B} = \frac{\partial I_{med}^i}{\partial B} + \frac{\partial I_{field}^i}{\partial B},$$

where, the medium contribution at  $T = 0$  is

$$\frac{\partial I_{med}^i}{\partial B} = \sum_n \frac{N_c \alpha_n}{2\pi^2} \left[ \ln \frac{p_{zmax}^i + \mu_i}{A_{n,i}} - \frac{n|q_i|B}{A_{n,i}^2} \frac{\mu_i}{p_{zmax}^i} \right]. \quad (3.65)$$

The field contribution to the derivative of  $I_i$  is given by

$$\frac{\partial I_{field}^i}{\partial B} = \frac{N_c}{2\pi^2} \left[ \ln \Gamma(x_i) + \frac{1}{2} \log \frac{x_i}{2\pi} + x_i - x_i \Psi^0(x_i) - \frac{1}{2} \right], \quad (3.66)$$

where  $\Psi^0(x_i) = \Gamma'(x_i)/\Gamma(x_i)$  is the logarithmic derivative of the Gamma function.

The magnetization  $M$ , described in Eq.(3.60) is shown in the left panel of Fig.[3.10] for  $T = 0$  and  $\mu_u = \mu_d = 400$  MeV.  $M$  exhibits rapid de Hass van Alphen oscillation. The irregularity in the oscillation is due to the unequal masses of the three quark flavors.  $M$  does not become constant even after all the quarks are in the lowest Landau level unlike Ref.[78]. This is because of the contribution from magnetization of the Dirac sea which is included here along with the Fermi sea contribution through  $M_{med}$ .

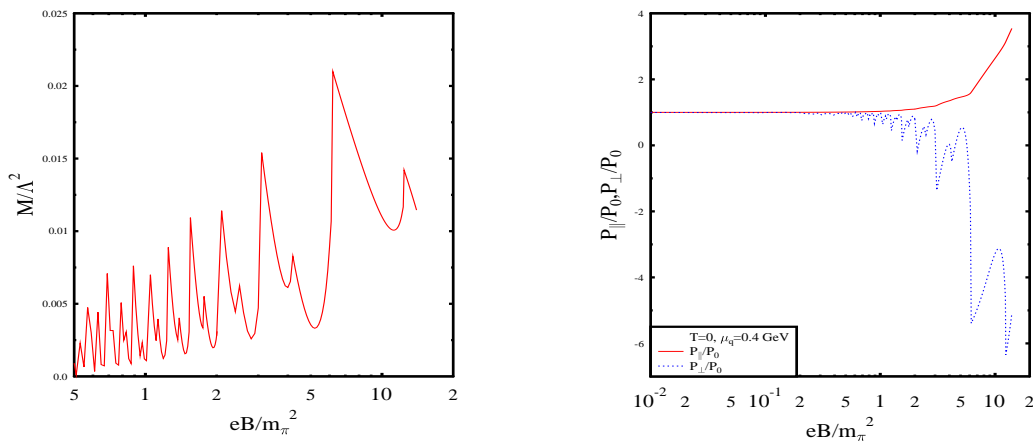


Figure 3.10: (Left panel) Magnetization in units of  $\Lambda^2$  as a function of magnetic field. (Right panel)  $P_{\parallel}$  and  $P_{\perp}$  of strange quark matter as functions of the magnetic field in units of pressure  $P_0$  for  $eB = 0$ . In both the plots, the magnetic field in units of  $m_\pi^2$  is plotted in a logarithmic scale and we have taken here  $T = 0$  and  $\mu_u = \mu_d = 0.4$  GeV.

The longitudinal pressure  $P_{\parallel}$  and the transverse pressure  $P_{\perp}$  for strange quark matter is plotted in the right panel of Fig.[3.10] for  $T = 0$  and  $\mu = 400$  MeV. The oscillatory behavior of the magnetization is reflected in the transverse pressure.  $P_{\parallel}$  and  $P_{\perp}$  start to differ significantly for magnetic field strengths of about  $eB = m_\pi^2$ , which corresponds to about  $10^{18}$  Gauss. Such field induced anisotropy in pressure is qualitatively similar to the case where the anisotropic properties of transport coefficients for strange quark matter were considered [78]. While considering neutron star structure, it is necessary to also include the free field energy  $B^2/2$  to the total energy and pressure. This term adds to  $P_{\parallel}$  and  $P_{\perp}$  with different signs [77]. This free field energy can make  $P_{\perp}$  negative and consequently may lead to mechanical instability [77]. While studying structural properties of compact astrophysical objects

endowed with magnetic fields such anisotropy in pressure should be taken into account as this can effect the structure and geometry of the star.

Finally we end this section with a comment regarding the axial fermion current density induced at finite chemical potential. From Eq.s(3.31) and Eq.(3.42),

$$\langle j_5^{i3} \rangle = \frac{N_c |q_i| B}{(2\pi)^2} \int dp_z \left[ \frac{1}{\exp(\sqrt{p_z^2 + M_i^2} - \mu_i)} - \frac{1}{\exp(\sqrt{p_z^2 + M_i^2} + \mu_i)} \right]. \quad (3.67)$$

Thus, although the lowest Landau level contributes to the above expectation value, because of its dependence on the constituent quark mass parameter  $M_i$ , the effects of all the higher Landau levels are implicitly there in Eq.(3.67) as the constituent masses here are calculated self consistently using Eq.(3.41) and Eq.(3.51). Further, because of dependence on the constituent quark mass the axial quark current density expectation value also depends upon the coupling in a non perturbative manner [26, 97].

## 3.5 Summary

We have analyzed here the effect of magnetic field on CSB in a 3-flavor NJL model with a KMT determinant interaction term. We calculated the Dirac spinors explicitly in presence of magnetic field and wrote the field operator expansion in terms of these spinors. An explicit variational construct for the ground state in terms of quark-antiquark pairing is used with respect to which the thermodynamic potential is calculated. The ground state ansatz includes the effect of finite temperature and density. In that sense it is a generalization of the 2-flavor NJL model at finite temperature and density [27].

The mass gap equation and the thermal distribution functions are obtained from the minimization of  $\Omega$ . The gap equation is self consistently solved for given values of  $T$ ,  $\mu_q$  and  $eB$ . At  $\mu_q = 0$  and high temperature, the nature of chiral transition remains a crossover transition even for magnetic field strength  $eB = 10m_\pi^2$ . The magnetic catalysis of CSB is also observed.

At finite densities, the effect of Landau quantization shows up in the kink structure of the constituent masses for  $T = 0$ . The order parameter shows oscillation similar to the de Haas van Alphen effect for magnetization in metals. However, in the present case of dense quark matter, the mass of the quark itself is dependent on the strength of magnetic fields which leads to a non periodic oscillation of the order parameter. Although the critical chemical potential,  $\mu_c$ , for chiral transition consistently decreases with increase in the strength of the magnetic field, the corresponding density increases with the magnetic field strength. The effect of the KMT term, which causes flavor mixing, is evident in the drop in strange quark mass. Imposing the electrical charge neutrality condition for the quark matter increases the value for  $\mu_c$  slightly. Since the mass of the strange quark plays an important role in maintaining the charge neutrality, this in turn affects the chiral restoration transition in quark matter. The presence of non zero magnetic field appears to make the equation of state steeper for charge neutral matter.

The hydrodynamic pressure can be anisotropic if the magnetization of the matter is significant. Within the model, this anisotropy starts to become relevant for field strengths around  $10^{18}$  Gauss. While considering the structural properties of astrophysical compact objects endowed with magnetic fields, this anisotropy in the equation of state should be taken into account as it can affect the geometry and structure of the star.

We have considered here quark-antiquark pairing in our ansatz for the ground state which is homogeneous with zero total momentum. However, it is possible that the condensate can be spatially non homogeneous with a net total momentum [98]. The effect of deconfinement transition can also be included by generalizing the present model to PNJL model for three flavors to investigate the inter relationship of deconfinement and the chiral transition in presence of strong magnetic fields considered here [99]. This will be particularly important for finite temperature calculations. At finite density and small temperatures, this ansatz can be generalized to include the diquark condensates in presence of magnetic field [82, 100].

# Chapter 4

## Strong CP violation at finite temperature and density

We shall discuss the effects of finite temperature and density on strong  $CP$  violation and the interplay of strong  $CP$  violation and CSB in this chapter. Strong interaction is known to respect space and time reflection symmetry to a very high degree as we have mentioned in the beginning of section[1.3.2]. However, these symmetries become questionable because of  $U(1)_A$  axial anomaly [30, 31]. The anomalous divergence of the axial current density can be obtained from inclusion of a  $CP$  violating  $\theta$ -term in the QCD Lagrangian which is, in principle, permitted from Lorentz invariance and gauge invariance. This  $\theta$ -term is give by

$$\mathcal{L}_\theta = \frac{\theta}{64\pi^2} g^2 F_{\mu\nu}^a \tilde{F}^{a\mu\nu}. \quad (4.1)$$

In Eq.(4.1),  $F_{\mu\nu}^a$  is the gluon field strength tensor and  $\tilde{F}^{a\mu\nu} = \epsilon^{\mu\nu\rho\sigma} F_{\rho\sigma}^a$  being its dual. This term violates  $CP$  unless  $\theta = 0 \text{ mod } \pi$ . However, extremely small value of intrinsic electric dipole moment (EDM) of neutron,  $|d_n| < 2.9 \times 10^{-26} e \text{ cm}$ , measured by precise experiments suggest that the QCD vacuum can be regarded as symmetric under  $CP$  [34]. Reliable theoretical calculation using this value of EDM of neutron imposes an upper bound on  $\theta$ ,  $|\theta| < 0.7 \times 10^{-11}$  [35]. This extreme smallness of  $\theta$  is framed as the strong  $CP$  problem. The strong  $CP$  problem is still unsolved although possible solutions have been

proposed by introducing axions [36] which arises from spontaneous breaking of the Peccei-Quinn symmetry [37].

According to the Vafa-Witten theorem, spontaneous  $CP$  violation does not happen for  $\theta = 0$  [38]. On the other hand, it has also been shown that spontaneous  $CP$  violation may take place in the QCD vacuum for  $\theta = \pi$  and degenerate vacuum states may arise which is known as Dashen phenomenon [41]. Even if  $CP$  is not broken for QCD vacuum, it is possible that it can be broken at finite density and finite temperature where the Vafa-Witten theorem need not be valid [39, 40]. It has been shown that metastable states with locally non vanishing  $\theta$  can be formed near the deconfinement phase transition region in the heavy ion collision experiments [43]. The most striking prediction regarding  $CP$  violation in the heavy ion collision experiments is the chiral magnetic effect (CME) [29]. This predicts, in presence of strong magnetic field, due to local  $CP$  violation, an electric current will be produced along the magnetic field axis since particles with right handed helicity move opposite to antiparticles with right handed helicity. CME may provide the proper explanation behind the charge separation phenomena that has been observed recently in the STAR experiment [44].

Because of the non perturbative nature of the  $\theta$ -term, strong  $CP$  violation is usually studied using lattice QCD or effective field theories. This has been extensively studied in low energy effective field theories like chiral perturbation theory [101] and linear sigma model [102]. The NJL model and its extensions have also been extensively used by incorporating  $CP$  violation through the Kobayashi-Maskawa-'t Hooft (KMT) determinant interaction term with a phase factor [103]. The NJL model has been used to study the spontaneous  $CP$  violation for  $\theta = \pi$  in the two flavor case [104]. This has been further extended to study  $CP$  restoration at high temperature [105]. The effect of  $\theta$  vacuum on deconfinement phase transition and chiral transition has also been analyzed in a 2-flavor PNJL model [106].

Here, we focus our attention on how chiral transition is affected in presence of a  $CP$  violating term in the Lagrangian. For this purpose, we adopt the 3-

flavor NJL model as an effective theory for CSB in strong interaction [24, 89]. The effect of  $CP$  violation is included through the KMT term with a phase  $\theta$ . We shall consider a variational ground state with quark-antiquark pairs that is related to CSB. The ground state ansatz is general enough to include both scalar and pseudo scalar condensates. We shall see that the pseudo scalar condensates arise for non zero values of  $\theta$  in the KMT term. The ansatz functions are to be determined through minimization of the thermodynamic potential. The mass gap equations for the scalar and the pseudo scalar condensates will also be obtained from the minimization of the thermodynamic potential. these gap equations will be self consistently solved and we shall discuss the phase structure at finite temperature and density for different values of  $\theta$ .

## 4.1 NJL model with CP violating term

To describe the chiral phase structure of strong interactions including the CP violating effects, we use the 3-flavor NJL model along with the flavor mixing KMT term. The Lagrangian is given by

$$\begin{aligned} \mathcal{L} = & \bar{\psi} (i\cancel{\partial} - m) \psi + G \sum_{A=0}^8 [(\bar{\psi}\lambda^A\psi)^2 + (\bar{\psi}i\gamma^5\lambda^A\psi)^2] \\ & - K [e^{i\theta} \det\{\bar{\psi}(1 + \gamma^5)\psi\} + e^{-i\theta} \det\{\bar{\psi}(1 - \gamma^5)\psi\}], \end{aligned} \quad (4.2)$$

where  $\psi^{i,a}$  denotes a quark field with color  $a$  ( $a = r, g, b$ ), and flavor  $i$  ( $i = u, d, s$ ), indices.  $\hat{m} = \text{diag}_f(m_u, m_d, m_s)$  is the current quark mass matrix in the flavor space. Here, we shall assume isospin symmetry for the two lightest flavors with  $m_u = m_d$ . In Eq.(4.2),  $\lambda^A$ ,  $A = 1, \dots, 8$  denote the Gell-Mann matrices in the flavor space and  $\lambda^0 = \sqrt{\frac{2}{3}} \mathbb{1}_f$ , where  $\mathbb{1}_f$  is the unit matrix in the flavor space. The four point interaction term  $\sim G$  is symmetric under  $SU(3)_V \times SU(3)_A \times U(1)_V \times U(1)_A$ . The determinant term  $\sim K$ , which generates a six point interaction for the case of three flavors, breaks  $U(1)_A$  symmetry for non vanishing values of  $\theta$ . The effect of topological term of Eq.(4.1) is simulated by the KMT term of Eq.(4.2) in the quark sector.

The field operator expansion for the quark fields is given as [81],

$$\psi(\mathbf{x}, t = 0) = \frac{1}{(2\pi)^{3/2}} \int [U_0(\mathbf{k})q^0(\mathbf{k}) + V_0(-\mathbf{k})\tilde{q}^0(-\mathbf{k})] e^{i\mathbf{k}\cdot\mathbf{x}} d\mathbf{k}. \quad (4.3)$$

The superscript ‘0’ indicates that the operators  $q^0$  and  $\tilde{q}^0$  are the two component operators for the quark annihilation and antiquark creation corresponding to the perturbative or the chiral vacuum  $|0\rangle$ . We have suppressed the color and flavor indices of the quark field operators.  $U^0(\mathbf{k})$  and  $V^0(-\mathbf{k})$  are the four component spinors which can be explicitly written as

$$U_0(\mathbf{k}) = \begin{bmatrix} \cos \frac{\chi^0}{2} \\ \boldsymbol{\sigma} \cdot \hat{\mathbf{k}} \sin \frac{\chi^0}{2} \end{bmatrix} \quad \text{and} \quad V_0(-\mathbf{k}) = \begin{bmatrix} -\boldsymbol{\sigma} \cdot \hat{\mathbf{k}} \sin \frac{\chi^0}{2} \\ \cos \frac{\chi^0}{2} \end{bmatrix}. \quad (4.4)$$

$\chi^0(\mathbf{k})$  in Eq.(4.4) is given as  $\cot \chi_i^0 = m_i/|\mathbf{k}|$ , for free massive fermion fields,  $i$  being the flavor index. For massless fields  $\chi^0(|\mathbf{k}|) = \pi/2$ .

## 4.2 Ground state and order parameters

Here, we shall construct a ground state for the Lagrangian in Eq.(4.2) to describe the phase structure. The ground state should be general enough to account for CSB as well as  $CP$  violation. We shall consider an ansatz for the ground state with quark-antiquark condensates which includes both the scalar as well as  $CP$  violating pseudo scalar channels. We consider an ansatz of the ground state at  $T = \mu = 0$  in terms of the chiral vacuum  $|0\rangle$  as

$$|\Omega\rangle = U_q|0\rangle, \quad (4.5)$$

where,  $U_q = U_{qI}U_{qII}$  is a unitary operator. In terms of creation and annihilation operators for quark and antiquark,  $U_{qI}$  and  $U_{qII}$  are given as

$$U_{qI} = \exp \left[ \int d\mathbf{k} q_r^0(\mathbf{k})^\dagger (\boldsymbol{\sigma} \cdot \hat{\mathbf{k}})_{rs} f(k) \tilde{q}_s^0(-\mathbf{k}) - h.c. \right], \quad (4.6)$$

$$U_{qII} = \exp \left[ \int d\mathbf{k} q_r(\mathbf{k})^\dagger r g(k) \tilde{q}_{-r}(-\mathbf{k}) - h.c. \right]. \quad (4.7)$$

$f(k)$  and  $g(k)$  are the ansatz functions which are to be determined later from the minimization of the thermodynamic potential. To include the effect of temperature and baryon density, we use the techniques of thermofield dynamics (TFD) [68]. The thermal ground state is constructed from the ground state  $|\Omega\rangle$  at  $T = \mu = 0$  through a thermal Bogoliubov transformation given as

$$|\Omega_{\beta,\mu}\rangle = \mathcal{U}_F|\Omega\rangle = e^{\mathcal{B}(\beta,\mu)^\dagger - \mathcal{B}(\beta,\mu)}|\Omega\rangle \quad (4.8)$$

with,

$$\mathcal{B}^\dagger(\beta, \mu) = \int \left[ \theta_-(\mathbf{k}, \beta, \mu) \underline{q}'(\mathbf{k})^\dagger \underline{q}'(-\mathbf{k})^\dagger + \theta_+(\mathbf{k}, \beta, \mu) \underline{\tilde{q}}'(\mathbf{k}) \underline{\tilde{q}}'(-\mathbf{k}) \right] d\mathbf{k}. \quad (4.9)$$

We shall see that the ansatz functions  $\theta_\pm(\mathbf{k}, \beta, \mu)$  in Eq.(4.9) will be related to the quark and the antiquark thermal distributions respectively and the underlined operators are associated with thermal doubling in TFD method.

To calculate the thermodynamic potential, we need the creation and annihilation operators for the thermal ground state  $|\Omega_{\beta,\mu}\rangle$ . We obtain these operators from the creation and annihilation operators for  $|0\rangle$  through Bogoliubov transformation similar to what we did in section[2.1.1] and section[3.2] in the context of BCS-BEC crossover and CSB respectively. Here, we have to perform two successive transformations for  $U_{qI}$  and  $U_{qII}$  described respectively in Eq.s(4.6,4.7). Here, we do not write the transformation matrices, instead, we write the following expectation value from which, the other expectation values can be calculated trivially,

$$\langle \Omega_{\beta,\mu} | \psi_\alpha^{ia}(\mathbf{x}) \psi_\beta^{jb}(\mathbf{y}) | \Omega_{\beta,\mu} \rangle = \delta^{ij} \delta^{ab} \int \frac{d\mathbf{k}}{(2\pi)^3} e^{-i\mathbf{k}\cdot(\mathbf{x}-\mathbf{y})} \Lambda^i(\mathbf{k}, \beta, \mu)_{\beta\alpha}, \quad (4.10)$$

where,

$$\begin{aligned} \Lambda^i(\mathbf{k}, \beta, \mu) &= \frac{1}{2} \left[ (\cos^2 \theta_+^i + \sin^2 \theta_-^i) + (\sin^2 \theta_-^i - \sin^2 \theta_+^i) (\gamma^0 \cos \phi^i \cos 2g^i \right. \\ &\quad \left. + \boldsymbol{\alpha} \cdot \hat{\mathbf{k}} \sin \phi^i \cos 2g^i) - i\gamma^0 \gamma^5 \sin 2g^i \right], \end{aligned} \quad (4.11)$$

where, we have introduced a new function  $\phi^i(\mathbf{k}) = \chi_0 + 2f^i(\mathbf{k})$  in terms of the condensate function  $f^i(\mathbf{k})$  of Eq.(4.6). From now on, we shall consider  $\phi^i(\mathbf{k})$  as the condensate function instead of  $f^i(\mathbf{k})$ . From Eq.(4.10), it is easy to calculate the scalar and pseudo scalar condensates. In terms of the ansatz functions  $\phi^i(\mathbf{k})$  and  $g^i(\mathbf{k})$  the scalar and pseudo scalar condensates for the  $i$ -th flavor can be respectively written as

$$\langle \bar{\psi}\psi \rangle_i = -\frac{2N_c}{(2\pi)^3} \int d\mathbf{k} \cos \phi^i \cos 2g^i (1 - n_-^i - n_+^i) \equiv -I_s^i, \quad (4.12)$$

$$\langle \bar{\psi}\gamma_5\psi \rangle_i = -i\frac{2N_c}{(2\pi)^3} \int d\mathbf{k} \sin 2g^i (1 - n_-^i - n_+^i) \equiv -iI_p^i, \quad (4.13)$$

where  $n_{\mp}^i = \sin^2 \theta_{\mp}^i$ . Thus a non vanishing  $I_s^i$  will imply CSB phase while a non vanishing  $I_p^i$  or equivalently  $g^i(\mathbf{k})$  will indicate  $CP$  violating phase. The condensate functions  $\phi^i(\mathbf{k})$ ,  $g^i(\mathbf{k})$  as well as the thermal functions  $\theta_{\mp}^i(\mathbf{k}, \beta, \mu)$  will be determined from the minimization of the thermodynamic potential which we shall carry out in the following section.

### 4.3 Effective potential and gap equations

Here, we shall evaluate the thermodynamic potential and the minimization of the same will lead us to the mass gap equations for the scalar and the pseudo scalar condensates. The thermodynamic potential is given by

$$\Omega = \epsilon - \mu\rho - \frac{S}{\beta}, \quad (4.14)$$

where  $\epsilon$  is the energy density,  $\mu$  is the quark chemical potential,  $\rho$  is the quark number density and  $S$  is the entropy density.  $\beta = 1/T$  is the inverse of temperature. The energy density  $\epsilon$  is given by the expectation value of the Hamiltonian corresponding to the Lagrangian given in Eq.(4.2) with respect to the thermal ground state  $|\Omega_{\beta,\mu}\rangle$  of Eq.(4.8). The energy density can be written as

$$\epsilon = T + V = T + V_S + V_D \quad (4.15)$$

where  $T$  is the expectation value of the kinetic term in Eq.(4.2) and using Eq.(4.10), it can be written as

$$\begin{aligned} T &= \langle \psi^\dagger (-i\boldsymbol{\alpha} \cdot \boldsymbol{\nabla} + \beta m) \psi \rangle \\ &= \frac{2N_c}{(2\pi)^3} \sum_i \int d\mathbf{k} (m^i \cos \phi^i + |\mathbf{k}| \sin \phi^i) \cos 2g^i (n_-^i + n_+^i - 1), \end{aligned} \quad (4.16)$$

where  $n_{\mp}^i = \sin^2 \theta_{\mp}^i$ .  $V_S$  is the contribution from the four point interaction term  $\sim G$  in Eq.(4.2) to the energy density and using Eq.(4.10), this can be written as

$$V_S = -2G \sum_i \left[ I_s^{i2} + I_p^{i2} \right]. \quad (4.17)$$

Finally,  $V_D$  is the contribution from the six point KMT term  $\sim K$  in Eq.(4.2) and using Eq.(4.10), it can be written as

$$V_D = 2K \left[ \cos \theta \left\{ \frac{|\epsilon_{ijk}|}{2} I_s^i I_p^j I_p^k - \prod_{i=1}^3 I_s^i \right\} + \sin \theta \left\{ \frac{|\epsilon_{ijk}|}{2} I_s^i I_s^j I_p^k - \prod_{i=1}^3 I_p^i \right\} \right] \quad (4.18)$$

The quark number density  $\rho$  is given by

$$\rho = \sum_{i=u,d,s} \langle \psi^\dagger \psi \rangle_i = \frac{2N_c}{(2\pi)^3} \sum_{i=u,d,s} \int d\mathbf{k} (1 - n_+^i + n_-^i). \quad (4.19)$$

The entropy density  $S$  is given as

$$S = \frac{2N_c}{(2\pi)^3} \sum_{i=u,d,s} \int d\mathbf{k} [n_-^i \ln n_-^i + (1 - n_-^i) \ln(1 - n_-^i) + (- \rightarrow +)]. \quad (4.20)$$

So the thermodynamic potential  $\Omega$  given in Eq.(4.14) is known in terms of the ansatz functions  $\phi^i(\mathbf{k})$ ,  $g^i(\mathbf{k})$  and  $\theta_{\mp}^i(\mathbf{k}, \beta, \mu)$ . Minimization of  $\Omega$  with respect to  $\phi^i(\mathbf{k})$  and  $g^i(\mathbf{k})$  respectively leads to

$$\tan \phi^i = \frac{|\mathbf{k}|}{M_s^i} \quad \text{and} \quad \tan 2g^i = \frac{M_p^i}{\sqrt{M_p^{i2} + |\mathbf{k}|^2}}, \quad (4.21)$$

where  $M_s^i$  and  $M_p^i$  are respectively the contributions to the constituent quark mass of the  $i$ -th flavor from the scalar and pseudo scalar condensates and they

are given by

$$\begin{aligned} M_s^i &= m^i + 4GI_s^i + K|\epsilon_{ijk}|\{\cos\theta(I_s^j I_s^k - I_p^j I_p^k) - \sin\theta(I_s^j I_p^k + I_p^j I_s^k)\}, \\ M_p^i &= 4GI_p^i - K|\epsilon_{ijk}|\{\cos\theta(I_s^j I_p^k + I_p^j I_s^k) - \sin\theta(I_p^j I_p^k - I_s^j I_s^k)\}. \end{aligned} \quad (4.22)$$

Minimizing  $\Omega$  with respect to the thermal ansatz functions  $\theta_{\pm}^i$  leads to

$$\sin^2 \theta_{\pm}^i = \frac{1}{\exp(\omega^i \mp \mu^i) + 1}, \quad (4.23)$$

where  $\omega^i(\mathbf{k}) = \sqrt{\mathbf{k}^2 + M^i{}^2}$  is the excitation energy of the  $i$ -th flavor with quark mass  $M^i$  where  $M^i = \sqrt{M_s^i{}^2 + M_p^i{}^2}$ . So it is evident that the constituent quark masses get contribution from both the scalar and pseudo scalar condensates.

Using Eq.(4.21), in Eq.s(4.12,4.13), the scalar and pseudo scalar condensates can be written as

$$I_s^i \equiv -\langle \bar{\psi}\psi \rangle_i = \frac{2N_c}{(2\pi)^3} \int d\mathbf{k} (1 - n_-^i - n_+^i) \frac{M_s^i}{\omega^i} \quad (4.24)$$

$$I_p^i \equiv i\langle \bar{\psi}\gamma_5\psi \rangle_i = \frac{2N_c}{(2\pi)^3} \int d\mathbf{k} (1 - n_-^i - n_+^i) \frac{M_p^i}{\omega^i}. \quad (4.25)$$

So from Eq.s(4.24,4.25), we can see that Eq.(4.22) represents the coupled self consistent equations for the scalar mass gap  $M_s^i$  and the pseudo scalar mass gap  $M_p^i$ . Using Eq.(4.22) and the extremized solution for the condensate functions from Eq.(4.21), the thermodynamic potential in Eq.(4.14) can be rewritten as

$$\begin{aligned} \Omega &= -\frac{2N_c}{(2\pi)^3} \sum_i \int d\mathbf{k} (\omega^i - |\mathbf{k}|) + 2G_s \sum_i [I_s^i{}^2 - I_p^i{}^2] + \sum_i M_p^i I_p^i \\ &\quad + 4K \cos\theta \prod_{i=1}^3 I_s^i - 2K \sin\theta \left[ \prod_{i=1}^3 I_p^i + \frac{1}{2} |\epsilon_{ijk}| I_s^i I_s^j I_p^k \right] \\ &\quad - \frac{2N_c}{\beta(2\pi)^3} \sum_i \int d\mathbf{k} \left[ \ln \{1 + e^{-\beta(\omega^i - \mu^i)}\} + \ln \{1 + e^{-\beta(\omega^i + \mu^i)}\} \right] \end{aligned} \quad (4.26)$$

In Eq.(4.26), we have subtracted the perturbative vacuum energy density contribution. It is important to mention here that the effective potential can also be evaluated at a mean field level after performing a chiral transformation for

the quarks so as to remove it from the KMT term [104, 106].

So we have Eq.(4.22) for the mass gap and Eq.(4.26) for  $\Omega$ . We shall solve Eq.(4.22) self consistently and calculate  $\Omega$  from Eq.(4.26) using the solutions for  $M_s^i$  and  $M_p^i$ . In the next section, this will be done and the resulting phase structure will be discussed.

## 4.4 Analysis of the phase structure

For numerical analysis, we have to fix the parameters of the 3-flavor NJL model. The model that we have considered here is similar to that we considered in the previous chapter while discussing CSB in presence of magnetic field. The only difference is the phase factor in the KMT term that we have taken here to incorporate the effect of  $CP$  violation. Here also, we have assumed isospin symmetry for the two lightest flavors with  $m_u = m_d$ . So we have to fix the same parameters here that we fixed in chapter-3. We have five parameters in total, namely the current quark masses for the non strange and strange quarks,  $m_q$  and  $m_s$ , the two couplings  $G$ ,  $K$  and the three momentum cutoff  $\Lambda$ . Here, we have chosen the same values of the parameters as in chapter-3. So we have  $\Lambda = 0.6023$  GeV,  $G\Lambda^2 = 1.835$ ,  $K\Lambda^5 = 12.36$ ,  $m^q = 5.5$  MeV and  $m^s = 0.1407$  GeV [89]. With these parameters, the constituent masses of the lightest quarks turn out to be  $M^{u,d} = 0.368$  GeV for quarks, while the same for strange quark turns out to be  $M^s = 0.549$  GeV, at  $T = \mu = 0$ .

For a given temperature  $T$  and the quark chemical potential  $\mu_q$ , we solve the coupled gap equations in Eq.(4.22) self consistently. Since we have assumed  $m^u = m^d$ , there are actually four coupled equations: two for the scalar condensates related to the two masses  $M_s^u = M_s^d$ ,  $M_s^s$  and two equations for the pseudo scalar condensate related to the corresponding mass parameters  $M_p^u = M_p^d$ ,  $M_p^s$ . The solutions to these equations are used to calculate  $\Omega$ . If there are more than one solutions, the one with the minimum  $\Omega$  is chosen.

Let us first discuss the ground state structure at  $T = \mu_q = 0$ . In the left panel of Fig.[4.1], the theta dependence of contributions to  $M^u$  from the scalar

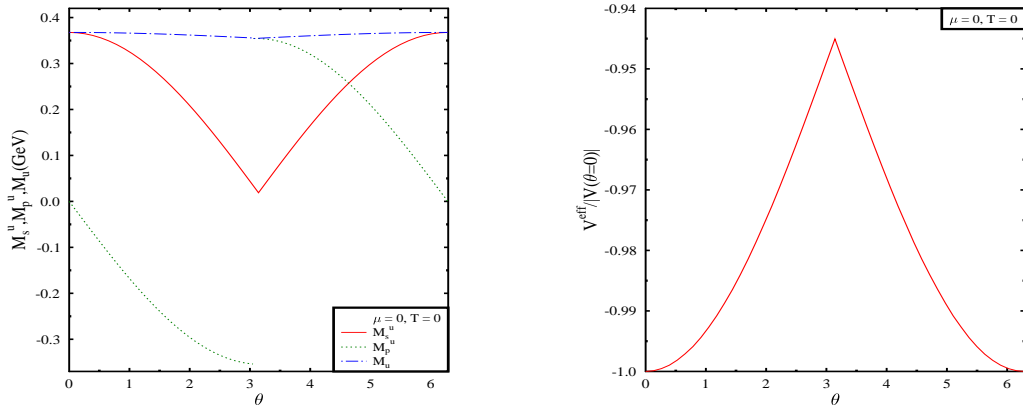


Figure 4.1:  $\theta$  dependence of scalar and pseudo scalar condensates for  $u$  quark (left panel) and the effective potential (right panel) at  $T = \mu_q = 0$ .

and pseudo scalar condensates are shown. As  $\theta$  increases the condensates in the two channels behave in a complimentary manner. While the contribution from the scalar condensates decreases with  $\theta$  (till  $\theta = \pi$ ), the pseudo scalar contribution increases so that the constituent quark mass  $M = \sqrt{M_s^2 + M_p^2}$  remains almost the same. Spontaneous CP violation is clearly seen for  $\theta = \pi$  with two degenerate solutions for  $M_p^u$  differing by a sign. The right panel of Fig.[4.1] shows the effective potential as a function of  $\theta$ . The effective potential is normalized with respect to the same at  $\theta = 0$ . The minimum of the potential is at  $\theta = 0$  which is consistent with the Vafa-Witten theorem and has a cusp at  $\theta = \pi$  which has also been observed in 2-flavor NJL model [104].

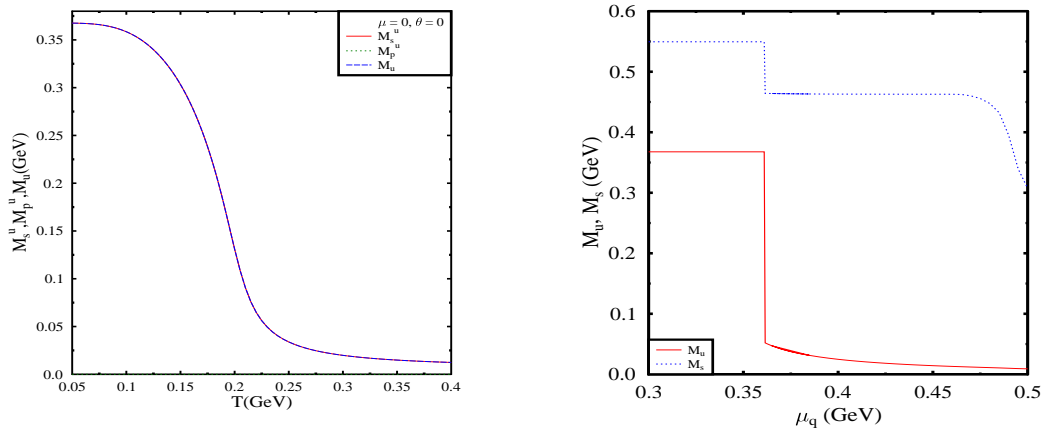


Figure 4.2: (Left panel) Temperature dependence of the constituent mass of  $u$  quark for  $\theta = \mu_q = 0$ . (Right panel) Constituent mass of  $u$  and  $s$  quark as functions of chemical potential at  $\theta = T = 0$ .

In Fig.[4.2], we show the temperature dependence of  $M^u$  at  $\theta = \mu_q = 0$

(left panel) and the dependence of  $M^u$  and  $M^s$  on  $\mu_q$  at  $\theta = T = 0$  (right panel). In both cases, the pseudo scalar channel contributes nothing and the constituent mass is equal to the contribution from the scalar channel. As expected, the chiral transition with temperature is a crossover. For finite density at  $T = 0$ , the (approximate) first order chiral transition takes place at  $\mu \sim 361$  MeV for  $u$  and  $d$  quarks with their masses decreasing discontinuously to  $M^{u,d} \sim 52$  MeV from their vacuum value of  $M^{u,d} = 368$  MeV. Because of the flavor mixing KMT term, this decrease is reflected also in the decrease in the strange quark mass to  $M^s = 464$  MeV from its vacuum value of  $M^s = 549$  MeV. These results are similar to the results obtained in the previous chapter while studying CSB in presence of magnetic field without the  $CP$  violating parameter  $\theta$ . These results are also similar to the results obtained in the context of color superconductivity in NJL model with a KMT term [107].

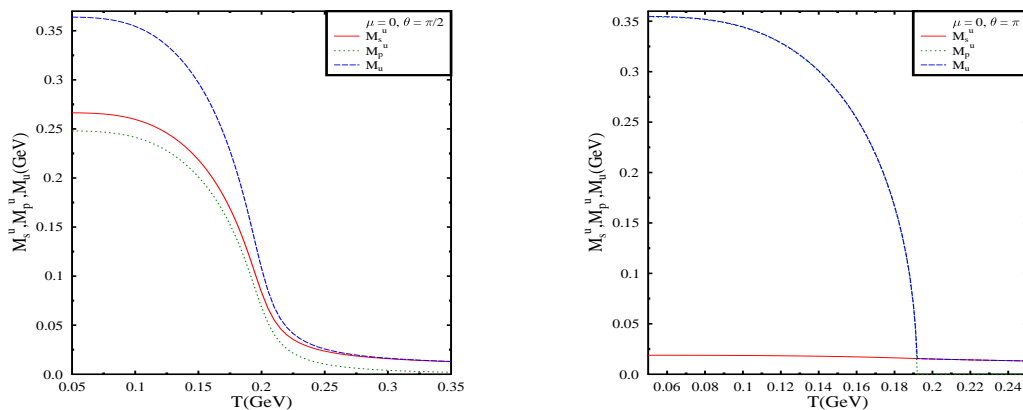


Figure 4.3: Constituent mass of  $u$  quark and the contributions from scalar and pseudo scalar condensates as a function of temperature at  $\mu_q = 0$  for  $\theta = \pi/2$  (left panel) and  $\theta = \pi$  (right panel).

Next we discuss the variations of the contributions from scalar and pseudo scalar condensates with temperature at  $\mu_q = 0$  for non zero values of  $\theta$ . The pseudo scalar contribution is non zero for  $\theta \neq 0$ . For  $\theta = \pi/2$ , masses arising from both type of condensates are shown in the left panel of Fig.[4.3]. Here, both the scalar and pseudo scalar masses show a crossover transition as temperature is increased. In the right panel of Fig.[4.3], the behavior of the masses for  $\theta = \pi$  is shown. The scalar contribution becomes negligible as compared

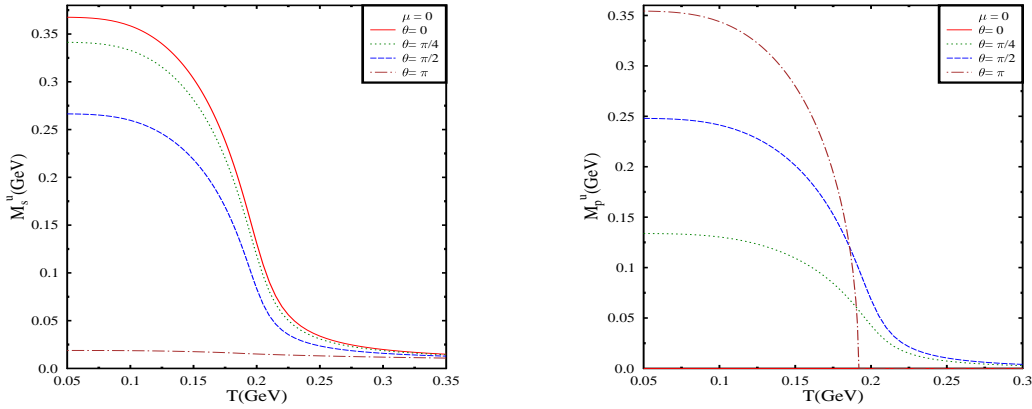


Figure 4.4: *The nature of transition of the scalar (left panel) and pseudo scalar (right panel) condensates with temperature at  $\mu_q = 0$  for different values of  $\theta$ .*

to the pseudo scalar contribution at  $\theta = \pi$  which is exactly the opposite to the case for  $\theta = 0$ . The pseudo scalar mass shows a second order transition at  $\theta = \pi$  instead of a crossover which was case for  $\theta = \pi/2$ . This feature is elaborated in Fig.(4.4) where  $\theta$  dependence of the nature of transition with temperature is shown for both scalar and pseudo scalar condensates at  $\mu_q = 0$ . The left panel of Fig.[4.4] shows the  $\theta$  dependence of the transition for the scalar condensate. The transition is always a crossover for scalar condensate. This is not the case for the pseudo scalar condensate which shows a second order transition at  $\theta = \pi$  and a crossover for other non zero values of  $\theta$ . This result is similar to the results obtained in 2-flavor NJL model [105]. This change in nature of the transition has been observed also in the linear sigma model but there the transition at  $\theta = \pi$  is a first order transition [102]. The reason behind such different behavior regarding the order of the transition is due to the non analytic vacuum term in the NJL model [105]. The  $CP$  restoring transition temperature for  $\mu_q = 0$  turns out to be 192 MeV. However, the constituent mass remains non zero as the scalar condensate remains non vanishing due to non zero current quark masses. This high temperature restoration of  $CP$  is expected as the instanton effects responsible for  $CP$  violation become suppressed exponentially at high temperature [6].

Next we consider the effect of nonzero density at  $T = 0$ . In Fig.(4.5), we show the variation of constituent masses of  $u$  and  $s$  quarks with  $\mu_q$  along with

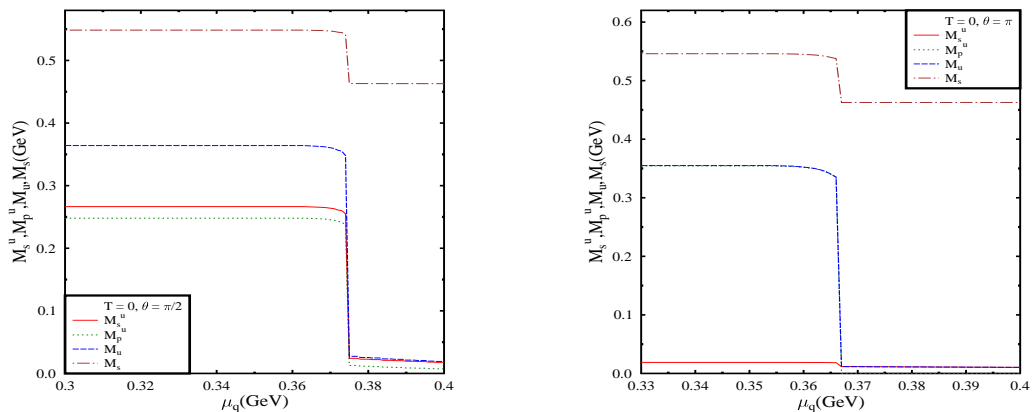


Figure 4.5: *Constituent masses of  $u$  and  $s$  quarks along with the contributions from scalar and pseudo scalar channels as functions of quark chemical potential  $T = 0$  for  $\theta = \pi/2$  (left panel) and  $\theta = \pi$  (right panel). The pseudo scalar contribution for strange quarks is negligible in this range of chemical potential.*

the variation of the contributions from scalar and pseudo scalar condensates at  $T = 0$  for  $\theta = \pi/2$  (left panel) and  $\theta = \pi$  (right panel). For  $\theta = \pi/2$ , the critical chemical potential for chiral transition is  $\mu_c \sim 375$  MeV where the mass contributions from scalar and pseudo scalar condensate become 24 MeV and 12 MeV respectively from their vacuum values of 266 MeV and 248 MeV. The total mass for the  $u$  and  $d$  quarks become 27 MeV from its vacuum value of 364 MeV. On the other hand the contribution of the pseudo scalar condensate to the strange quark mass is negligible ( $\sim 12$  MeV) compared to the contribution from the scalar condensate ( $\sim 548$  MeV). Because of flavor mixing, strange quark mass also falls to 463 MeV at  $\mu_c = 375$  MeV. For  $\theta = \pi$  the scalar condensate almost vanishes but for the non zero current quark masses while the contributions to the constituent masses of  $u$  and  $d$  quarks come solely from the pseudo scalar condensate as shown in the right panel of Fig.[4.5]. However, the strange quark mass gets almost no contribution from the pseudo scalar channel as  $CP$  violation is not expected to happen for strange quark in the chemical potential range that we are considering. As  $\mu_q$  is increased there is a first order transition at  $\mu_c \sim 368$  MeV. At  $\mu_c$  the pseudo scalar condensate vanishes and the contribution to quark mass arises solely from the scalar condensate which is non vanishing because of the nonzero current quark masses.

Though the  $CP$  restoring transition with  $\mu_q$  is first order at  $T = 0$ , it becomes a second order transition at high temperature. This change in nature of the transition is shown in the left panel of Fig.(4.6) where we have shown the dynamical mass,  $M_p^u$  arising from the pseudo scalar condensate as a function of  $\mu_q$  for different temperatures for  $\theta = \pi$ . While at zero temperature, the order parameter decreases discontinuously, as the temperature increases, it becomes less sharp and finally results in a second order transition at high temperature.

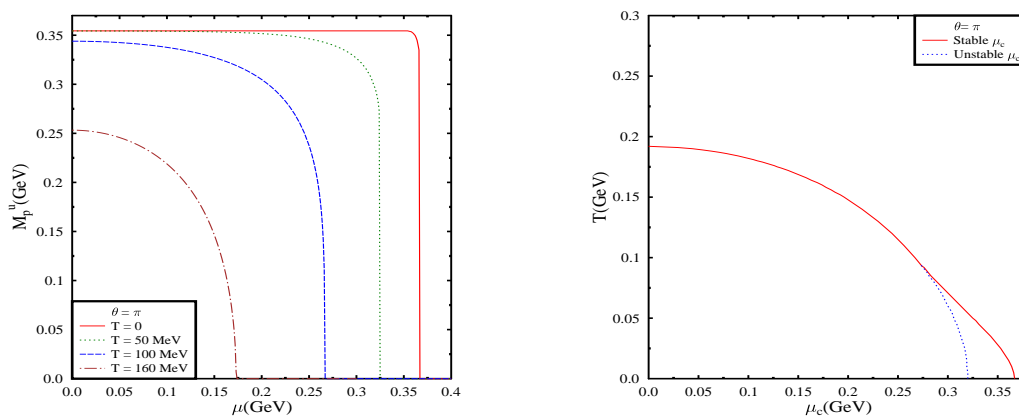


Figure 4.6: (Left Panel) Contribution from the pseudo scalar condensates to the  $u$  quark mass as a function of  $\mu_q$  for different temperatures for  $\theta = \pi$ . (Right panel) The phase diagram for  $CP$  restoring transition in the  $T - \mu$  plane for  $\theta = \pi$ . The region between the solid line and the dotted line represents the unstable  $CP$  restored phase with  $\Omega$  higher than the  $CP$  violated phase.

In the right panel of Fig.(4.6), we show the phase diagram in the  $T - \mu$  plane for the  $CP$  restoring transition for  $\theta = \pi$ . Since the transition is first order at  $T = 0$  and second order at  $\mu_q = 0$ , there is a tri-critical point for this transition in this plane. This turns out to be  $(\mu_c, T_c) = (273, 94)$  MeV. Including Polyakov loop in the two flavor NJL model, such a tri-critical point occurs at  $(209, 165)$  MeV [106]. First order transitions are associated with existence of metastable states where  $CP$  is restored. However the pressure for these metastable lower than the  $CP$  broken phase. In the phase diagram that we have shown, such metastable states exist in the region between solid line and the dotted line.

## 4.5 Summary

In this chapter, we have studied the effects of  $CP$  violation and the interplay of  $CP$  violation and CSB in quark matter at finite temperature and density. For this, we have adopted 3-flavor NJL model with the KMT determinant interaction term. The effect of  $CP$  violation is included through a phase  $\theta$  in the KMT term. The thermal ground state is obtained through successive Bogoliubov transformations of the perturbative vacuum  $|0\rangle$  for including the effects of both CSB and  $CP$  violation.  $CP$  violation takes place through the pseudo scalar channel and the CSB happens through the scalar channel. The scalar and pseudo scalar mass gap equations are obtained from the minimization of the thermodynamic potential  $\Omega$  with respect to the condensate functions. These gap equations are solved self consistently and  $\Omega$  is calculated numerically using the solutions to check the thermodynamic stability.

For  $\theta = 0$ , we have not observed any  $CP$  violation which is perfectly in accordance with the Vafa-Witten theorem [38]. For  $\theta = \pi$ , we have observed spontaneous  $CP$  violation and degenerate vacuum states are formed. This is exactly what is expected from Dashen phenomenon [41]. This has been observed in 2-flavor NJL model also [104]. The effective potential is minimum for  $\theta = 0$  and has a cusp at  $\theta = \pi$ . The CSB and  $CP$  violation behaves in a somewhat complimentary manner as CSB solely accounts for the constituent masses for  $\theta = 0$  and the chiral symmetry gets almost restored for  $\theta = \pi$ . The constituent mass remains almost the same for different values of  $\theta$ .

At finite temperature also, CSB and  $CP$  violation exhibits the same complimentary behavior. At finite temperature, the  $CP$  restoring transition is a crossover similar to the chiral transition for  $\theta \neq \pi$  at zero density. However, at  $\theta = \pi$ , the transition becomes a second order one unlike the case in linear sigma model where it becomes a first order one for  $\theta = \pi$  [102]. The chiral transition at finite temperature remains a crossover for all values of  $\theta$  at zero density.

At finite chemical potential, the  $CP$  restoring transition is a first order

transition for all values of  $\theta$  at  $T = 0$ . However, at high temperature, it becomes a second order transition. In the range of chemical potential that we have considered, there is negligible contribution from the pseudo scalar condensates to the strange quark mass. In this range, the  $CP$  violating effects on the constituent mass of strange quark can be neglected though strange quark affects the other quarks through the KMT term.

We have also shown the phase diagram for the  $CP$  restoring transition in the  $T - \mu$  plane. There exist a tri-critical point at  $(\mu_c, T_c) = (273, 94)$  MeV in this plane because of the different nature of transition at finite temperature and finite density. This tri-critical point turns out to be at  $(209, 165)$  MeV in 2-flavor PNJL model [106]. We have also observed region with the existence of metastable states in the phase diagram. These metastable states arise when the transition is a first order one.

This study is important in the context of heavy ion collision experiments and the compact stars. However, strong magnetic fields are associated with both cases. So for a more complete study, the effect of magnetic field should be included which has been done in linear sigma model [102]. In the context of heavy ion collision experiments, the effect of deconfinement phase transition should be considered which has been studied in 2-flavor PNJL model [106].

# Chapter 5

## Summary and outlook

This thesis covers the studies on some aspects of matter under the influence of extreme conditions such as high temperature, high density as well as strong magnetic fields. The main motivation of our work was to analyze some phases that have been conjectured in the QCD phase diagram. Because of the non-perturbative nature of the strong interaction, these phases are usually studied using either lattice QCD or effective models. However, because of the limitations of lattice QCD in the finite density regime, it can not be employed to study the finite density phases. In our analysis, we resort to effective models. Here, we have discussed three different aspects: (i) the transition from BCS type superconducting state at weak coupling to BEC type spatially localized bound state for strong coupling for a relativistic fermionic system, (ii) CSB in presence of magnetic field and (iii) the interplay of CSB and strong  $CP$  violation at finite temperature and density. For studying the BCS-BEC crossover, we have used a general model with two species of relativistic fermions with or without a mismatch in their relative population. While analyzing the effects of magnetic field on CSB, we have used the 3-flavor NJL model with a KMT determinant interaction term which causes flavor mixing. We have used the same model also to study the interplay between CSB and strong  $CP$  violation with the effect of  $CP$  violation being incorporated through a  $CP$  violating phase in the KMT term. Throughout our analysis, our approach has been variational. This involves constructing a ground state explicitly in

terms field operators acting on the perturbative vacuum state  $|0\rangle$  for each case. The effect of temperature is included through a unitary transformation on the ground state where the unitary operator encodes the effect of temperature within the framework of thermo-field dynamics method. The ansatz functions and the thermal distribution functions are determined from minimization of the thermodynamic potential. While our methodology is non perturbative, it is limited by the choice of the ansatz for the ground state.

In chapter-2, we have discussed the BCS-BEC crossover with two species of relativistic fermions. We considered a relativistic Lagrangian with four fermion interaction term. We have considered particle-particle and antiparticle-antiparticle pairing for the ground state.

First, we studied the BCS-BEC transition within the mean field approximation where the condensate field is treated as a classical auxiliary field and its expectation value is taken to be constant. The thermal ground state is constructed from the vacuum  $|0\rangle$  through a thermal Bogoliubov transformation. The ansatz functions and the superfluid gap equation are obtained by minimizing the thermodynamic potential. This gap equation is solved self consistently to see the transition.

The transition from BCS to BEC phase is observed to be a crossover similar to the case with cold atoms. It is observed that the antiparticle degrees of freedom plays a significant role even for  $k_f/m \ll 1$ , particularly for large values of  $\eta \equiv 1/k_f a$ . For a mismatch in chemical potentials of the two species, we have not observed any gapless modes in the BCS regime but in the deep BEC regime gapless modes with one Fermi surface have been observed. We have not seen any breached pairing modes with two Fermi surfaces. The phase structure is qualitatively similar to that obtained in a boson-fermion model [59].

Then we extended our study to see the crossover beyond the mean field approximation by treating the condensate field as a dynamical bosonic field in a model with quartic self interactions of the boson field. The scalar field mass gap was also calculated self consistently. A decrease in the critical temperature

in the BEC regime is observed. It is observed that the transition can be a first order one for larger quartic coupling.

Our study is important in the context of cold dense matter where these superfluid phases might be realized. The results obtained here is limited by our choice of ansatz. We have not considered an ansatz with non zero momentum of the Cooper pair like the FFLO condensate which would give rise to crystalline superconductivity. Our study can be extended to a more phenomenological models like the NJL model. Nevertheless, the results we obtained here can serve as a good reference solution in the appropriate limit with which the results obtained from a more generalized ansatz for the ground state can be compared.

In chapter-3, we have analyzed the effects of magnetic field on CSB within a framework of 3-flavor NJL model. Here, we have included the KMT determinant interaction term which causes flavor mixing. In contrast with our analysis of BCS-BEC crossover, here we have considered quark-antiquark terms in the Lagrangian which is relevant for CSB. We have explicitly calculated the Dirac spinors in presence of magnetic field. The thermal ground state is constructed in a similar manner to that in the study of BCS-BEC crossover with the difference being our choice of ansatz which here, accounts for the quark-antiquark pairing. The ansatz functions and the mass gap equation is obtained from the minimization of the thermodynamic potential and solved in a self consistent manner.

We have observed the magnetic catalysis of CSB at finite temperature. At zero baryon density, the transition from the chiral symmetry broken phase to the chiral symmetry restored phase with temperature remains a crossover even for magnetic field as high as  $eB = 10m_\pi^2$ . The chiral transition with density is observed to be a first order transition for the two lightest flavors at  $T = 0$ . The effect of flavor mixing through the KMT term is reflected in the drop of strange quark mass at the critical chemical potential  $\mu_c$  for the first order transition for the two lightest flavors.  $\mu_c$  is seen to decrease with increase in the strength of magnetic field which has been observed in case of holographic

QCD also and is termed as inverse magnetic catalysis (IMC) [28]. However, we observe that the first order transition becomes stronger with increase in magnetic field leading to a smaller value of the quark mass. This in turn leads to a larger baryon density as compared to the zero field case at the transition chemical potential  $\mu_c$ . At  $T = 0$ , for non zero magnetic field, the quark masses oscillate rapidly for  $\mu > \mu_c$  similar to the de Haas van Alphen effect in metals.

When the charge neutrality condition is imposed, the critical chemical potential  $\mu_c$  increases slightly as compared to the same when charge neutrality condition is not imposed. At finite temperature, the transition becomes smoother and the kink structure in the quark masses arising from Landau quantization disappears. For charge neutral matter, the equation of state becomes more steep if the magnetic field is increased. We have also observed the anisotropy in the hydrodynamic pressure due to significant magnetization of quark matter in presence of very strong magnetic field. The pressure in the direction of the magnetic field becomes large as compared to the same in the transverse direction to the magnetic field. This anisotropy becomes appreciable at magnetic field strength  $\sim 10^{18}$  Gauss. This can have possible ramification in the structural properties of highly magnetized compact stars. The magnetization also exhibits the de Haas van Alphen oscillation and consequently the pressure in the transverse direction to the magnetic field also shows oscillation.

We have analyzed CSB in presence of magnetic field both at finite temperature as well as finite densities so that, our results can be of relevance in the context of both heavy ion collision experiments and compact stars. However, our analysis is not complete even within the 3-flavor NJL model. We have considered here quark-antiquark pairing only with zero total momentum. However, the formation of spatially non homogeneous condensates with non zero net momentum is also possible [98]. We also have not considered the interplay of chiral transition and deconfinement transition in presence of magnetic field. This can be studied with Polyakov loop extended NJL (PNJL) model [99]. This is particularly important at finite temperature in the context

of heavy ion collision experiments. At finite density and low enough temperatures, the diquark condensates in presence of magnetic field can also be studied [82, 100] apart from the quark-antiquark condensates that have been investigated in this thesis.

In chapter-4, we have examined the effect of a  $CP$  violating  $\theta$ -term and the interplay of CSB and  $CP$  violation in the context of quark matter at finite temperature and density. Here also, we have used the 3-flavor NJL model with the KMT term with the effect of  $CP$  violation being simulated through a phase factor in the KMT term. We constructed the thermal ground state through a thermal Bogoliubov transformation of the vacuum  $|0\rangle$ . The ground state incorporates the scalar as well as the  $CP$  violating pseudo scalar condensates. The scalar and pseudo scalar mass gap equation is obtained from the minimization of the thermodynamic potential.

We have not observed any  $CP$  violation for  $\theta = 0$  which is consistent with the Vafa-Witten theorem [38]. Spontaneous  $CP$  violation is seen for  $\theta = \pi$  in accordance with the Dashen phenomenon [41]. This is qualitatively opposite to the CSB which is dominant for  $\theta = 0$  and negligible for  $\theta = \pi$ . In between, both CSB and  $CP$  violation contribute to the constituent quark mass. With temperature, the transition from the  $CP$  violating phase to the  $CP$  restored phase is a crossover for  $\theta < |\pi|$ . However, at  $\theta = \pi$ , the transition is a second order transition unlike the case with linear sigma model, where a first order transition has been observed [102]. With density, the transition is seen to be a first order transition at  $T = 0$  and becomes a second order transition when the temperature is increased. In the range of temperature and chemical potential that we have considered, the effect of  $CP$  violation on the strange quark is negligible but it does affect the  $u$  and  $d$  quarks through the KMT term. We have also shown the phase diagram for  $\theta = \pi$  where a tri-critical point,  $(\mu_c, T_c) = (273, 94)$  MeV, exists because of the different nature of transition at zero density and zero temperature.

Our result is important in the context of the present heavy ion collision experiments at LHC and RHIC as well as the future planned experiments

with finite density like FAIR, NICA and BES at RHIC. However, the effect of confinement which we have not considered here should also be taken into account and the effect of magnetic field should be studied in order to get a complete picture.

Thus we have presented here, our analysis of some phases relevant for the QCD phase structure as a function of temperature, density as well as strong magnetic fields. While the variational method that we have used and a simplified ansatz for the ground state within NJL type of models show a rich phase structure, it also calls for more reliable and systematic non perturbative techniques to be developed so as to lead us to a more complete understanding of properties of matter under the influence of extreme conditions.

# Bibliography

- [1] S. Glashow, Nucl. Phys. **22**, 579 (1961); S. Weinberg, Phys. Rev. Lett. **19**, 1264 (1967); A. Salam in Elementary particle physics ed. N. Svarthom pg. 367.
- [2] D. Gross and F. Wilczek, Phys. Rev. Lett. **30**, 1343 (1973); H. D. Politzer, Phys. Rev. Lett. **30**, 1346 (1973).
- [3] Y. Dokshitzer, Sov. Phys. JETP, **46**, 641 (1977); V. Gribov and L. Lipatov, Sov. J. Nucl. Phys. **15**, 438 (1972); G. Altarelli and G. Parisi, Nucl. Phys. B **126**, 298 (1977).
- [4] K. Wilson, Phys. Rev. D **10**, 2445 (1974).
- [5] A. Polyakov, Phys. Lett. B **72**, 477 (1978).
- [6] D. Gross, R. Pisarski and L. Yaffe, Rev. Mod. Phys. **53**, 43 (1981);
- [7] L. Yaffe and B. Svetitsky, Phys. Rev. D **26**, 963 (1982).
- [8] P. Powell and G. Baym, arXiv:1111.5911 [hep-ph].
- [9] D. Bandyopadhyaya, S. Chakrabarty and S. Pal, Phys. Rev. Lett. **79**, 2176 (1997); S. Chakrabarty and S. Mandal, Phys. Rev. C **75**, 015805 (2007).
- [10] D. Lai and S. Shapiro, Astrophys. J. **383**, 745 (1991); R. Duncan and C. Thompson, Astrophys. J. **392**, L9 (1992); Astrophys. J. **408**, 194 (1993); Mon. Not. R. Astron. Soc. **275**, 255 (1995); Astrophys. J. **473**, 322 (1996); C. Cardall, M. Prakash and J. Lattimer, Astrophys. J. **554**,

- 322 (2001); A. Broderick, M. Prakash and J. Lattimer, Phys. Lett. B **531**, 167 (2002).
- [11] D. Kharzeev, L. McLerran and H. Warringa, Nucl. Phys. A **803**, 227 (2008).
- [12] V. Skokov, A. Illarionov and V. Toneev, Int. J. Mod. Phys. A **24**, 5925 (2009).
- [13] Y. Nambu and G. Jona-Lasinio, Phys. Rev. **122**, 345 (1961); Y. Nambu and G. Jona-Lasinio, Phys. Rev. **124**, 246 (1961).
- [14] L. N. Cooper, Phys. Rev. **104**, 1189 (1956).
- [15] J. Bardeen, L. Cooper, and J. Schrieffer, Phys. Rev. **106**, 162 (1957); J. Bardeen, L. Cooper, and J. Schrieffer, Phys. Rev. **108**, 1175 (1957).
- [16] P. Meisinger and M. Ogilvie, Phys. Lett. B **379**, 163 (1996); K. Fukushima, Phys. Lett. B **591**, 277 (2004); C. Ratti, M. Thaler and W. Weise, Phys. Rev. D **73**, 014019 (2006); C. Sasaki, B. Friman and K. Redlich, Phys. Rev. D **75**, 074013 (2007); S. Rößner, C. Ratti and W. Weise, Phys. Rev. D **75**, 034007 (2007).
- [17] M. Alford, K. Rajagopal and F. Wilczek, Nucl. Phys. B **537**, 443 (1999).
- [18] B. Barrois, Nucl. Phys. B **129**, 390 (1977); D. Bailin and A. Love, Nucl. Phys. B **190**, 175 (1981); Nucl. Phys. B **205**, 119 (1982); Phys. Rep. **107**, 325 (1984).
- [19] H. Abuki, T. Hatsuda and K. Itakura, Phys. Rev. D **65**, 074014 (2002).
- [20] M. Kitazawa, D. Rischke and I. Shovkovy, Phys. Lett. B **663**, 228 (2008).
- [21] P. Fulde and R. Ferrel, Phys. Rev. A **135**, 550 (1964); A. Larkin, Y. Ovchinnikov, Sov. Phys. JETP **20**, 762 (1965);

- [22] E. Gubankova, W. Liu and F. Wilczek, Phys. Rev. Lett. **91**, 032001 (2003); M. Forbes, E. Gubankova, W. Liu and F. Wilczek, Phys. Rev. Lett. **94**, 017001 (2005).
- [23] Y. Aoki, et al., JHEP **0906**, 88 (2009); S. Borsanyi, et al., JHEP **1009**, 073 (2010).
- [24] S. Klevansky, Rev. Mod. Phys. **64**, 649 (1992).
- [25] V. Gusynin, V. Miranski and I. Shovkovy, Phys. Rev. Lett. **73**, 3499 (1994); Phys. Lett. B **349**, 477 (1995); Nucl. Phys. B **462**, 249 (1996); E. Ferrer and V. Incerra, Phys. Rev. Lett. **102**, 050402 (2009); Nucl. Phys. B **824**, 217 (2010); D. Ebert and K. Klimenko, Nucl. Phys. A **728**, 203 (2003).
- [26] E. Gorbar, V. Miransky and I. Shovkovy, Phys. Rev. C **80**, 032801(R) (2009).
- [27] J. Boomsma and D. Boer, Phys. Rev. D **81**, 074005 (2010).
- [28] F. Preis, A. Rebhan and A. Schmitt, JHEP **1103**, 033 (2011).
- [29] K. Fukushima, D. Kharzeev and H. Warringa, Phys. Rev. D **78**, 074033 (2008); Phys. Rev. Lett. **104**, 212001 (2010); D. Kharzeev and D. Son, Phys. Rev. Lett. **106**, 062301 (2011).
- [30] S. Adler, Phys. Rev. **177**, 2426 (1969); J. Bell and R. Jackiw, Nuovo Cimento A **60**, 47 (1969).
- [31] A. Belavin, A. Polyakov, A. Shvarts and Y. Tyupkin, Phys. Lett. B **59**, 85 (1975).
- [32] G. 't Hooft, Phys. Rev. Lett. **37**, 8 (1976).
- [33] G. 't Hooft, Phys. Rev. D **14**, 3432 (1976).
- [34] C. Baker, et al., Phys. Rev. Lett. **97**, 131801 (2006).

- [35] J. Kim and G. Carosi, *Rev. Mod. Phys.* **82**, 557 (2010).
- [36] S. Weinberg, *Phys. Rev. Lett.* **40**, 223 (1978); F. Wilczek, *Phys. Rev. Lett.* **40**, 279 (1978).
- [37] R. Peccei and H. Quinn, *Phys. Rev. Lett.* **38**, 1440 (1977); *Phys. Rev. D* **16**, 1791 (1977).
- [38] C. Vafa and E. Witten, *Phys. Rev. Lett.* **53**, 535 (1984); *Nucl. Phys. B* **234**, 173 (1984).
- [39] D. Son and M. Stephanov, *Phys. Rev. Lett.* **86**, 592 (2001).
- [40] T. Cohen, *Phys. Rev. D* **64**, 047704 (2001).
- [41] R. Dashen, *Phys. Rev. D* **3**, 1879 (1971).
- [42] T. Lee, *Phys. Rev. D* **8**, 1226 (1973); T. Lee and G. Wick, *Phys. Rev. D* **9**, 2291 (1974).
- [43] D. Kharzeev, R. Pisarski and M. Tytgat, *Phys. Rev. Lett.* **81**, 512 (1998).
- [44] B. Abelev et al. [STAR Collaboration], *Phys. Rev. Lett.* **103**, 251601 (2009); *Phys. Rev. C* **81**, 054908 (2010).
- [45] M. Kobayashi and T. Maskawa, *Prog. Theor. Phys.* **44**, 1422 (1970).
- [46] K. Rajagopal and F. Wilczek, hep-ph/0011333; D. Hong, *Acta Phys. Polon. B* **32**, 1253 (2001); M. Alford, *Ann. Rev. Nucl. Part. Sci.* **51**, 131 (2001); T. Schäfer, hep-ph/0304281; D. Rischke, *Prog. Part. Nucl. Phys.* **52**, 197 (2004); H. Ren, hep-ph/0404074; M. Huang, *Int. J. Mod. Phys. E* **14**, 675 (2005); I. Shovkovy, *Found. Phys.* **35**, 1309 (2005); M. Alford, A. Schmitt, K. Rajagopal and T. Schafer, *Rev. Mod. Phys.* **80**, 1455 (2008).
- [47] D. Son, *Phys. Rev. D* **59**, 094019 (1999).

- [48] D. Hong, V. Miransky, I. Shovkovy and L. Wijewardhana, *Phys. Rev. D* **61**, 056001 (2000); T. Schäfer and F. Wilczek, *Phys. Rev. D* **60**, 114033 (1999); S. Hsu and M. Schwetz, *Nucl. Phys. B* **572**, 211 (2000).
- [49] R. Pisarski and D. Rischke, *Phys. Rev. D* **60**, 094013 (1999); *Phys. Rev. D* **61**, 051501 (2000); *Phys. Rev. D* **61**, 074017 (2000).
- [50] K. Rajagopal and E. Shuster, *Phys. Rev. D* **62**, (2000) 085007.
- [51] T. Schwarz, S. Klevansky and G. Papp, *Phys. Rev. C* **60**, 055205 (1999).
- [52] M. Alford, K. Rajagopal and F. Wilczek, *Phys. Lett. B* **422**, 247 (1998); R. Rapp, T. Schäfer, E. Shuryak and M. Velkovsky, *Phys. Rev. Lett.* **81**, 53 (1998).
- [53] A. Bodmer, *Phys. Rev. D* **4**, 1601 (1971); E. Witten, *Phys. Rev. D* **30**, 272 (1984); C. Alcock, E. Farhi and A. Olinto, *Astrophys. J.* **310**, 261 (1986).
- [54] W. Liu and F. Wilczek, *Phys. Rev. Lett.* **90**, (2003) 047002; E. Gubankova, F. Wilczek and E. Mishchenko, *Phys. Rev. Lett.* **94**, 110402 (2005); E. Gubankova, E. Mishchenko and F. Wilczek, *Phys. Rev. B* **74**, 184516 (2006); E. Gubankova, A. Schmitt and F. Wilczek, *Phys. Rev. B* **74**, 064505 (2006).
- [55] B. Deb, A. Mishra, H. Mishra and P. Panigrahi, *Phys. Rev. A* **70**, 011604(R) (2004).
- [56] M. Kitazawa, D. Rischke and I. Shovkovy, *Phys. Lett. B* **663**, 228 (2008).
- [57] A. Rezaean and H. Pirner, *Nucl. Phys. A* **779**, 197 (2006).
- [58] G. Sun, L. He, and P. Zhuang, *Phys. Rev. D* **75**, 096004 (2007); L. He and P. Zhuang, *Phys. Rev. D* **76**, 056003 (2007).
- [59] J. Deng, A. Schmitt and Q. Wang, *Phys. Rev. D* **76**, 034013 (2007).

- [60] L. He and P. Zhuang, Phys. Rev. D **75**, 096003 (2007); Y. Nishida and H. Abuki, Phys. Rev. D **72**, 096004 (2005); H. Abuki, Nucl. Phys. A **791**, 117 (2007).
- [61] J. Deng, J. Wang and Q. Wang, Phys. Rev. D **78**, 034014 (2008).
- [62] T. Brauner, Phys. Rev. D **77**, 096006 (2008).
- [63] K. Rajagopal and A. Schmitt, Phys. Rev. D **73**, 045003 (2006).
- [64] A. Mishra and H. Mishra, Eur. Phys. J. D **53**, 75 (2009).
- [65] M. Mannarelli, G. Nardulli and M. Ruggieri, Phys. Rev. A **74**, 033606 (2006).
- [66] H. Mishra and J. Parikh, Nucl. Phys. A **679**, 597 (2001); A. Mishra and H. Mishra, Phys. Rev. D **71**, 074023 (2005).
- [67] A. Mishra and H. Mishra, Phys. Rev. D **69**, 014014 (2004).
- [68] H. Umezawa, H. Matsumoto and M. Tachiki, Thermofield Dynamics and Condensed States (North-Holland, Amsterdam, 1982); P. Henning, Phys. Rep. **253**, 235 (1995); A. Mishra and H. Mishra, J. Phys. G **23**, 143 (1997).
- [69] C. Sa de Melo, M. Randeria and J. Engelbrecht, Phys. Rev. Lett. **71**, 3202 (1993).
- [70] S. Chang, J. Carlson, V. Pandharipande and K. Schmidt, Phys. Rev. A **70**, 043602 (2004); J. Carlson and S. Reddy, Phys. Rev. Lett. **95**, 060401 (2005); Y. Nishida and D. Son, Phys. Rev. Lett. **97**, 050403 (2006); G. Rupak, T. Schafer and A. Kryjevski, Phys. Rev. A **75**, 023606 (2007); J. Chen and E. Nakano, Phys. Rev. A **75**, 043620 (2007).
- [71] G. Amelino-Camelia and S. Pi, Phys. Rev. D **47**, 2356 (1993); D. Rischke and J. Lenaghan, J. Phys. G **26**, 431 (2000).

- [72] I. Giannakis, D. Hou, H. Ren and D. Rischke, *Phys. Rev. Lett.* **93**, 232301 (2004).
- [73] I. Giannakis and H. Ren, *Phys. Lett. B* **611**, 137 (2005); *Nucl. Phys. B* **723**, 255 (2005).
- [74] D. Kharzeev, *Annals Phys.* **325**, 205 (2010); M. D'Elia, S. Mukherjee and F. Sanfilippo, *Phys. Rev. D* **82**, 051501 (2010).
- [75] A. Mizher, M. Chenodub and E. Fraga, *Phys. Rev. D* **82**, 105016 (2010).
- [76] K. Fukushima, M. Ruggieri and R. Gatto, *Phys. Rev. D* **81**, 114031 (2010).
- [77] E. Ferrer, V. Incera, J. Keith, I. Portillo and P. Springsteen, *Phys. Rev. C* **82**, 065802 (2010).
- [78] X. Huang, M. Huang, D. Rischke and A. Sedrakian, *Phys. Rev. D* **81**, 045015 (2010).
- [79] D. Menezes, M. Benghi Pinto, S. Avancini, A. Martinez and C. Providencia, *Phys. Rev. C* **79**, 035807 (2009); D. Menezes, M. Benghi Pinto, S. Avancini and C. Providencia, *Phys. Rev. C* **80**, 065805 (2009).
- [80] K. Bhattacharya, arXiv:0705.4275 [hep-th]; M. Aguiano-Galicia, A. Bashir and A. Raya, *Phys. Rev. D* **76**, 127702 (2007).
- [81] H. Mishra and S. Misra, *Phys. Rev. D* **48**, 5376 (1993).
- [82] T. Mandal, P. Jaikumar and S. Digal, arXiv:0912.1413 [nucl-th].
- [83] M. Metlitsky and A. Zhitnitsky, *Phys. Rev. D* **72**, 045011 (2005).
- [84] E. Ferrer, V. Incera and C. Manuel, *Nucl. Phys. B* **747**, 88 (2006).
- [85] T. Hatsuda and T. Kunihiro, *Phys. Rep.* **247**, 221 (1994); M. Buballa, *Phys. Rep.* **407**, 205 (2005).
- [86] J. Berges and K. Rajagopal, *Nucl. Phys. B* **538**, 215 (1999).

- [87] J. Noornah and I. Shovkovy, *Phys. Rev. D* **76**, 105030 (2007).
- [88] E. Elizalde, *J. Phys. A* **18**, 1637 (1985).
- [89] P. Rehberg, S. Klevansky and J. Huefner, *Phys. Rev. C* **53**, 410 (1996).
- [90] M. Lutz, S. Klimt and W. Weise, *Nucl. Phys. A* **542**, 521 (1992).
- [91] S. Ruester, I. Shovkovy and D. Rischke, *Nucl. Phys. A* **743**, 127 (2004).
- [92] K. Schertler, S. Leupold and J. Schaffner-Bielich, *Phys. Rev. C* **60**, 025801 (1999).
- [93] K. Klimenko and V. Zhukovsky, *Phys. Lett. B* **665**, 352 (2008).
- [94] D. Ebert, K. Klimenko, M. Vdovichenko and A. Vshivtsev, *Phys. Rev. D* **61**, 025005 (1999).
- [95] K. Fukushima and H. J. Warringa, *Phys. Rev. Lett.* **100**, 032007 (2008).
- [96] V. Canuto and J. Ventura, *Fundam. Cosmic Phys.* **2**, 203 (1977).
- [97] D. Hong, *Phys. Lett. B* **699**, 305 (2011).
- [98] D. Nickel, *Phys. Rev. D* **80**, 074025 (2009); G. Baser, G. Dunne and D. Kharzeev, *Phys. Rev. Lett.* **104**, 232301 (2010); I. Frolov, V. Zhukovsky and K. Klimenko, *Phys. Rev. D* **82**, 076002 (2010).
- [99] R. Gatto and M. Ruggieri, *Phys. Rev. D* **82**, 054027 (2010).
- [100] E. Ferrer, V. Incera and C. Manuel, *Phys. Rev. Lett.* **95**, 152002 (2005); E. Ferrer and V. Incera, *Phys. Rev. Lett.* **97**, 122301 (2006); *Phys. Rev. D* **76**, 114012 (2007). S. Fayazbakhsh and N. Sadhooghi, *Phys. Rev. D* **82**, 045010 (2010).
- [101] P. Vecchia and G. Veneziano, *Nucl. Phys. B* **171**, 253 (1980); A. Smilga, *Phys. Rev. D* **59**, 114021 (1999); M. Tytgat, *Phys. Rev. D* **61**, 114009 (2000); G. Akemann, J. Lenaghan and K. Splittorff, *Phys. Rev. D* **65**,

- 085015 (2002); M. Creutz, Phys. Rev. Lett. **92**, 201601 (2004); M. Metlitsky and A. Zhitnitsky, Nucl. Phys. B **731**, 309 (2005); Phys. Lett. B **633**, 721 (2006).
- [102] A. Mizher and E. Fraga, Nucl. Phys. A **820**, 247c (2009); Nucl. Phys. A **831**, 91 (2009).
- [103] T. Fujihara, T. Inagaki and D. Kimura, Prog. Theo. Phys. **117**, 139 (2007).
- [104] D. Boer and J. Boomsma, Phys. Rev. D **78**, 054027 (2008).
- [105] D. Boer and J. Boomsma, Phys. Rev. D **80**, 034019 (2009).
- [106] Y. Sakai, H. Kouno, T. Sasaki and M. Yahiro, Phys. Lett. B **705**, 349 (2011).
- [107] A. Mishra and H. Mishra, Phys. Rev. D **74**, 054024 (2006).



## **Publications attached with the thesis**

1. **“BCS-BEC crossover and phase structure of relativistic systems: A variational approach”**

B. Chatterjee, A. Mishra and H. Mishra

Phys. Rev. D **79**, 014003 (2009) [arXiv:0804.1051 [hep-ph]]

2. **“Vacuum structure and chiral symmetry breaking in strong magnetic fields for hot and dense quark matter”**

B. Chatterjee, A. Mishra, H. Mishra

Phys. Rev. D **84**, 014016 (2011) [arXiv:1101.0498 [hep-ph]]

